NASA/CR—2020-220489

Fuel Flexible Combustor for High-OPR Compact-Core N+3 Propulsion Engine

Final Technical Report

Lance L. Smith
United Technologies Research Center, East Hartford, Connecticut

March 2020

NASA STI Program . . . in Profile

Since its founding, NASA has been dedicated to the advancement of aeronautics and space science. The NASA Scientific and Technical Information (STI) Program plays a key part in helping NASA maintain this important role.

The NASA STI Program operates under the auspices of the Agency Chief Information Officer. It collects, organizes, provides for archiving, and disseminates NASA's STI. The NASA STI Program provides access to the NASA Technical Report Server—Registered (NTRS Reg) and NASA Technical Report Server—Public (NTRS) thus providing one of the largest collections of aeronautical and space science STI in the world. Results are published in both non-NASA channels and by NASA in the NASA STI Report Series, which includes the following report types:

- TECHNICAL PUBLICATION. Reports of completed research or a major significant phase of research that present the results of NASA programs and include extensive data or theoretical analysis. Includes compilations of significant scientific and technical data and information deemed to be of continuing reference value. NASA counter-part of peer-reviewed formal professional papers, but has less stringent limitations on manuscript length and extent of graphic presentations.

- TECHNICAL MEMORANDUM. Scientific and technical findings that are preliminary or of specialized interest, e.g., "quick-release" reports, working papers, and bibliographies that contain minimal annotation. Does not contain extensive analysis.

- CONTRACTOR REPORT. Scientific and technical findings by NASA-sponsored contractors and grantees.

- CONFERENCE PUBLICATION. Collected papers from scientific and technical conferences, symposia, seminars, or other meetings sponsored or co-sponsored by NASA.

- SPECIAL PUBLICATION. Scientific, technical, or historical information from NASA programs, projects, and missions, often concerned with subjects having substantial public interest.

- TECHNICAL TRANSLATION. English-language translations of foreign scientific and technical material pertinent to NASA's mission.

For more information about the NASA STI program, see the following:

- Access the NASA STI program home page at http://www.sti.nasa.gov

- E-mail your question to help@sti.nasa.gov

- Fax your question to the NASA STI Information Desk at 757-864-6500

- Telephone the NASA STI Information Desk at 757-864-9658

- Write to:
  NASA STI Program
  Mail Stop 148
  NASA Langley Research Center
  Hampton, VA 23681-2199

NASA/CR—2020-220489

Fuel Flexible Combustor for High-OPR Compact-Core N+3 Propulsion Engine

Final Technical Report

Lance L. Smith
United Technologies Research Center, East Hartford, Connecticut

Prepared under Contract NNC14CA30C

National Aeronautics and
Space Administration

Glenn Research Center
Cleveland, Ohio 44135

March 2020

This work was sponsored by the Advanced Air Vehicle Program
at the NASA Glenn Research Center

Level of Review: This material has been technically reviewed by expert reviewer(s).

Available from

NASA STI Program
Mail Stop 148
NASA Langley Research Center
Hampton, VA 23681-2199

National Technical Information Service
5285 Port Royal Road
Springfield, VA 22161
703-605-6000

This report is available in electronic form at http://www.sti.nasa.gov/ and http://ntrs.nasa.gov/

Final Technical Report

This document reports unlimited-rights data relating to technical work under NASA contract NNC14CA30C, performed throughout the full period of the effort. This period comprises Fiscal Years 2015 through 2019 (inclusive); this period includes the 4th Quarter of Calendar Year 2014, all of Calendar Years 2015 through 2018, and the first three Quarters of Calendar Year 2019. Limited-rights data relating to technical progress during this period are provided in a separate document, a Limited Rights version of this report having limited rights markings.

Section I – Technical Progress Summary

As reported here and in detail below, the N+3 small-core combustor effort was successfully completed, having accomplished all its milestones and having met all its delivery requirements. The significant accomplishments and activities during the program were the following:

- Selection of a target N+3 engine cycle (Pratt & Whitney's SGTF2065 cycle), for combustor rig design and performance evaluation, including specification of combustor requirements for N+3.
- Combustor sub-component testing at UTRC, including high-pressure high-temperature autoignition testing of multiple alternative fuels (leading to publication of AIAA Paper No. AIAA-2017-4985), and ambient testing of main- and pilot-injectors.
- Concept design studies and concept downselection for a small-core N+3 combustor configuration, to be experimentally evaluated at UTRC and NASA.
- Detailed design and fabrication of a water-cooled single-sector N+3 combustor rig for UTRC testing.
- Detailed design and fabrication of an air-cooled single-sector N+3 combustor rig for NASA testing.
- Completion of high-pressure N+3 combustor testing in UTRC's Jet Burner Test Stand, with Jet-A and with alternative fuels, and with test results obtained that meet NASA's N+3 emissions goals.
- Support of N+3 combustor testing at NASA, including on-site rig installation support at NASA, rig operation and test planning, and rig servicing and re-instrumentation for continued NASA testing.
- Completion of choked-exit full-annular combustor testing (using hardware from ERA Phase-II) with engine-like acoustic boundary conditions in Pratt & Whitney's X960 facility, for evaluation of combustion dynamics in the ACS combustor.
- Completion of choked-exit dynamics testing of the single-sector N+3 combustor rig at UTRC, with Jet-A and with alternative fuels, and for three different pilot-injector configurations. Acoustically-forced spray testing and modeling were also performed to support the dynamics investigations.
- Prediffuser CFD modeling and analysis (leading to publication of AIAA Paper No. AIAA-2019-1186) toward development of a validated tool for design of prediffusers.
- Completion of documentation describing the N+3 combustor concept selected, the results of design, analysis, and testing of the selected N+3 combustor concept, lessons learned (e.g. as summarized in Section V of this report), and recommendations for additional research and development (see Section IV of this report). To-date this documentation has been provided in the various Quarterly and Annual Technical Progress Reports, and is compiled and completed in this Final Technical Report.

The above activities have supported development of an ACS (Axially Controlled Stoichiometry) combustor technology for future small-core N+3 propulsion engines, having high bypass ratios and attendant high efficiency. Accordingly, during the first year of this effort a target N+3 engine cycle and core-size was selected by the N+3 combustor stakeholders – UTRC, Pratt & Whitney, and NASA. The chosen cycle was based on MIT's N+3 aircraft studies with propulsion analysis by Pratt & Whitney, and

meets NASA's N+3 fuel-burn goal in the D8.6 concept aircraft. Pratt & Whitney performed turbomachinery and combustor flowpath analysis to define the target combustor envelope (see Figure I.1.5 below), and with this input the ERA Phase-II ACS combustor design was scaled to N+3 engine size and conditions, to provide an initial N+3 combustor "baseline" design. In the second year, the effort was directed toward design refinement for improved emissions performance, including component evaluation using CFD and ambient testing, followed by configuration downselection and detailed design and fabrication of a single-sector N+3 combustor rig for experimental performance evaluation at UTRC. In the third year, the focus was on actual combustion testing, both of the single-sector N+3 combustor hardware fabricated for UTRC testing and of the full-annular ERA Phase-II combustor hardware for its engine-like acoustic boundary conditions (enabling dynamics evaluation). The results provided significant learning regarding small-core and ACS combustor performance, both in terms of achievable emissions (meeting NASA's goals) and challenges to be faced in mitigating combustion dynamics. In the final period of the effort the focus was on fabrication and delivery of a new single-sector N+3 combustor rig for testing in NASA's CE-5 facility, as well as continued testing at UTRC of the existing N+3 combustor rig to further evaluate combustion dynamics and emissions performance, including configuration variations to evaluate alternative pilot injectors.

Task 1 – Define & specify combustor requirements

Selection & Analysis of Cycle & Core Size for N+3 Combustor Development

A significant goal for this effort is to develop combustor technologies consistent with all of NASA's N+3 objectives, including 80% reduction in NOx and 60% reduction in fuel burn as measured against 2005-defined baseline levels. Aircraft fuel burn reductions exceeding this goal have been predicted by the Massachusetts Institute of Technology (MIT) and Pratt & Whitney (P&W) team for the D8.6 concept aircraft, under previous NASA-sponsored N+3 aircraft studies (Greitzer et al. 2010, Lord et al. 2014). Therefore the target engine cycle for this N+3 combustor development effort was selected from the MIT/P&W work, and specifically from the Pratt & Whitney cycle studies for the D8.6 aircraft (Lord et al. 2014). A detailed P&W NPSS model for the D8.6 aircraft engine was used to provide an accurate and complete set of operating conditions for N+3 combustor evaluation and design. These conditions were used for refinement of preliminary performance predictions for the N+3 combustor, and for further N+3 combustor development and design, as discussed in more detail in subsequent sections of this report.

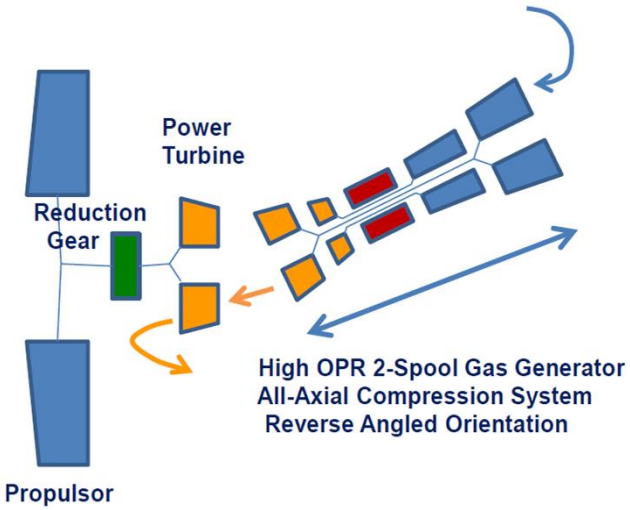

Figure I.1.1. *Implementation of N+3 engine as a 2-spool core aerodynamically coupled to the separate propulsor (fan drive system), as shown by Lord et al. (2015).*

The initial MIT-defined engine cycle assumed a 3-engine D8.5 aircraft configuration (Greitzer et al., 2010), with each engine having a core-size of around 1.0 (at or below the core-size limit for a high-OPR axial compressor; see Figures I.1.3 and I.1.4 and the discussion below). In the configuration update defined by Lord et al. (2014, 2015) the aircraft concept was modified to use only 2 engines (each of 3-spool design), increasing the core-size to ~1.5 and enabling each engine core to be canted away from the adjacent engine, to prevent cascading failure in the event of a disk burst (i.e. to prevent a failure in one engine from damaging the second engine). This 2-engine aircraft concept is designated the D8.6 configuration, and is illustrated in Figures I.1.1 and I.1.2 (from Lord et al., 2015) with the above-mentioned canting of the engines. In Figure I.1.2, two D8.6 engine configurations are shown – an "initial concept" having an aggressively-small 1.5 core-size, and a "revised installation" that further pushes the core-size down to 1.3 to bring the core air inlet inside the fan diameter. The 1.5 core-size is depicted (annotated) in Figure I.1.3 from Lord et al. (2015) at 13k-lbf thrust-class (corresponding to the required thrust from each engine in the 2-engine D8.6 aircraft).

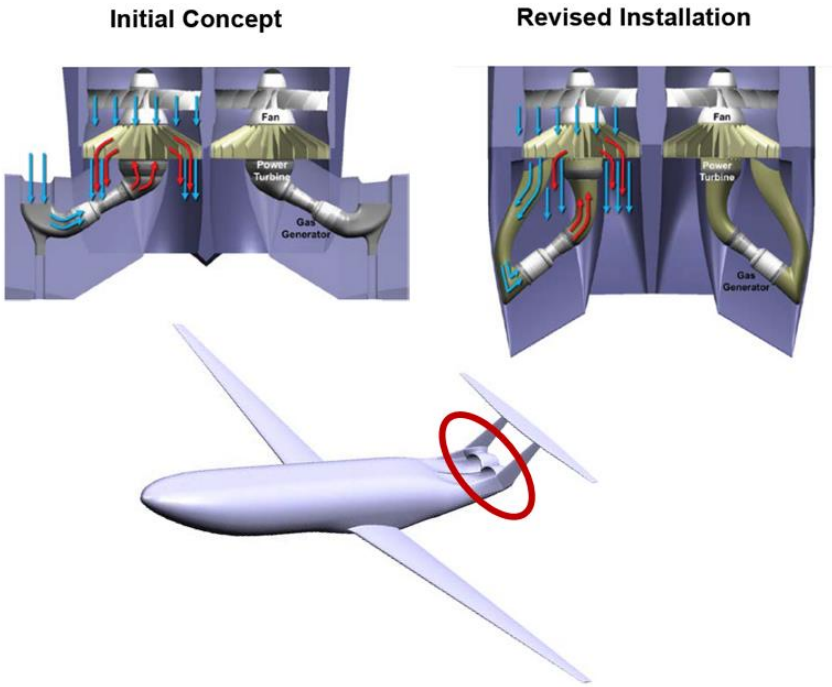

Figure I.1.2. *Conceptual installation of two N+3 engines on the D8.6 aircraft, from Lord et al. (2015), showing the twin rear-mount configuration for Boundary Layer Ingestion (BLI) efficiency benefits. The upper-left panel shows the initial 1.5 core-size concept, and the upper-right shows the revised 1.3 core-size concept.*

Figure I.1.4 from Lord et al. (2014) shows the challenges associated with achieving high-OPR operation at the small core-sizes required for the D8.5 aircraft concept, by contrasting the required compressor operating conditions to current compressor operating regimes. The figure illustrates the need for engine and compressor technology development to achieve core sizes below 3 with high-efficiency axial compressors. As described above, the architecture limit at core-size ~3 can be overcome (moved) by changing to a 3-spool architecture with a mechanically decoupled fan (Lord et al., 2014, 2015). However, additional compressor development is required to achieve very small core sizes (below ~2), for operation in the desired N+3 region shown at the top-left of Figure I.1.4 (in the region designated by

the annotation “Advanced Concepts N+3”). The 2.0 core-size selected for N+3 combustor development is thus consistent with the need for small-core engines in future high-efficiency aircraft, and consistent with achievable compressor operation in an N+3 technology engine. This target corresponds to an approximate 15 k-lbf thrust class for the MIT-defined N+3 engine cycle.

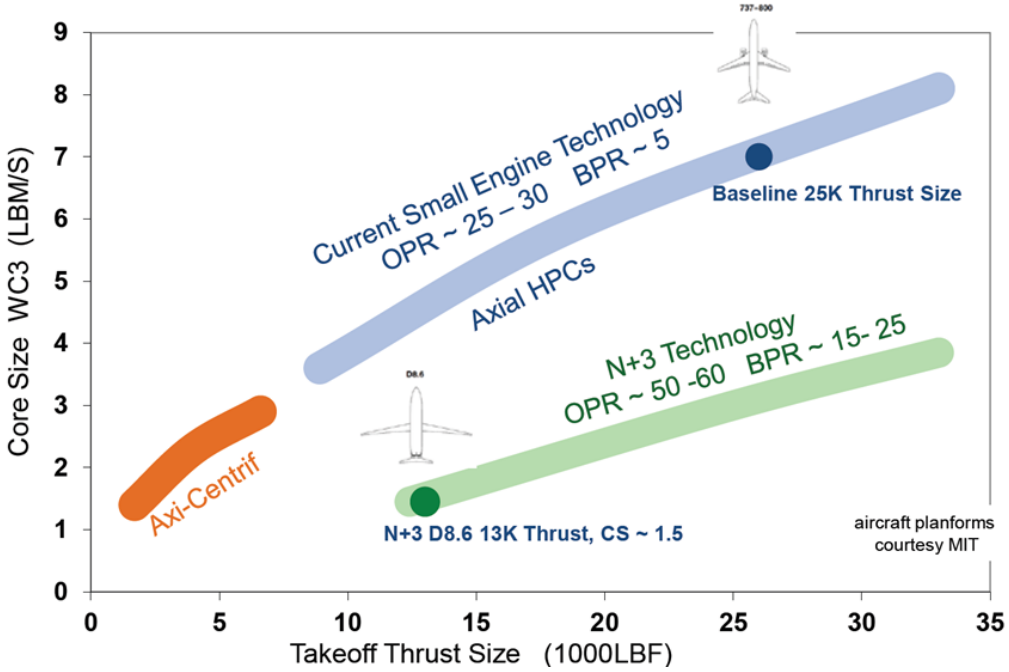

Figure I.1.3. Map of core-size vs. takeoff thrust size from Lord et al. (2015), showing N+3 core-sizes from ~1.5 to 3.5 for thrust class from ~13 to 30 k-lbf.

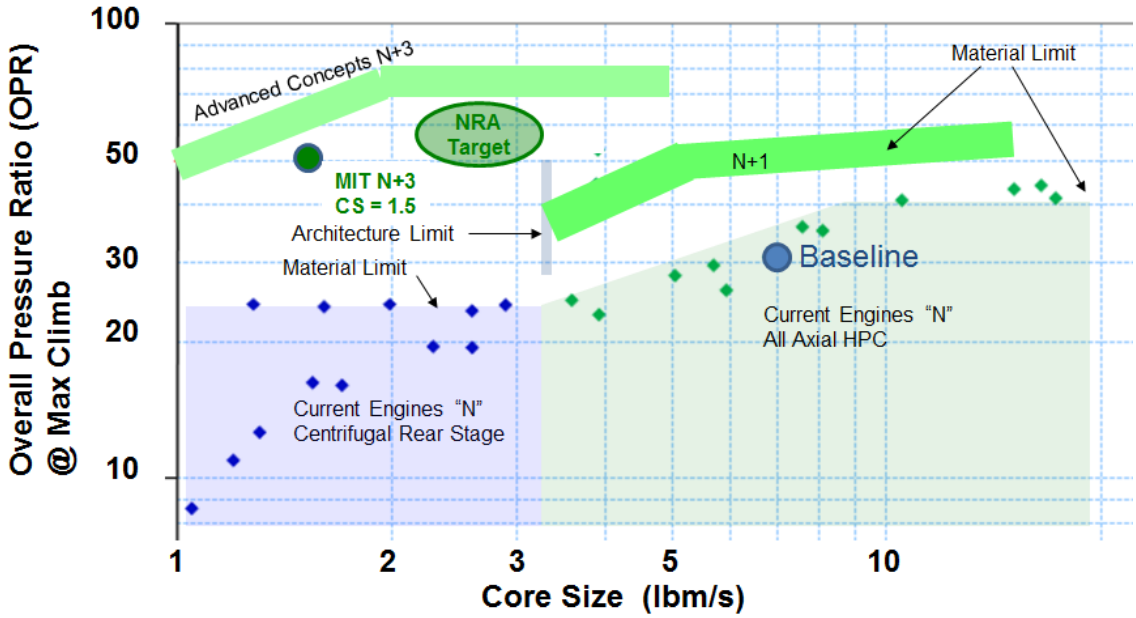

Figure I.1.4. *Map of OPR vs. core-size for engine technology generations (N, N+1, and N+3), from Lord et al. (2014), showing technology development need for high-OPR compressors of core-size < 3.*

With selection of the specific cycle and core-size for the N+3 combustor, Pratt & Whitney provided NPSS cycle analysis and initial sizing analysis using their aerothermal design engineering tools. These were used as input for detailed CFD analysis at UTRC.

In addition to the cycle analysis, Pratt & Whitney also provided flowpath results for the SGTF2065 cycle. The Pratt & Whitney flowpath tool uses a mean-line turbomachinery analysis to calculate compressor and turbine information including vane and blade elevations (radius and span). This geometric information is then used, together with the cycle conditions, to calculate approximate combustor dimensions, ensuring an appropriate match to the compressor exit and turbine inlet geometries, and allowing adequate length and volume for the combustor-section aerodynamic and aerothermal functions based on Pratt & Whitney design rules and experience. Mechanical design considerations are also included, such as space allocation for fuel-nozzles. On this basis Pratt & Whitney provided a preliminary N+3 combustor layout for the SGTF2065 cycle and flowpath, scaled to a core-size of 2.0. The combustor dimensions (and corresponding turbomachinery elevations) are based on the D8.6 engine concept as discussed by Lord et al. (2014) in which a reverse-flow configuration is implemented to avoid passing the fan shaft through the engine core (thus enabling reduced turbomachinery diameters and concomitantly larger spans). Pratt & Whitney's preliminary combustor sizing was used as the basis for more detailed CFD analysis.

Characteristics of High-BPR Cycles for N+3

It is worth noting that modern high bypass-ratio (BPR) engines have cycle conditions that trend differently from legacy engines, as discussed further below, and that therefore pose different challenges for achieving combustion efficiency and low NOx across the required aircraft mission. In addition, integration of the airframe and propulsion engine can provide unique benefits, offering significant improvements in overall system efficiency (mission fuel burn). The D8.5 and D8.6 concepts utilize such airframe/propulsion engine integration, as reported by the Massachusetts Institute of Technology (MIT) team in partnership with Pratt & Whitney (P&W), Aerodyne Research, and Aurora Flight Sciences, under their NASA-sponsored project to develop "Aircraft and Technology Concepts for an N+3 Subsonic Transport" (Greitzer et al., 2010). The initial MIT-defined N+3 engine-cycle conditions for the D8.5 aircraft are summarized in Figure I.1.5 below. This cycle corresponds to an integrated ultra-high bypass ratio (BPR = 20) engine design, having advanced materials and high component efficiencies to minimize fuel burn (Greitzer et al. 2010; Lord et al. 2014).

As shown in Figure I.1.5 and described in the MIT project final report (Greitzer et al., 2010), the MIT-defined engine cycle provides a cruise Thrust Specific Fuel Consumption (TSFC) of 0.37 lbm/hr/lbf (fuel-flow/thrust) when installed in the D8.5 concept aircraft and configured to provide Boundary Layer Ingestion (BLI) to effectively reduce ram drag. In this configuration, the integrated engine-airframe concept (see Figure I.1.2) provides a mission fuel burn that is 70% below the 2005 baseline fuel burn (B737-800 with CFM56-7B engines) as measured in units of Payload Fuel Energy Intensity (PFEI, or kJ/kg-km). Thus, the MIT engine-airframe combination more than meets NASA's Aircraft Fuel Energy Consumption objective (fuel burn objective) for N+3. For reference, the 2005 baseline CFM56-7B24 engine is cited in the subsequent Phase 2 final report (Lord et al., 2014) as having a TSFC of approximately 0.60 lbm/hr/lbf (at 35k-ft altitude/ 0.80 Mach/ ISA/ uninstalled).

Note in Figure I.1.5 that the MIT-defined N+3 engine has an ultra-high bypass ratio of 20 or more (depending on flight condition), and demonstrates characteristics common to ultra-high-bypass engines that are relevant to the combustor design. In particular, we note that OPR (overall pressure ratio) and temperature ratio (TT4/TT2, i.e. burner outlet temperature to engine inlet temperature) are both much

higher at cruise than at takeoff. This behavior of high bypass engines, or equivalently low Fan Pressure Ratio (FPR) engines, is discussed by Cumpsty (2010): "Reducing FPR at cruise…does more than…raise propulsive efficiency. The lower cruise FPR makes possible higher overall pressure ratio and turbine inlet temperature at cruise, thereby increasing thermal efficiency and making the core relatively smaller and lighter. The explanation lies with the so-called lapse rate… Higher thrust ratio [takeoff thrust / cruise thrust] for lower cruise FPR means…proportionately more [available] thrust at take-off." This trend is also reported by Epstein (2014) as shown in Figure I.1.6, which shows that low FPR engines (i.e. high BPR engines) show less variation in T4 (turbine inlet temperature) from takeoff to cruise than "legacy" engines with higher FPRs in the range of 1.7. Figure I.1.6 clearly shows that lowering FPR (e.g. to FPR=1.4 for the MIT-defined N+3 engine) reduces T4 at the Sea Level Static thrust condition where NOx emissions are regulated. On the other hand, T4 at cruise may increase with reduced FPR. Thus, future high-bypass engines are likely to be more challenged at cruise than at takeoff with respect to NOx emissions.

Table 10: D8.5 Engine Performance Parameters

Parameter	Sea Level Static	Rolling / Rotation	Takeoff	Cutback	Top of climb	Cruise	Approach
Net thrust (kN)	37.7	29.0	27.7	14.2	5.9	5.9	1.9
Ram drag (kN)	N/A	9.2	11.8	9.2	11.7	11.7	4.1
TSFC' (lb/lb h)	0.174	0.228	0.239	0.243	0.370	0.370	0.418
Engine mass flow (kg/s)	201.9	207.8	210.3	163.0	57.6	57.4	78.7
BPR	22.8	23.3	23.5	25.7	20.0	20.0	23.6
Cooling flows (kg/s)	0.125	0.126	0.126	0.090	0.040	0.040	0.047
OPR	33.7	33.4	33.2	21.4	50.2	50.0	9.0
TT4/TT2	5.6	5.6	5.5	2.57	6.63	6.62	2.98
Fan efficiency (%)	96.5	96.5	96.5	97.3	95.1	95.1	98.0
High compressor efficiency (%)	90.0	90.0	90.0	90.0	90.0	90.0	90.0
Low compressor efficiency (%)	93.0	93.0	93.0	93.0	93.0	93.0	93.0
High turbine efficiency (%)	92.5	92.5	92.5	92.5	92.5	92.5	92.4
Low turbine efficiency (%)	90.4	90.5	90.5	86.9	93.0	93.0	80.5
Fan pressure ratio	1.25	1.24	1.24	1.14	1.43	1.42	1.04
Low pressure compressor pressure ratio	1.92	1.92	1.92	1.62	2.27	2.27	1.22
High pressure compressor pressure ratio	17.56	17.40	17.33	13.24	22.07	22.0	7.36
Low Pressure Turbine Pressure Ratio	0.14	0.14	0.14	0.20	0.08	0.09	0.47
High Pressure Turbine Pressure Ratio	0.25	0.25	0.25	0.25	0.25	0.25	0.25
Core Inlet Pressure Recovery	0.995	0.995	0.994	0.994	0.962	0.962	0.994
Core Exhaust Duct Recovery	0.995	0.995	0.995	0.995	0.995	0.995	0.995
Fan Exhaust Duct Recovery	0.985	0.985	0.985	0.985	0.985	0.985	0.985

Figure I.1.5. *Summary table from 2010 MIT Final Report (Greitzer, 2010), providing N+3 engine cycle conditions corresponding to the D8.5 concept aircraft mission.*

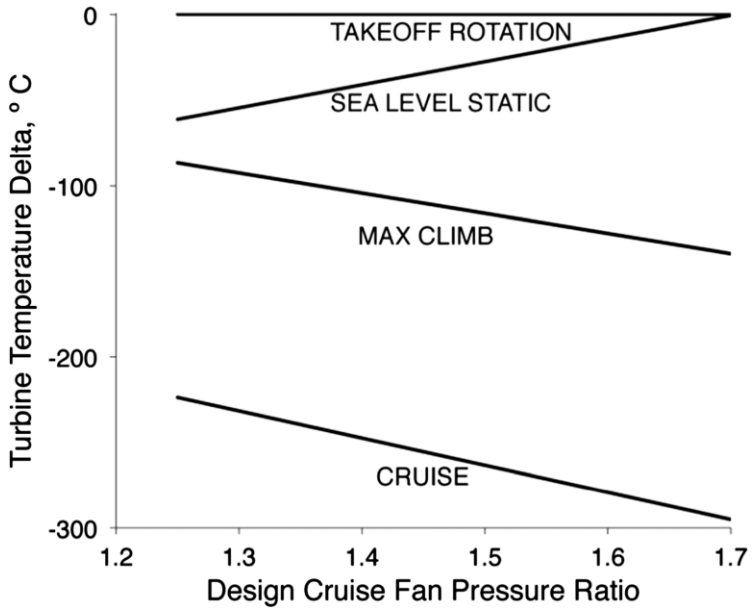

Figure I.1.6. *Lapse of turbine temperature, from takeoff to cruise, vs. FPR (or BPR), from Epstein (2014).*

For high-bypass engines the wide "lapse" in OPR from cruise or top-of-climb conditions (at high altitude and high Mach number) down to takeoff conditions (at low altitude and low Mach number) is also an important consideration for combustor design. As shown in Figure I.1.5, the MIT-defined N+3 cycle drops from 50 OPR at cruise or top-of-climb to 33 OPR at takeoff. As a result, low-FPR high-bypass engines do not exhibit the extremely high combustor inlet pressures and temperatures (P3 and T3) one might expect to be associated with a high-OPR core. To some extent, therefore, low FPR technologies will help ameliorate the risk of autoignition and flashback in future lean-burn combustion systems.

Aircraft Operating Condition	Combustor Inlet Pressure, P3 (psia)	Combustor Inlet Temperature, T3 (F)	Combustor Outlet Temperature, T4 (F)
Sea Level Static (100% Foo)	493 psia	1042 F	2445 F
Takeoff/Rotation (0.19 Mach)	501 psia	1048 F	2466 F
Cruise (0.74 Mach)	145 psia	949 F	2407 F

Figure I.1.7. *Calculated combustor operating conditions for MIT-defined N+3 engine cycle of Figure I.1.2, for three different engine cycle conditions: cruise (M=0.74 at 45k feet altitude), sea-level takeoff (M=0.19), and SLS rated thrust. Calculations are based on the parameters provided in Figure I.1.2, assuming constant specific heat ratio (1.4 in the engine inlet and LPC, and 1.39 in the HPC) and aircraft operation within International Standard Atmosphere (ISA) conditions.*

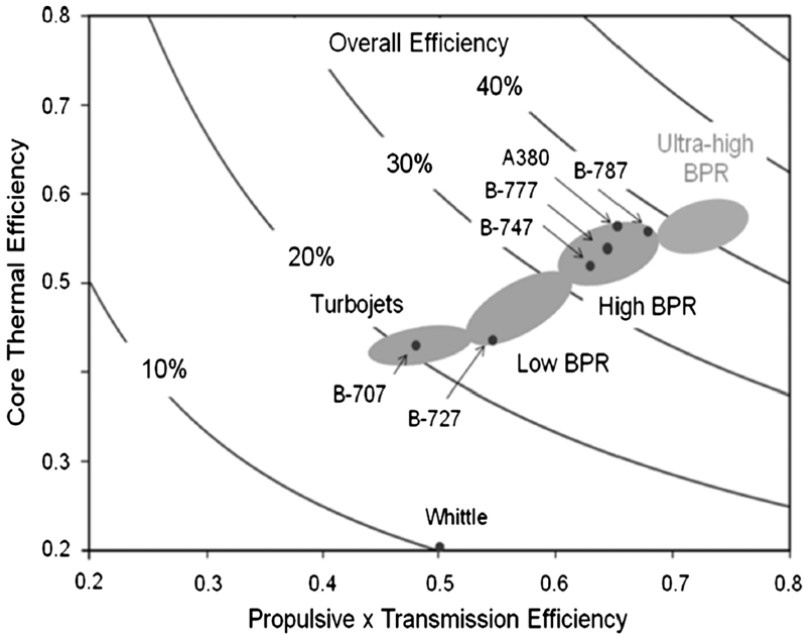

Figure I.1.8. *Efficiency trend with propulsive efficiency (BPR), from Epstein (2014).*

The numerical values in Figure I.1.5 can be used to calculate combustor operating conditions, for MIT's D8.5 aircraft operation in the International Standard Atmosphere (ISA) at the speeds specified in Greitzer et al. (2010) and Lord et al. (2014), i.e. 0.74 Mach at cruise (45000 feet) and 0.19 Mach at takeoff (sea level). On this basis, combustor conditions are tabulated in Figure I.1.7 for cruise, takeoff rotation, and 100% rated thrust (sea level static). As noted, for this high-bypass low-FPR engine the combustor outlet temperature (T4) "lapses" very little from takeoff to cruise (cruise T4 is within ~50F of its high thrust value), meaning that cruise NOx goals may be more difficult to achieve than LTO NOx (landing-takeoff NOx) goals. In addition, we note that combustor inlet pressure and temperature at takeoff are moderate (500 psia and ~1050 F) despite the use of a high-OPR cycle. Again, this is attributable to the high-bypass low-FPR design, which will necessarily be a key feature in future high-efficiency engines as demonstrated in Figure I.1.8 (from Epstein, 2014), especially noting the "Ultra-high BPR" region of the chart where maximum efficiency gains are achieved.

Combustor Requirements for N+3

To guide and constrain the N+3 combustor design, a target "combustor requirements list" for N+3 was developed with Pratt & Whitney during the first year of the effort. This "requirements list" includes metrics appropriate for both near-term development (up to TRL3) and far-term development (to TRL6 and beyond), but which are all useful to help define the technical direction. Broadly, there are two categories of targeted metrics – *performance* metrics desirable for an N+3 combustor, and *scalability* metrics to ensure the developed N+3 technologies will be useful for high-OPR, ultra-high-bypass cycles in a wide range of future aircraft (including both single-aisle and wide-body). At the present TRL level for N+3 (below TRL3) this "combustor requirements list" represents target values only, and is expected to be refined and expanded as the technology matures and the TRL level increases:

- Targeted N+3 *Performance* Metrics:
  - Emissions & Efficiency –
    - Meet NASA's N+3 NOx goals for LTO & cruise
    - Combustion efficiency: target 99% for idle, 99.5% for approach, 99.9% for cruise
    - Smoke & PM: SN < 1; PM equivalent to reported data for lean-burn systems

- Ignition & Blowout –
  - High-altitude ignition/re-light → apply P&W combustor sizing rules; test
  - LBO (lean blowout): adequate blowout margin from minimum transient FAR

➢ Targeted N+3 *Scalability* Metrics:

- Meet above performance metrics across full range of expected core-sizes (<2 to >6)
- Cost, Weight, Complexity, Maintainability –
  - Minimize fuel-nozzle count
  - Combustor diam. & length: comparable to Talon-X combustor at same core-size

TECHNOLOGY BENEFITS*	TECHNOLOGY GENERATIONS (Technology Readiness Level = 4-6)		
	N+1 (2015)	N+2 (2020**)	N+3 (2025)
Noise (cum margin rel. to Stage 4)	-32 dB	-42 dB	-71 dB
LTO NOx Emissions (rel. to CAEP 6)	-60%	-75%	-80%
Cruise NOx Emissions (rel. to 2005 best in class)	-55%	-70%	-80%
Aircraft Fuel/Energy Consumption‡ (rel. to 2005 best in class)	-33%	-50%	-60%

Figure I.1.9. *Summary of NASA's objectives for N+3 technologies, including 60% fuel-burn reduction and 80% NOx reduction, as compared to 2005 baseline levels.*

The first item from the "requirements list" above (under Emissions & Efficiency) refers to NASA's stated goals for an N+3 engine. As shown in Figure I.1.9, the LTO NOx goal is to achieve emissions that are 80% below the ICAO CAEP/6 standard. This is a well-defined goal that can easily be calculated from measured NOx emissions and the known (selected) engine cycle. The cruise NOx goal, analogously, is to achieve emissions that are 80% below a 2005 "best in class" baseline. This goal is less well-defined, however, since there is no existing ICAO cruise NOx standard – and therefore no existing cruise NOx metric – and since the 2005 baseline requires definition.

For the cruise NOx metric, a measure is needed representing the quantity of NOx deposited in the atmosphere for any given flight mission. For this purpose, a useful metric for comparing cruise NOx emissions from different engines is NOx per thrust, or more specifically grams NOx emitted per minute per kN thrust at cruise. This can be calculated from measured EINOx emissions (for cruise combustor conditions), along with the engine cycle's cruise Thrust Specific Fuel Consumption (TSFC). Since TSFC is usually quoted in units of lbm/hr fuel flow per lbf thrust, we have:

$$\text{Cruise\_NOx} = (\text{ g\_NOx / min }) / \text{kN\_thrust} = 1.7*\text{EINOx}*\text{TSFC}$$

when EINOx is in units of g_NOx/kg_fuel and TSFC is in units of pph_fuel/lbf_thrust. The above units conversion comes from evaluating the expression below:

$$EINOx \cdot TSFC = \frac{g_{NOx}}{kg_{fuel}} \cdot \frac{lbm_{fuel}/hr}{lbf_{thrust}} \cdot \frac{hr}{60\ min} \cdot \frac{kg}{2.2046\ lbm} \cdot \frac{224.8\ lbf}{kN} = \frac{g_{NOx}/min}{kN_{thrust}} \cdot \frac{224.8}{60 * 2.2046}$$

which is equivalent to the above (i.e. to multiplying EINOx*TSFC by 1.7). Note that this cruise NOx metric (Cruise_NOx = 1.7*EINOx*TSFC) is a better measure of aircraft-mission NOx emissions than pure EINOx, since the Cruise_NOx metric replaces fuel-burn with thrust in the denominator, and therefore accurately represents emitted NOx regardless of whether the aircraft fuel burn rate is high or low. Thus, this Cruise_NOx metric is closer in meaning than pure EINOx to the ICAO LTO NOx standard (g_NOx/kN for the duration of the LTO cycle, or Dp/Foo), and it recognizes the NOx reductions possible with increased aircraft and engine efficiency.

Finally, we note that the original cycle and core-size selections were made in 2015 to enable detailed N+3 combustor evaluation and design to begin, prior to N+3 compressor definition from Pratt & Whitney's parallel NASA-sponsored N+3 effort. As a result, there are some differences in the target conditions for the combustor versus compressor efforts, but in general the N+3 combustor targets remain relevant to Pratt & Whitney needs for future N+3 type engines. In addition, since 2015 NASA has directed MIT to study requirements for a higher Mach number cruise capability than the D8.6 aircraft, targeting 0.8 Mach number cruise (versus e.g. 0.74 for the earlier D8.6 aircraft). NASA therefore recommended, during the December 17th first Annual Review for this N+3 combustor effort, that we communicate with MIT about possible updates to engine thrust requirements for their D8-series N+3 aircraft concept. The engine cycle we selected for N+3 combustor development was based on the D8.6 rated thrust requirement [Greitzer et al., 2010] of about 13k-lbf (or 15 to 16k-lbf when scaled to our selected 2.0 core-size), whereas per NASA's comments MIT's most recent studies have shown a rated thrust requirement closer to 25k-lbf. In follow-up correspondence with P&W and MIT, we learned that the 25k-lbf value was based on MIT's D8.2S aircraft, which is a lower technology concept (e.g. aluminum, not composite) than the D8.6, and configured for 0.8 Mach number cruise (hence the "S" designation). In brief, the D8.2S requires 25k-lbf thrust because it is heavier and faster than the D8.6. Based on back-to-back comparison of the D8.2 (0.72 Mach) and D8.2S (0.8 Mach), MIT's studies show that the higher Mach number requires a thrust increase of about 14% and core-size growth of about 17%. These trends indicate that our selected 2.0 core-size remains an appropriate target for N+3 combustor development.

Task 2 – Layout & design studies for small-core combustor

Introduction

Using the detailed N+3 cycle and geometry information provided by Pratt & Whitney under Task 1, UTRC performed detailed aerodynamic design and analysis of ACS (Axially Controlled Stoichiometry) combustor performance at N+3 conditions. One combustor design challenge, discussed further below, is to ensure a high enough fuel-air ratio within the burning zone that combustion is stable at idle, while at the same time limiting the local fuel-air ratio at cruise to a low enough value that NOx emissions are not excessive. A successful design depends on balancing this tradeoff, via airflow allocation and fuel-staging between the pilot and mains, and also depends on the detailed function and design of the pilot and main injectors themselves.

Combustor Flow Split, Fuel Staging, and Geometrical Configuration and Sizing

A demonstrated path to staged lean burn combustion utilizes a diffusion or partially premixed pilot stage supporting a main premixed stage. Therefore, it is desirable to design the smallest pilot and largest main possible while meeting all performance requirements, so that the pilot fuel split (fraction of fuel to the pilot) can be set to a minimum during full stage (high power) operation, thus minimizing NOx emissions. In general, the main stage is ideally designed to maximize airflow, thus minimizing main-stage fuel-air ratio (or equivalence ratio ϕ) and therefore minimizing NOx. However, for the ACS

concept, high power efficiency is a concern if the main ϕ is too low. Based on the SGTF2065 N+3 engine cycle, the pilot injector and main injector airflow splits and fuel flow splits were selected for an initial N+3 combustor design, and were evaluated against prior data from the NASA ERA program and from CFD models using the initial geometrical sizing provided by Pratt & Whitney. These evaluations were then used for development of a final design.

Task 3 – Assess alternative-fuel and high-OPR effects

Existing Autoignition Data and Modeling for Aircraft Fuels

Initial assessments of aircraft fuel autoignition times were obtained from data and models available in the literature. A survey of the open literature was made focusing on data illustrating experimental Jet A ignition delay times as functions of temperature and pressure. One such figure is shown below (Figure I.3.1) for premixed, prevaporized stoichiometric blends of Jet A and air. The data shown are based on shock tube studies; for the pressures shown, at temperatures above 1000 K, the fuel chemistry occurs in the "high temperature" region. The so-called NTC ("negative temperature coefficient") region exists between approximately 1000 K and 750 K, with "low temperature" region below 750 K.

The experimental data in Figure I.3.1 are plotted against corresponding detailed chemical kinetic reaction models utilizing surrogate blends of two or three hydrocarbon species to simulate Jet A (model results based on the Dryer group at Princeton University). As indicated, the models do a reasonable job predicting both the absolute value of the ignition delay time and the locations of the three (high, NTC, low) chemistry regions as functions of temperature and pressure. As noted, the locations of the experimental NTC regions are somewhat broadened by the simulations.

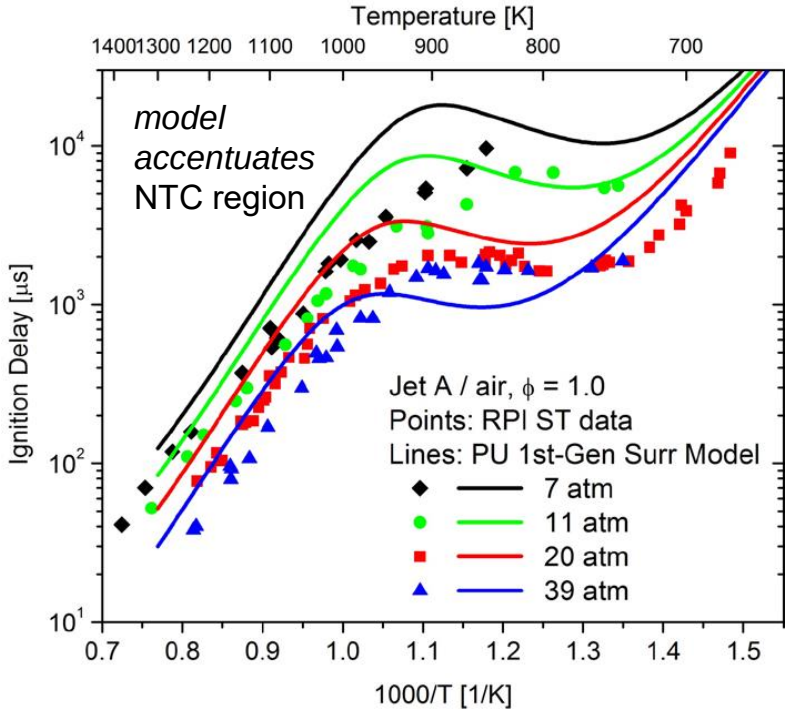

Figure I.3.1. *Experimental and Numerical Ignition Delay Times for Stoichiometric Jet A/Air Mixtures for the Conditions Shown (symbols: experiments, lines: model). Data from RPI Professor Matthew Oehlschlaeger, as provided in his 2012 MACCCR meeting pdf available at: http://kinetics.nist.gov/RealFuels/macccr/macccr2012/MACCCR_2012_Oehlschlaeger.pdf.*

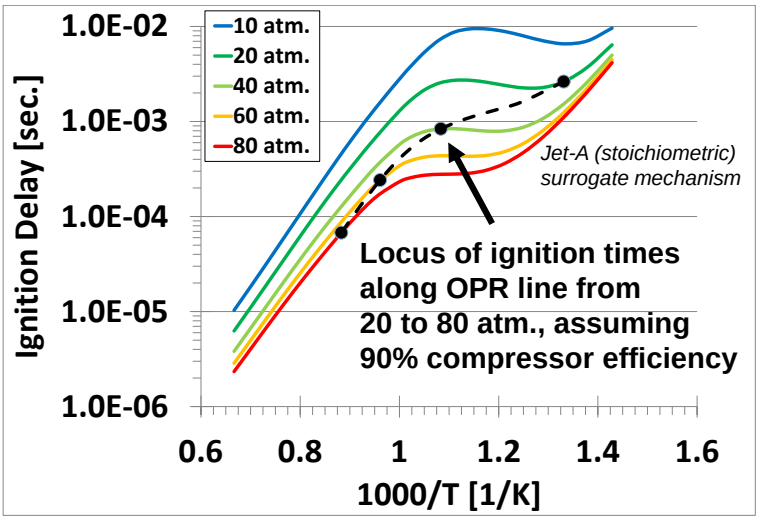

Figure I.3.2. *Numerical Ignition Delay Times for Stoichiometric Jet A/Air Mixtures for the Conditions Shown.*

A comparable set of numerical ignition delay times as a function of temperature and pressure is shown in Figure I.3.2. The numerical predictions in both Figures I.3.1 and I.3.2 are comparable at the same pressure-temperature conditions, providing an estimate of ignition delay times over a wide range of conditions. Due to the nature of turbine operation, however, combustor inlet pressures and temperatures cannot be controlled independently and are linked. Of greater interest in combustor design would be the range of ignition delay times based on combustor inlet conditions. Therefore Figure I.3.2 also shows the locus of ignition delay times generated along an OPR line from 20 to 80 atm. (assuming a compressor efficiency of 90%). As shown, at OPR's above 40, characteristic ignition times are one millisecond or less, and at these conditions the fuel is essentially reacting in the high temperature region of the curves.

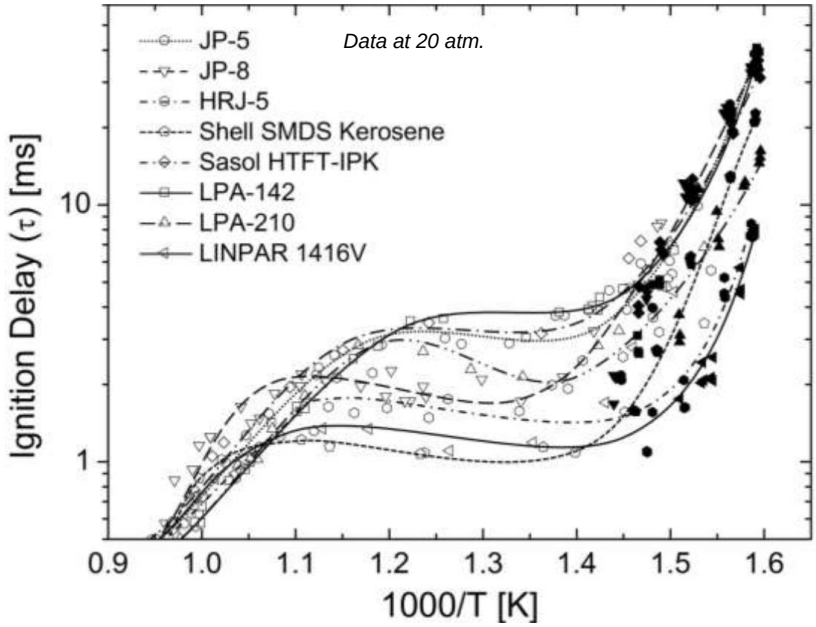

Figure I.3.3. *Experimental Ignition Delay Times for Stoichiometric Mixtures of Various Fuels for the Conditions Shown (symbols: experiments, lines: model)*

While understanding and quantifying the absolute values of ignition delay times for Jet A is important, it is also important to understand its relative ignition delay time characteristics compared to alternative fuels. The data shown in Figure I.3.3 illustrate this sensitivity of ignition delay time to fuel composition. Figure I.3.3 is from "Autoignition Behavior of Synthetic Alternative Jet Fuels: An Examination of Chemical Composition Effects on Ignition Delays at Low to Intermediate Temperatures," Valco, Gentz, Allen, Colket, Edwards, Gowdagiri, Oehlschlaeger, Toulson and Lee and was presented at the recent 35th International Symposium on Combustion. At the pressure for which this data was acquired (20 atm), it can be seen that fuel composition had greatest impact on ignition delay in the NTC and low temperature regions. Above 1000 K (~ comparable to OPR-45 inlet air temperatures), it can be seen there is far less impact of fuel type on ignition delay. Note that JP-5 and JP-8 are logistics fuels, HRJ-5 is a hydro-treated alternative fuel formulation for JP-5, Shell SMDS –*Shell Middle Distillate Synthesis*- is a Fischer-Tropsch alternative fuel, Sasol HTFT –*High Temperature Fischer Tropsch*- is a predominantly iso-paraffinic fuel, and LPA-142, -210, and LINPAR 1416V are industrial hydrocarbon solvent blends.

Autoignition Assessment for Aircraft Fuel Injectors/Mixers (liquid sprays)

A first order analysis for chemical kinetic times and droplet characteristic times as a function of OPR (engine overall pressure ratio) was performed and is described below. The intent was to assess the characteristic ignition times associated with premixed Jet-A/Air mixtures at elevated conditions. The rationale for this analysis is the following: As engine cycle OPRs continue to increase, the combustor inlet air temperature must necessarily increase as well. Since fuel-air ignition delay times strongly decrease as temperature increases, calculations were performed to determine if any of the proposed operating conditions might generate autoignition within the main injector mixing region of the combustor.

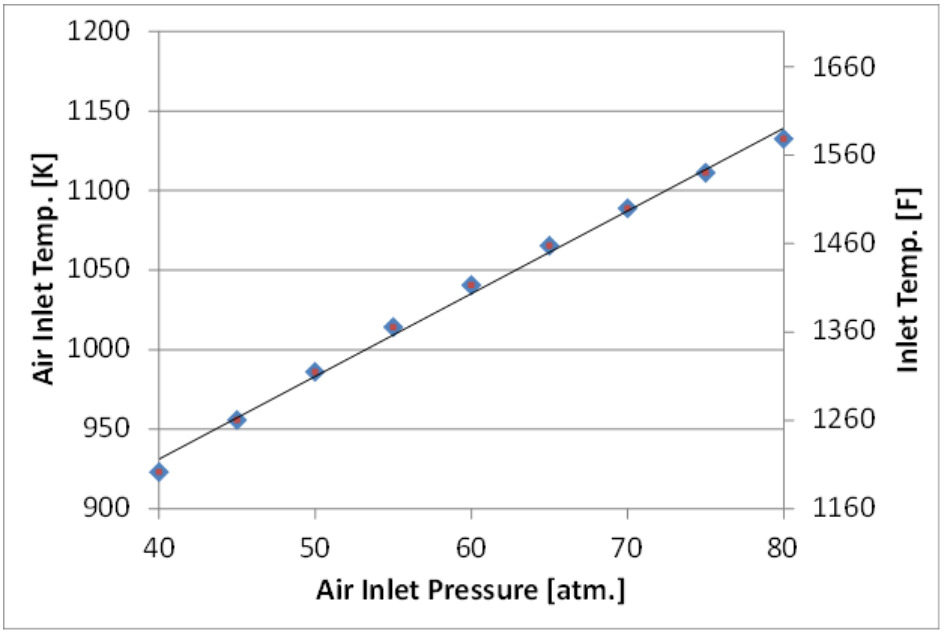

Figure I.3.4. *Combustor air inlet temperature versus pressure (90% compressor efficiency assumed).*

The region of interest was estimated by assuming that the OPR range of interest spanned 40 to 80. Based on STP inlet conditions and assuming overall compressor efficiencies of 90%, a map of inlet air temperatures and pressures was generated and is shown above in Figure I.3.4. Characteristic kinetic

ignition delay times associated with lean, stoichiometric, and rich fuel-air mixtures (Φ: 0.5, 1.0, 1.5) were determined for the inlet conditions shown in Figure I.3.4. The initial state of the fuel was a 98% liquid, 2% vapor blend at 311 K. The liquid fuel was assumed to follow a Rosin-Rammler size distribution with an exponent of 2.0 and a Sauter mean diameter (SMD) of 20 microns. It was further assumed that any vaporized fuel instantaneously fully mixed into the bulk gas phase so that only one vapor phase fuel-air ratio existed. (The code used in this analysis is based on the Chemkin-II Senkin application and was previously modified by UTRC to treat liquid fuel systems.)

The kinetics associated with the above analysis was the complete Lawrence Livermore National Labs n-heptane-air kinetic mechanism. This mechanism had previously been found suitable for estimating Jet-A/air characteristic chemical times. Another example of its utility for calculating Jet-A/air chemical times is shown in Figure I.3.5. Recent shock-tube ignition delay data for Jet-A-oxygen (4%)/nitrogen (96%) mixtures (Hanson group, Figure I.3.5) at pressures of approximately 13 and 54 atm and various initial temperatures are compared against simulations made using the above heptane mechanism at identical initial conditions (the calculations were performed assuming a constant-volume boundary condition). As indicated, the simulated ignition times are within a factor of 2 of the experimental times at the lower pressure and yield excellent agreement to the experimental data at the higher pressure.

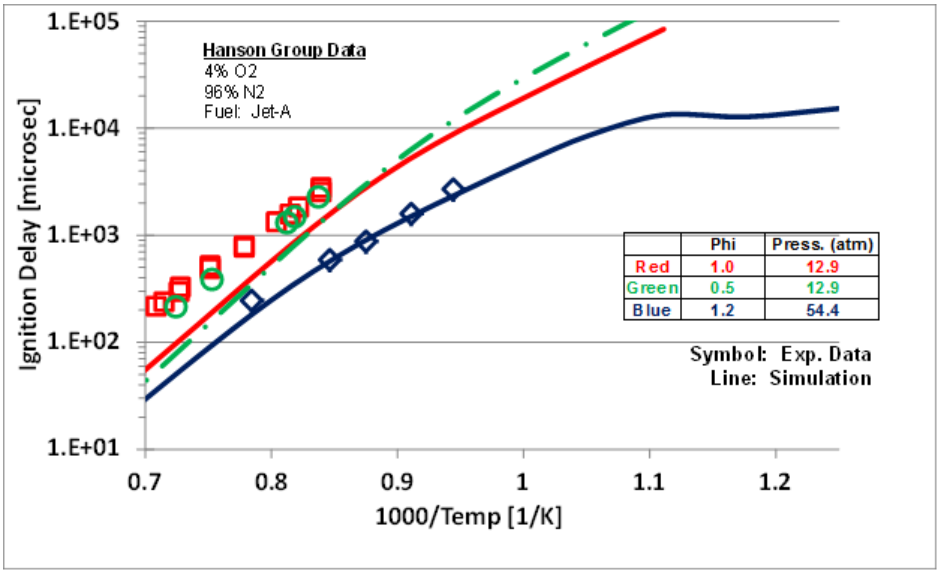

Figure I.3.5. *Comparison of experimental (shock tube) and numerical (constant volume) ignition delay times for conditions shown.*

Two bounding methods were then used to calculate the characteristic ignition times. The first method followed analysis procedures described in Lefebvre's "Gas Turbine Combustion" book (Lefebvre, 1998) and assumed that the overall characteristic time was the sum of the sequential, independent vaporization times and the kinetic times (i.e., all liquid fuel fully vaporized prior to any fuel-air kinetic interactions). The second method relaxed this assumption and assumed that fuel-air chemistry simultaneously occurred with the vaporization process. Examples of the definitions of vaporization and ignition times utilized in the first sequential analysis method are given in Figures I.3.6 and I.3.7, respectively. Essentially, the code distributes the liquid fuel mass into ten bins. Each bin contains liquid droplets of a constant diameter. Following the "d^2" law, the mass in each bin is reduced based on the local environmental conditions. The total fuel mass in all the bins is tracked and the time at which 99% of the liquid fuel has vaporized is considered to be the vaporization time (these calculations are made in

the absence of chemical reaction). The ignition delay determination employs the kinetic mechanism described above, but assumes the fuel-air mixture is fully premixed and prevaporized. As time evolves and the fuel and oxygen react, the system temperature increases. The time at which the system maximum temperature temporal derivative occurs is defined to be the ignition delay time.

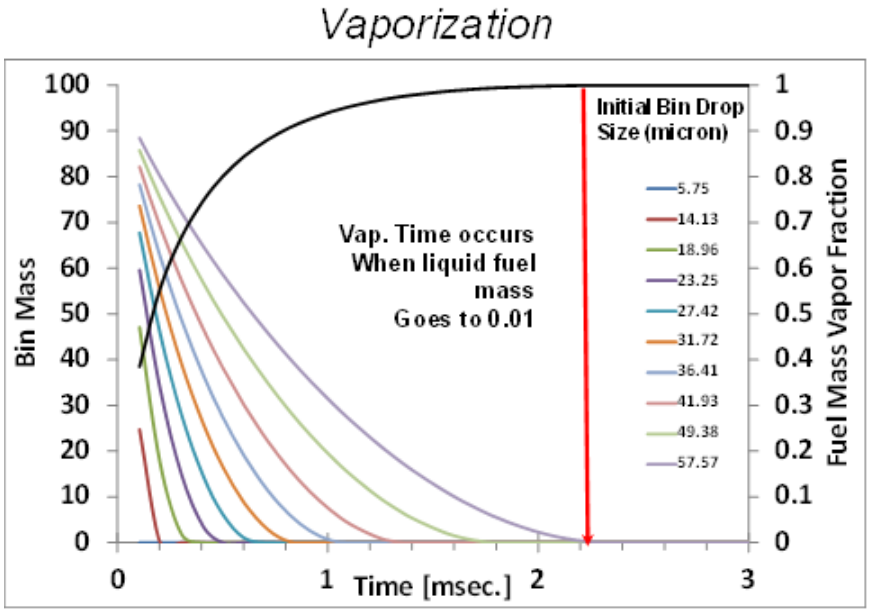

Figure I.3.6. *Graphical illustration of the vaporization characteristic time.*

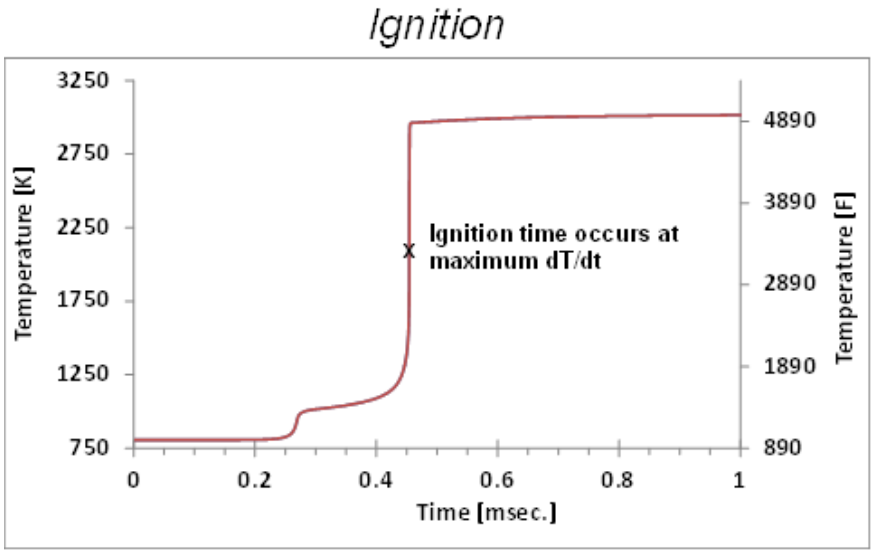

Figure I.3.7. *Graphical illustration of the ignition characteristic time.*

Again, the above methods were based on sequential physical and chemical processes. The liquid fuel first vaporizes and then the gaseous fuel reacts. The second analysis method allowed both processes to occur simultaneously. An example of such an analysis is shown in Figure I.3.8. Initially, essentially all the fuel mass is in the liquid state. Thus, although the bulk equivalence ratio is rich, the vapor phase equivalence is zero. As time evolves and droplets evaporate according to the "d^2" law, the relative fraction of liquid fuel decreases, the relative fraction of vapor fuel increases, and the vapor equivalence

ratio also increases. At early times, the system temperature decreases as the fuel vaporizes and the vapor phase equivalence ratio is fairly inactive and/or too lean to liberate much energy. By approximately 0.8 msec, all the fuel has vaporized and by 1 msec, the system fully ignites.

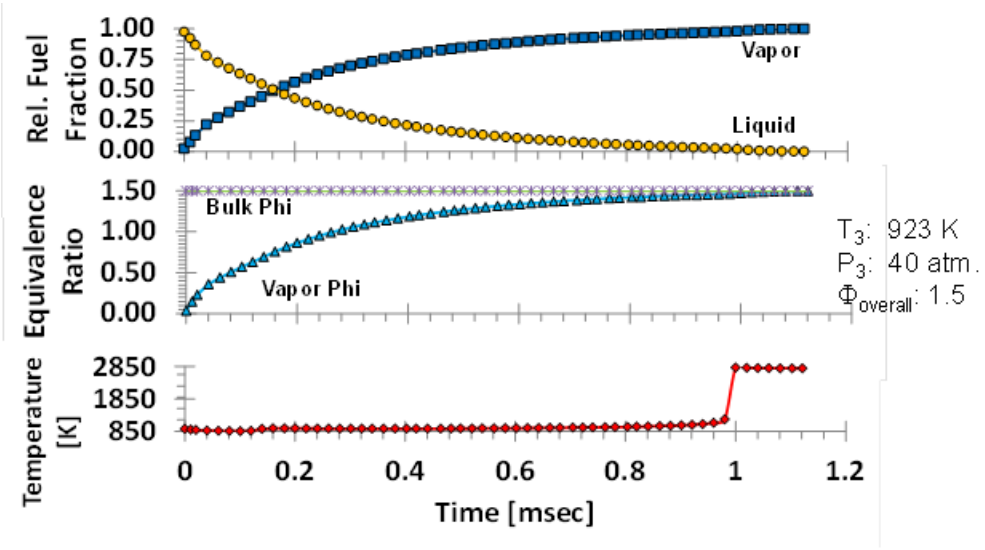

Figure I.3.8. *Graphical illustration of the concurrent vaporization-ignition characteristic time for the conditions shown.*

Comparisons of these sequential and simultaneous ignition times over the inlet conditions shown in Figure I.3.4 are illustrated in Figure I.3.9. Also shown are the characteristic vaporization times at all conditions. The difference between the sequential time and the vaporization time at any condition represents the premixed, prevaporized ignition delay time at that condition. As can be seen, it is much less than the corresponding vaporization time. However, as Figure I.3.9 also illustrates, for all three fuel-air mixtures, the simultaneous ignition time is less than the sequential time and this discrepancy increases at the higher OPR conditions. Also, even though for premixed, prevaporized systems, stoichiometric systems have shorter ignition delay times than rich systems, the above results indicate that the rich liquid fueled system has slightly faster ignition times than the stoichiometric system. These findings highlight the importance of treating both vaporization and kinetics as concurrent processes.

Based on the above ignition times, maximum characteristic length scales can be obtained (i.e., maximum traversed distances without autoignition) for the various inlet conditions. Based on an average injector velocity of 50 m/sec and without including any safety factors, these length are given in Figure I.3.10. The code described above is currently linked exclusively to the LLNL heptane mechanism, and is expected to give reasonable results for Jet-A. For specific alternative fuels, mechanisms associated with these fuels can be identified and linked to the above code, for prediction of autoignition times and combustor performance with alternative fuels.

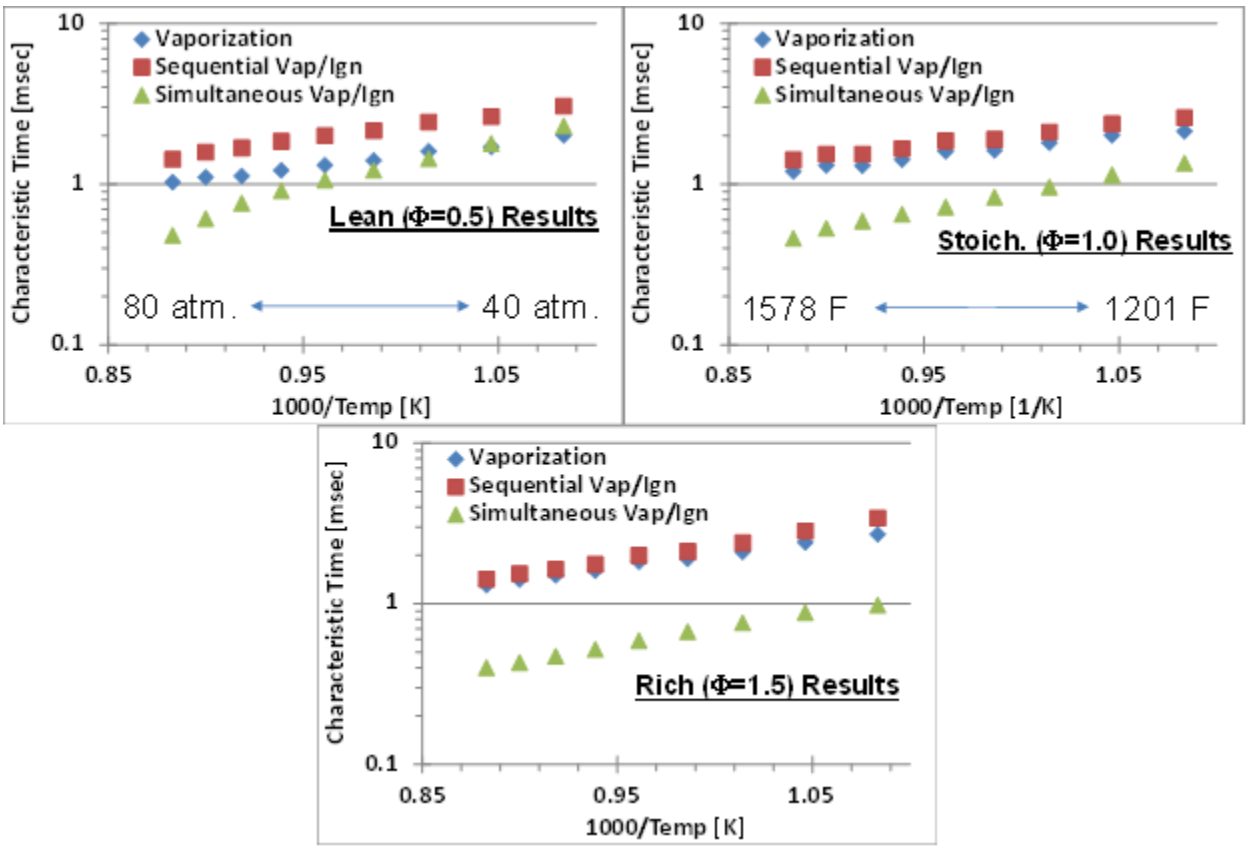

Figure I.3.9. *Characteristic times associated with sequential and simultaneous vaporization and reaction for lean, rich, and stoichiometric Jet-A/Air mixtures at conditions shown.*

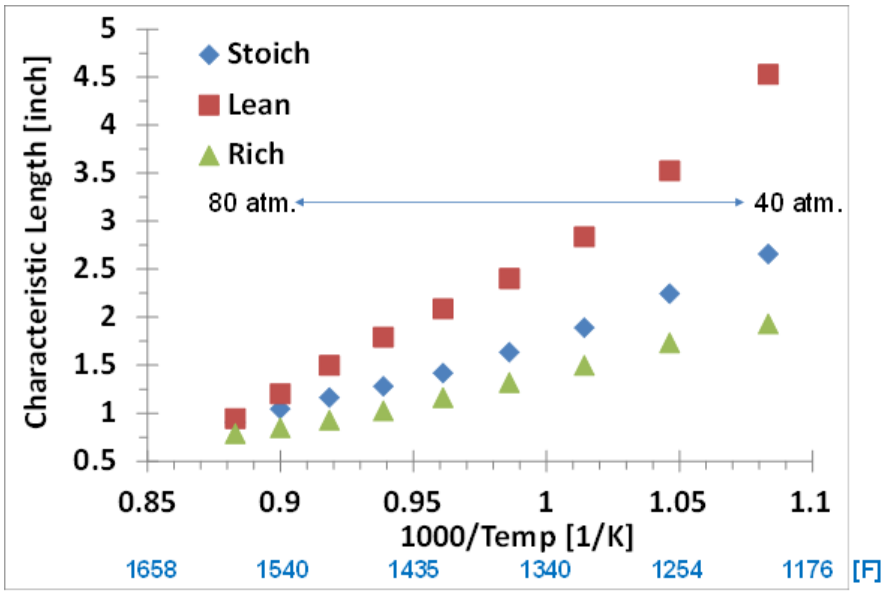

Figure I.3.10. *Characteristic lengths associated with simultaneous vaporization and reaction for lean, rich, and stoichiometric Jet-A/Air mixtures at conditions shown (50 m/sec flow assumed, no safety factor).*

Alternative Fuel Analysis, Requirements, and Selection for N+3 Combustor Tests

For assessing alternative fuels, a finite set of alternative fuels were selected for analysis and initial testing under the N+3 combustor program. Selection was based on identifying and targeting key requirements and metrics associated with operating on alternative fuels in the N+3 combustor program.

Fuel prop\impact	Fuel	Emissions	Hardware	Operability	Example of Fuel(s)
Fast vaporization	Low MW, low viscosity	-	-	-	**Shell GTL**
Slow vaporization	High MW, high Viscosity	Higher NOx	-	Loss of LBO margin	**HRJ-8** or **C-3 (POSF 12341)**
Fast Chemistry	High CN number	Higher NOx	Flashback in premixer	-	**Rentek (POSF 7898)** or nC12
Slow Chemistry Baseline	Low CN number	-	--	Loss of LBO margin	**Gevo ATJ** **Cat. A-2**

NASA, NJFCP, AFRL

Table I.3.1. *Listing of fuel properties & impacts on combustor metrics, and some example fuels.*

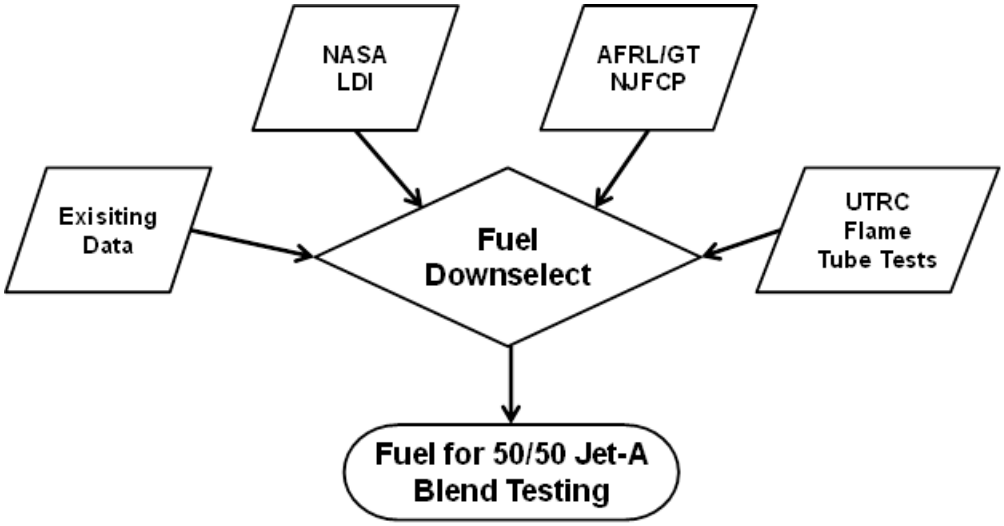

Figure I.3.11. *Data-driven decision flowchart for selecting alternative fuel for use in blended-fuel tests.*

Fuel physical and chemical properties were identified that could potentially modify combustor emissions, hardware, and operability. For instance, fuels with very fast chemistry could potentially lead to flashback risk to the premixer. These identified properties were then associated with example

alternative fuels. This analysis is summarized in Table I.3.1. (The entries are colored coded based on availability from NASA, AFRL, or the FAA-sponsored "National Jet Fuel Combustion Program".)

Figure I.3.11 depicts the assessment methodology used to make the final alternative fuel down-selection for testing with a 50/50 alternative/Jet-A fuel blend in the UTRC N+3 combustor rig tests, and consists of utilizing existing data sets and data from the UTRC flame tube ignition tests (described in more detail under Task 4, i.e. Section I.4 of this report).

Alternative Fuel Selection, for Autoignition Testing and N+3 Combustor Testing

For UTRC autoignition testing of an N+3 combustor's main mixer/injector, UTRC downselected specific alternative fuels to be evaluated: four alternative fuels were selected for initial autoignition testing (Table I.3.2, discussed below) in addition to a Jet-A standard. Recall there are two objectives (two end uses) for the selected fuels: autoignition testing and combustor performance testing. The autoignition testing activity refers to the sub-component auto-ignition testing conducted in UTRC's high-pressure high-temperature rig, while the combustor performance testing activity refers to the sector rig testing conducted using a 50-50 blend of Jet-A and an alternative fuel.

Basis for Selection of Alternative Fuels

For the autoignition tests, the intent is to characterize the fuels' autoignition behavior at the high-OPR conditions expected in future engine cycles such as N+3, where information is limited or non-existent for many fuels today. For this purpose, it is desirable to select a set of fuels with dissimilar characteristics, covering a wide range of fuel property values, to best evaluate the expected range of behaviors. In addition, it is also desirable to select a set of fuels that are traceable in terms of composition and origin, and for which known property data are available. Finally, it is also necessary to select fuels for testing that are available for procurement.

As mentioned previously, the FAA and AFRL are investigating the impact of alternative fuels on gas-turbine performance under the ASCENT program, and have selected a set of fuels (along with physical batches of fuels) that are being evaluated. The synergies between the ASCENT program and the N+3 activities enabled UTRC to find several fuels that meet UTRC's requirements and that are available in sufficient quantities for rig testing (Table I.3.2, described further below). One important fuel property that is indicative of a fuel's autoignition tendencies is Cetane number, so fuels were selected that span a wide range in Cetane number and will thus give an indication of the expected range in autoignition times when using alternative fuels.

The five fuels selected by UTRC for evaluation are listed in Table I.3.2 – four of these are alternative fuels, and one is a specific batch of Jet-A fuel that has been well characterized under the ASCENT program. The first four fuels listed in Table I.3.2 (Jet-A and the first three alternative fuels) come from the ASCENT program, and will be provided to UTRC by AFRL. Each of these ASCENT fuels is batch-specific, traceable via its POSF number, and is under evaluation as a combustion fuel by various participants in the ASCENT program (see Table I.3.4). The UTRC tests provide additional data regarding autoignition characteristics under high-OPR combustion conditions. The last fuel listed (Rentech) is also batch-specific and traceable via its POSF number, but is provided to UTRC by NASA, and is outside the ASCENT program. This fuel is of interest because it was used for NASA testing of Pratt & Whitney's ERA Phase-2 ASC combustor, and because it has an especially high Cetane number. NASA is providing the Rentech fuel to UTRC in two forms: one barrel of "pure" Rentech, and one barrel of Rentech mixed with Jet-A fuel (in 50/50 proportions).

	Fuel	POSF	ASCENT Designation	Selection Rationale	Performance Impact
1	Jet-A	10325	A-2	Baseline Properties	Baseline Performance
2	Gevo	11498	C-1	Low Cetane #	Longer ignition delay
3	JP-5 (64v%)/Farnesane(36v%)	12341	C-3	High Viscosity/High Surface Tension	Droplet SMD Increase, slower fuel air mixing
4	iso-C10s (73v%)/trimethylbenzene(27v%)	12345	C-5	Flat distillation curve; Low Boiling Pt.	Faster vaporization, fuel-air mixing
5	Rentech	7898	-	High Cetane #	Shorter ignition delay, mixer length impact?

Table I.3.2. *Fuels selected for UTRC sub-component autoignition testing at high pressure.*

The basis for the selection of the fuels in Table I.3.2 is shown in the "Selection Rationale" column, and the expected impact of the individual fuel in both the autoignition and sector rig tests is given in the "Performance Impact" column. Jet-A was chosen as a test fuel to provide a reference point around "conventional" fuel performance, for comparison to the alternative fuels performance. In fact, the POSF of the chosen Jet-A fuel is such that AFRL considers it to be the "nominal" performance fuel.

Significant chemical and physical properties of the chosen fuels are given in Table I.3.3 below. As mentioned earlier, fuel Cetane number is an important property for assessing a fuel's autoignition tendency. The baseline Cetane number for "nominal" Jet-A is 48.8. The Gevo alternative fuel ("C-1") has a much lower Cetane number, 17.1. In contrast, the Rentech alternative fuel has a Cetane number of 70. Based on these Cetane numbers, at identical conditions the Gevo fuel is expected to have a longer ignition delay time than the base Jet-A, and the Rentech is expected to have a shorter ignition delay time than the Jet-A. For comparison, measured autoignition times are shown in Figure I.3.12 below for several of the ASCENT fuels, based on preliminary shock tube ignition studies conducted at Stanford University at the specified conditions (12 atmospheres pressure and equivalence ratio of 1). The UTRC tests provide autoignition data at higher pressures.

	Surface Tension	Viscosity	Density	Flash Point	Smoke Point	Hydrogen Content	MW	Cetane Number
	[dyne/cm, 20 C]	[cSt, -20 c]	[kg/L, 15 C]	[C]	[mm]	[% mass]	[g/mol]	[-]
Mil Spec JP-8 Max Limit		8.00	0.8400					
Jet-A	24.9	4.70	0.8032	48.0	24.0	13.80	159	48.8
C-1	23.4	5.00	0.7597	49.5	34.5	15.43	178	17.1
C-3	26.1	8.00	0.8077	65.5	25.2	14.18	180	47.0
C-5	23.8	1.96	0.7689	43.5	21.4	13.96	135	39.6
Rentech	23.5 (est.)	6.20	0.7630	48.0	50.0	15.30	185 (est.)	70.0
Mil Spec JP-8 Min Limit			0.7750	38.0	25.0	13.40		

Table I.3.3. *Specific properties of the fuels selected for UTRC sub-component testing at high pressure.*

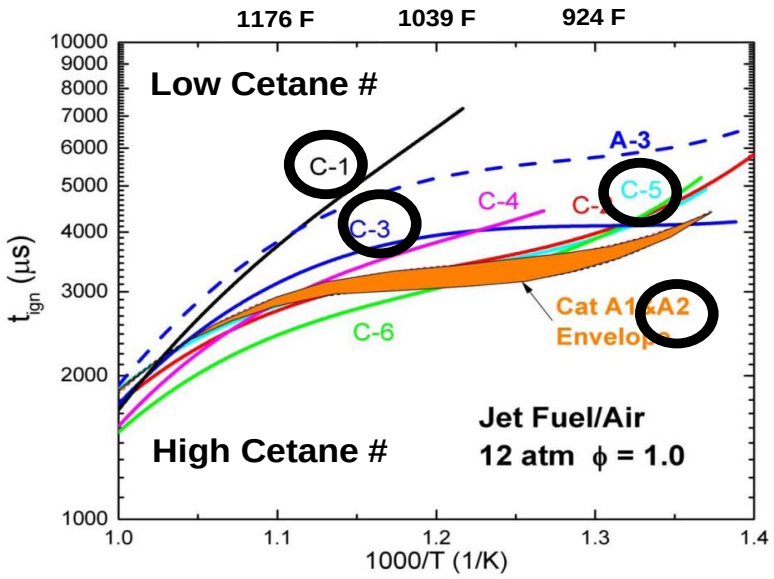

Figure I.3.12. *Trend-lines for autoignition time of ASCENT alternative fuels, based on preliminary shock-tube data at 12 atm pressure and 1.0 equivalence ratio (ϕ). The trend with Cetane number is annotated. Data courtesy of the Hanson group at Stanford University.*

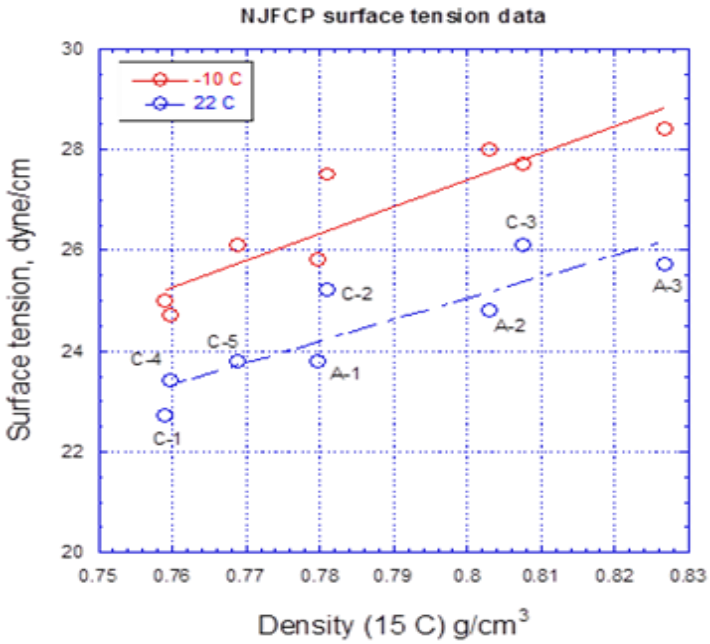

Figure I.3.13. *Fuel surface tension at indicated temperatures for ASCENT alternative fuels. Data courtesy of Tim Edwards at AFRL.*

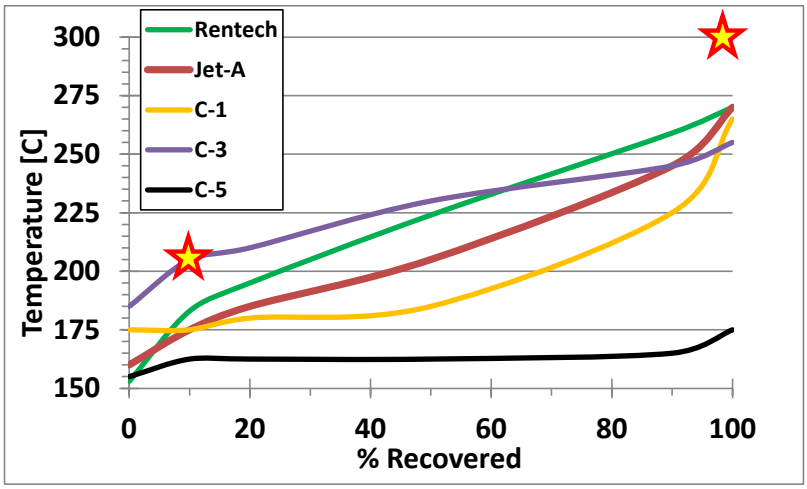

Figure I.3.14. *Distillation curves associated with the downselected alternative fuels (Mil Spec Limits denoted by stars, and are as follows: maximum temperature for 10% vaporized – 205 C, maximum final boiling point – 300 C).*

While the chosen fuels do indeed span a full range of Cetane numbers, their other physical and chemical properties also span a useful range of fuel properties. For example, as shown in Figure I.3.13, the chosen fuels span a wide range of surface tension values ("C-3" is the JP-5/Farnesane blend; "A-3" is neat JP-5). Also, the chosen fuels span a range of low temperature viscosity values; in fact, the "C-3" fuel is at the Mil Spec JP-8 limits, as indicated in Table I.3.3. Lastly, each selected fuel has a unique distillation curve, as shown in Figure I.3.14. In fact, the "C-5" fuel has essentially a flat distillation curve: its initial and final boiling point values are within 14 C of each other. Thus, in addition to the impact of Cetane number on the autoignition characteristics of the fuels, the chosen fuels also enable UTRC to acquire knowledge on the impact of these other physical and chemical property variations from the subcomponent testing results.

Fuel	Referee Rig Operation & Combustor Instabilities	Flow Reactor & Shock Tube	Spray Characterization	High Altitude Relight & LBO	Spray Burner LBO	7 Point LDI Emissions & Diagnostics	9 Point LDI Emissions	High OPR Autoignition Assessment
						(30 and 75 psi)	(100, 150, 250 psi)	
A-2	UDRI	Stanford	Purdue/NRC Canada	NRC Canada	DLR Germany	NASA	NASA	UTRC
C-1	UDRI	Stanford	Purdue/NRC Canada	NRC Canada	DLR Germany			UTRC
C-3	UDRI	Stanford	Purdue/NRC Canada	NRC Canada		NASA (2 C Fuels Total)	NASA (2 C Fuels Total)	UTRC
C-5	UDRI	Stanford	Purdue/NRC Canada	NRC Canada				UTRC
Rentech								UTRC

Table I.3.4. *Summary of performance and kinetic data to be acquired under the ASCENT and N+3 programs, for the selected alternative fuels.*

Additionally, because of the synergy between these chosen fuels and the ASCENT program, data/results acquired from that program can be used together with the UTRC-acquired data for the N+3 downselection decision process regarding which alternative fuel to use in the 50-50 fuel blend tests at

UTRC and at NASA. Table I.3.4 summarizes the performance and kinetic data acquired for the selected fuels under both the ASCENT and N+3 programs. The UTRC autoignition tests are highlighted in blue, and provide unique data not provided by the ASCENT participants. In particular, the UTRC tests provide autoignition data at actual high-OPR combustor conditions, including pressure, temperature, and fuel-air mixture strengths, obtained in actual combustor hardware at the appropriate flow (velocity) conditions.

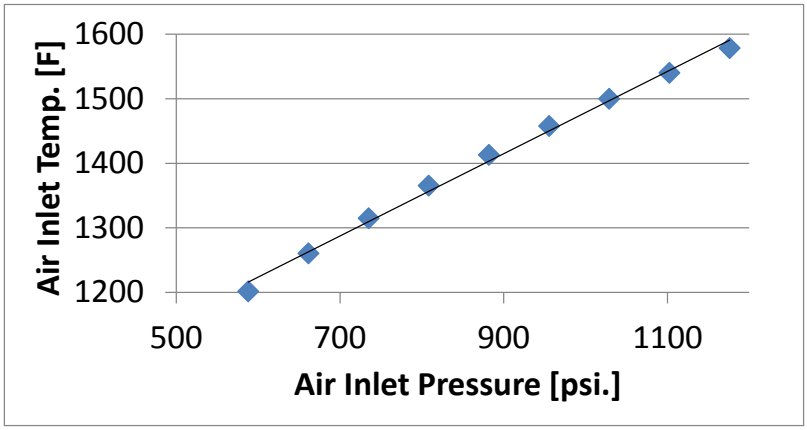

Figure I.3.15. *Representative operating line, showing combustor inlet pressure vs. temperature, as used for alternative-fuel/air ignition delay calculations.*

In an effort to investigate the impact of the alternative-fuel composition on ignition times at high OPR conditions, the previously used operating line (reproduced above in Figure I.3.15) was used to conduct preliminary homogenous ignition delay times using the current UTRC surrogate fuel model, consisting of the components listed in the top row of Table I.3.5. Earlier kinetic calculations for a Jet-A-like fuel were made utilizing the LLNL detailed n-heptane mechanism exclusively, which has been previously validated against shock tube data at elevated pressures in the temperature range of interest for N+3 conditions. (This validated mechanism was used to set the maximum main injector residence times for the N+3 combustor design program). The current UTRC surrogate model does not include low temperature chemistry reactions and was instead used to qualitatively assess the relative impact of alternative fuel composition on the high OPR autoignition times. In making these calculations, the best choice between available surrogate fuel kinetics species and actual fuel components was made. For example, the UTRC kinetic model does not include the chemistry for trimethylbenzene, a real fuel in the "C-5" alternative fuel. Accordingly, m-xylene was used as a surrogate for the corresponding calculations.

	n-C12	n-C16	i-C12	m-Xylene	ButylCyclohex
Jet-a	0.04	0.55	0.20	0.21	0.00
JP-5/Farnesane	0.00	0.52	0.27	0.16	0.05
Gevo	0.00	0.00	1.00	0.00	0.00
i-C10/TMB	0.00	0.00	0.75	0.25	0.00
Rentech	0.89	0.00	0.75	0.01	0.10

Table I.3.5. *Surrogate-fuel blends used to calculate alternative-fuel autoignition delay times.*

Table I.3.5 lists the specific surrogate fuels used to represent each of the five fuels, for calculating relative autoignition delay times. The results of these autoignition calculations, shown in Figure I.3.16, are qualitatively in agreement with what one would expect based on the fuel's Cetane number. Specifically, the fuel with the lowest Cetane number, Gevo, had the longest ignition delay time and the

fuel with the highest Cetane number, Rentech, had a slightly faster ignition delay time compared to the baseline Jet-A fuel. The range in times for these two fuels was 2.65 at the 588 psi/1201 F condition and 1.6 at the 1176 psi/1578 F condition.

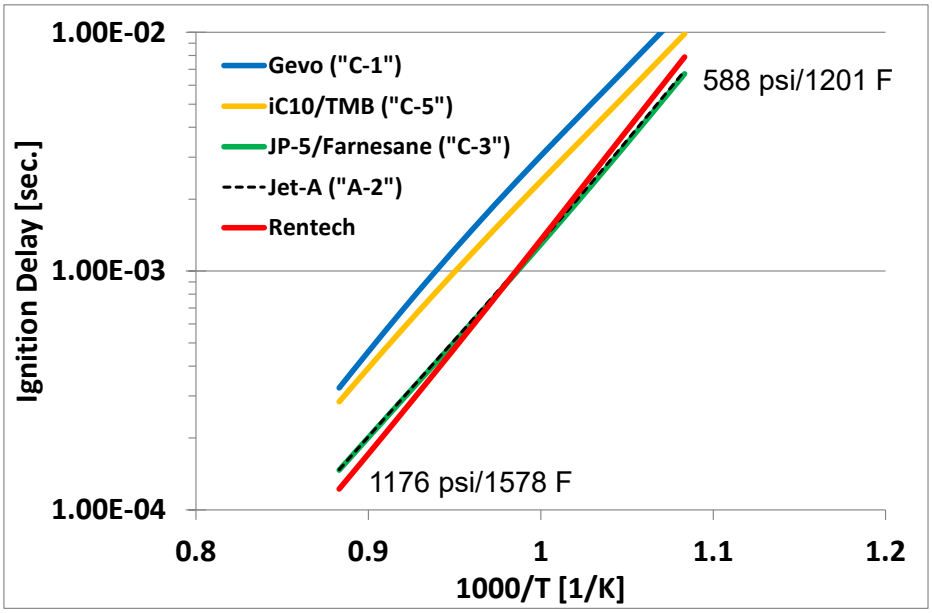

Figure I.3.16. *Ignition delay calculations for stoichiometric homogenous fuel-air mixtures, for operating line given in Figure I.3.4, and based on the surrogate-fuel blends listed in Table 1.3.4.*

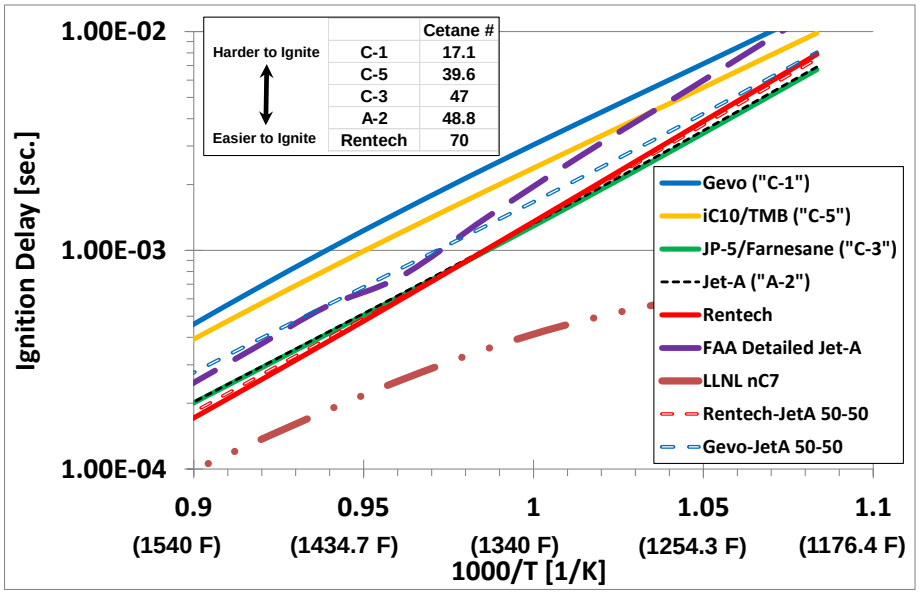

Figure I.3.17. *Computational Ignition Delay Profiles for Planned Fuels (Stoichiometric Prevaporized Mixtures on notional operating line between 40 to 80 atm and corresponding combustor inlet temperatures).*

The calculations shown in Figure I.3.16 were extended to include blends of these alternative fuels with Jet-A. As for Figure I.3.16, ignition delay times were calculated along the notional operating line between combustor inlet pressures of 40 to 80 atm and associated inlet temperatures assuming 90%

compressor efficiency (Figure I.3.15). The results are shown in Figure I.3.17. As shown, all the fuels and blends have ignition delay times that are approximately within a factor of two of each other over this range of conditions. It can also be seen that 50/50 blends of some fuels (Rentech/Jet-A; Gevo/Jet-A) also fall within the range and that the blend ignition time is skewed closer to the ignition delay time of the component with the faster ignition delay time. Also shown in the figure is an estimate of Jet-A autoignition times based on the recently developed FAA National Jet Fuels Combustion Program detailed Jet-A kinetic model. Ignition times associated with this mechanism are consistent with those of the UTRC detailed model and provide a reasonable confidence level in these time estimates. Finally, the figure also shows ignition delay times associated with the Lawrence Livermore National Labs detailed n-heptane mechanism. This mechanism is often utilized to highlight the impact of so-called NTC chemistry on ignition times.

Task 4 – Sub-component testing at UTRC

Autoignition Testing at UTRC

The UTRC autoignition rig consists of an ACS combustor main-mixer, as depicted in Figure I.4.1, installed with its primary axis along the centerline of UTRC's High-Pressure High-Temperature (HPHT) combustion rig, as depicted in Figure I.4.2. The assembly prior to installation in the rig is shown in the photograph of Figure I.4.3, which depicts an early rig configuration that used a quartz tube to visualize ignition downstream of fuel injection. An image of autoignition in this rig is given in Figure I.4.4 as obtained using UTRC's high-speed camera. The uniqueness of this autoignition rig is that it uses fuel-injector hardware (swirler and fuel nozzle) representative of a gas turbine combustor, and specifically from an advanced lean-burn gas-turbine combustor design (the ACS combustor).

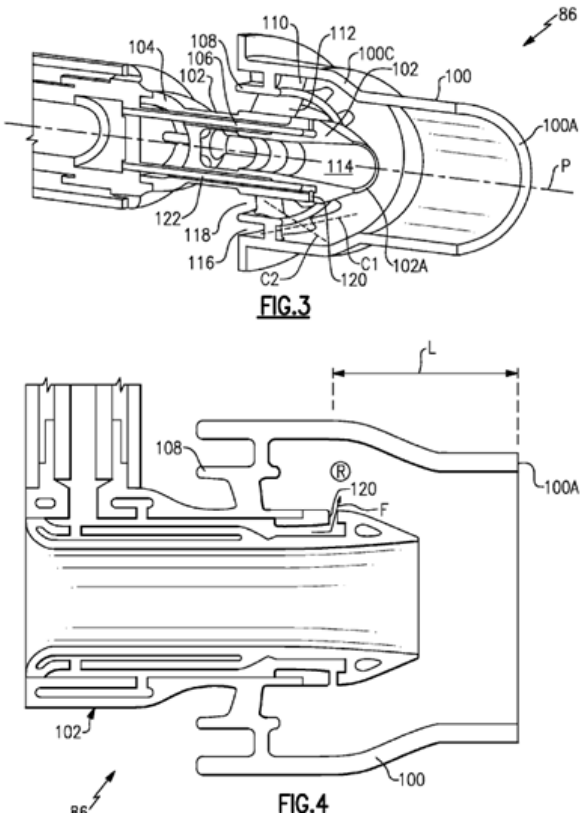

Figure I.4.1. *Main-mixer design for UTRC alternative-fuel autoignition testing, as shown in figure from US Patent Application Publication US 2013/0232978.*

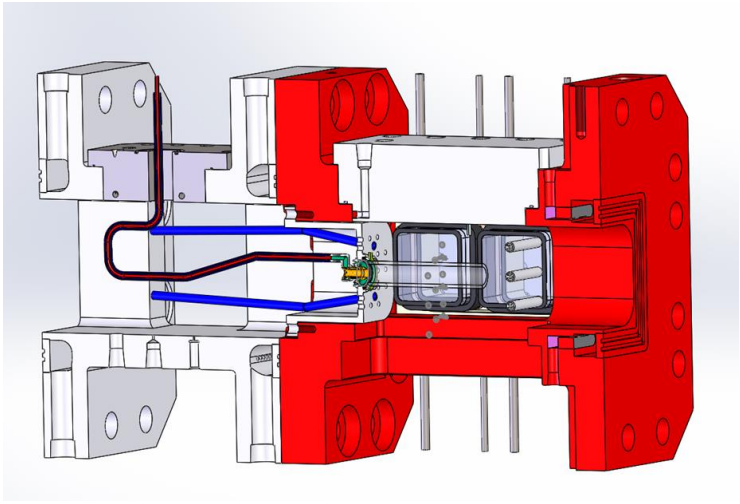

Figure I.4.2. *Illustration of rig components and layout for high-pressure autoignition tests of alternative fuels at UTRC, in cross-sectional depiction of UTRC high-pressure combustion rig. Flow is left-to-right.*

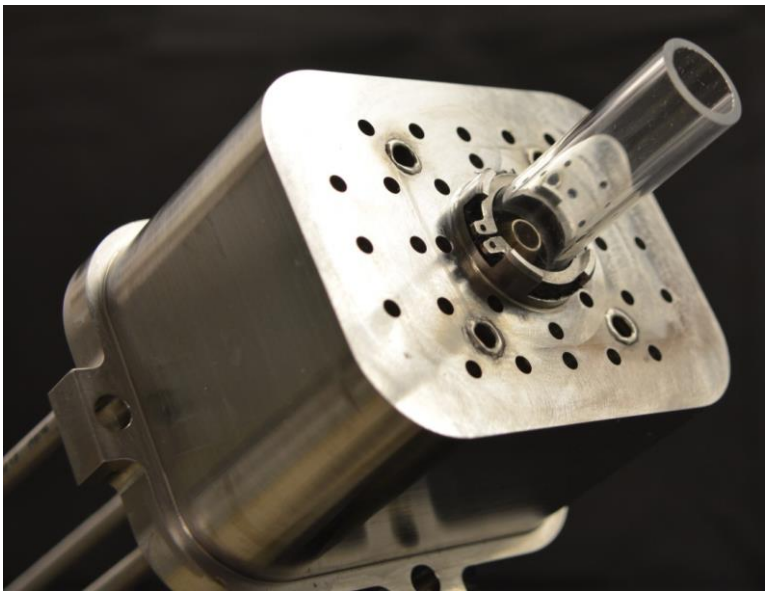

Figure I.4.3. *Photograph of fuel injector (swirler and fuel nozzle) installed in bulkhead, prior to installation in UTRC's High-Pressure High-Temperature (HPHT) rig. Note this photograph shows an early rig configuration in which a quartz tube was used to visualize autoignition.*

The original intended operation of this unique rig was to perform autoignition testing at swirler equivalence ratios up to 1.0. During testing, however, these high equivalence ratios resulted in combustion and flame propagation in the exhaust gases downstream of the test section immediately following autoignition. The large volume of compressible gas in the piping downstream of the test section (but upstream of the backpressure valve) caused unsteady flow when autoignition and flame propagation occured, with a resulting velocity reduction and occasional flow reversal in the test section. These transient events made it difficult to determine autoignition location and time. Therefore the test procedure was modified to keep equivalence ratios below the lean flammability limit, so that flame propagation could not lead to rapid transient events upon autoignition. As shown in Figure I.4.5 below,

calculations were performed to confirm that even at the high inlet temperatures tested the flammability limit remained around 0.3 equivalence ratio, indicating that quality autoignition tests could be conducted at equivalence ratios below about 0.3.

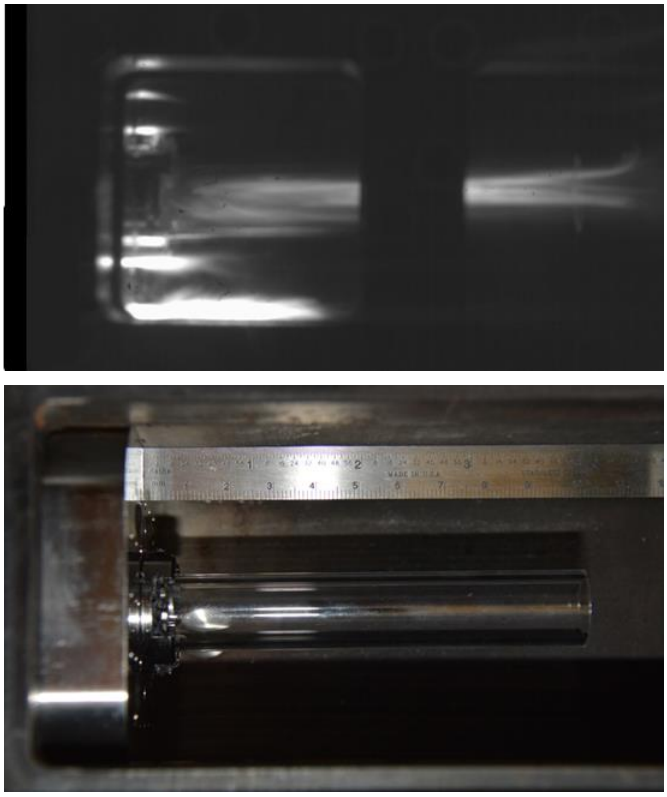

Figure I.4.4. *Image of autoignition event in UTRC's autoignition rig while operating at rig inlet conditions of 150 psia air pressure and 1000 F air temperature (top panel). The bottom panel shows the rig with the windows removed, with a ruler to show length scale. Flow is from left to right, and the fuel injector is mounted in the bulkhead at the left-hand side of the test section.*

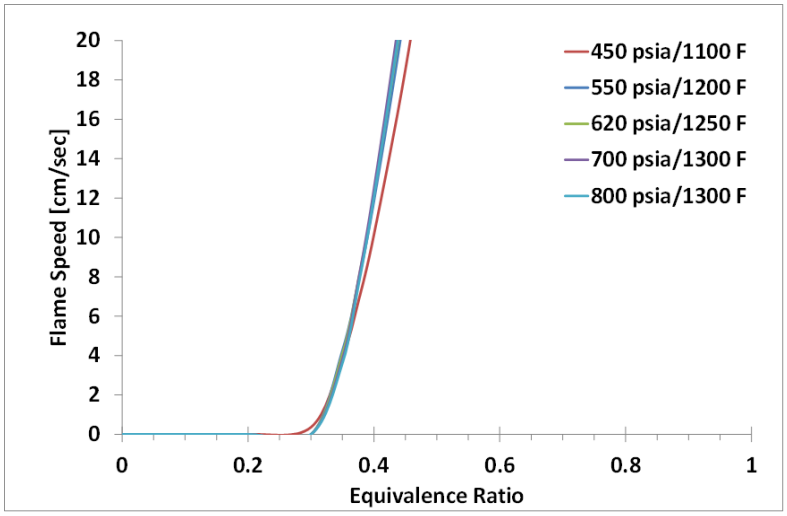

Figure I.4.5. *Predicted flame speeds and flammability limits for Jet-A/air mixtures at the planned autoignition test conditions, focusing on region near the lean flammability limit.*

As shown in the photographs in Figures I.4.3 and I.4.4, the original autoignition rig used a quartz tube downstream of the fuel injector, in which fuel/air mixing and eventually autoignition occurred, without dilution from bulkhead or rig cooling air. The quartz material allowed for visual access to the flow within the injector tube and for determining changes to the flow field and location and establishment of the ignition process within the tube. After successfully solving several flow sealing issues between the bulkhead, injector, and quartz and metal interfaces, it was determined (experimentally, by quartz tube failure) that the quartz walls were not able to withstand the highest pressure test conditions at 700 and 800 psia. Consequently, the injector tube material was changed to 316 stainless steel. This design allowed for one piece construction of the injector, inclusion of the captured carbon seal at the injector base, and external threads for attachment of the bulkhead locking nut. The new tube construction greatly simplified rig installation and hardware durability (see Figure I.4.6), but at the expense of visual access to the flow within the injector. To help overcome this visual limitation, two photo-multiplier tubes (PMTs) were used to measure light emissions from the ignition process as a function of time, and thus serve as an unambiguous reference as to the moment of autoignition.

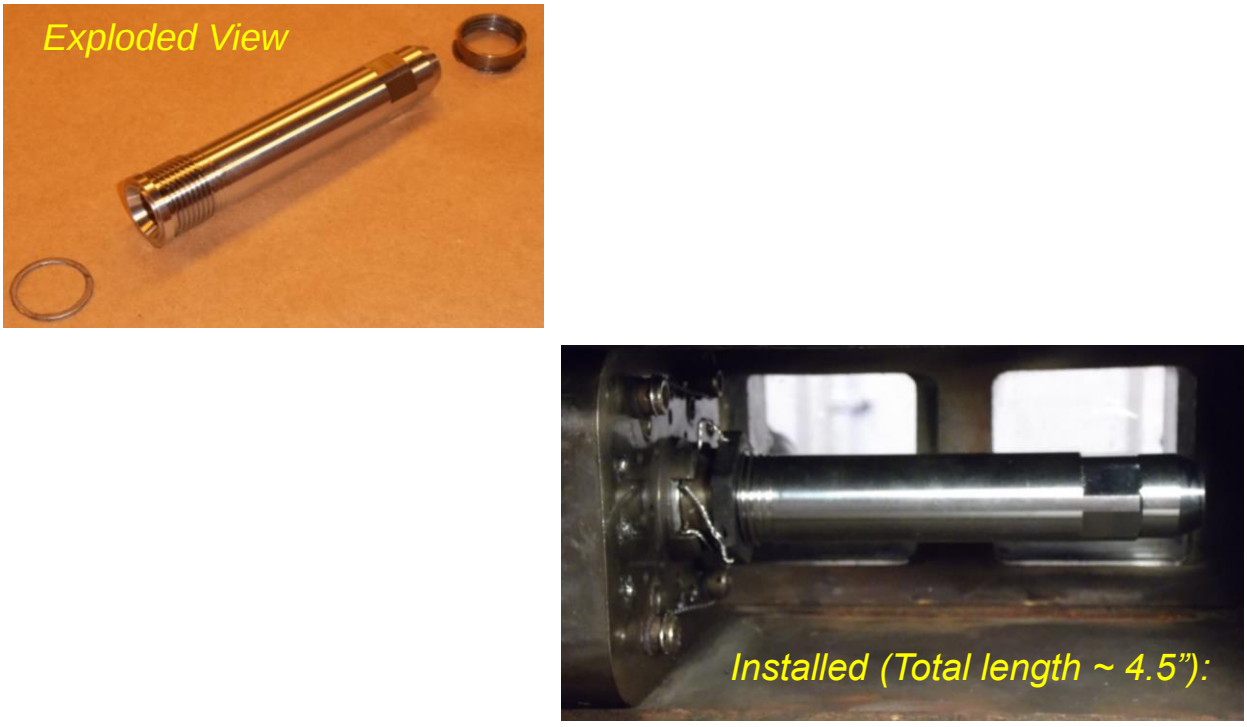

Figure I.4.6. *Final configuration of UTRC's autoignition rig, using a stainless steel mixing tube downstream of the fuel injector.*

Figure I.4.7 illustrates the use of the PMT tubes for determining autoignition. The black trace represents the fuel-air equivalence ratio within the injector tube and the green and red traces are the PMT signal outputs. Figure I.4.7a denotes PMT response during a non-ignition event. (The PMT spike when the fuel is turned off - "purge flash" - is due to nitrogen injector purge flow mixing with the fuel flow and presumably flash-vaporizing the fuel.) In contrast, the PMT signal of a successful ignition is illustrated in Figure I.4.7b. As shown here, the PMTs outputs are non-zero (due to an ignition event) as soon as the fuel flow is increased such that the overall injector equivalence ratio is 0.3.

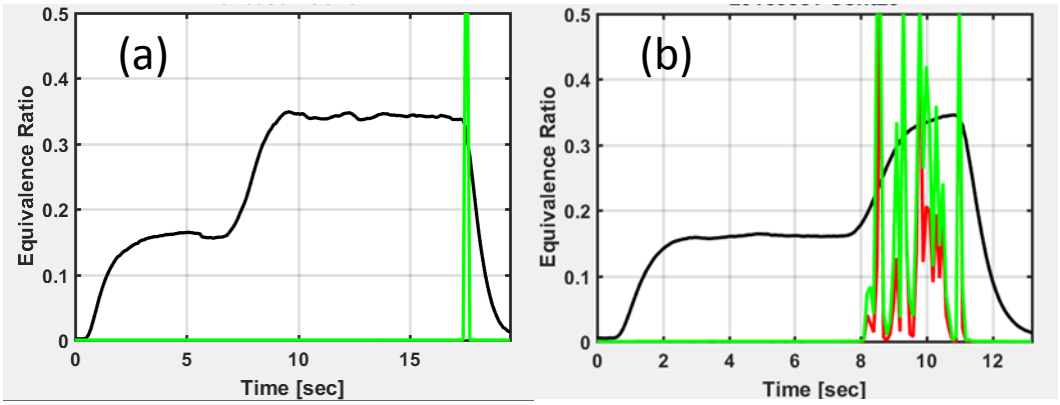

Figure I.4.7. *PMT Signals during: (a) Non-Ignition and (b) Ignition Experiments.*

Initial Testing Methodology

Testing of the alternative fuels occurred in two rounds, to quickly compare all of the fuels on a "go/no-go" basis, and then later to provide a finer comparison by evaluating equivalence ratio at ignition. The first test method for assessing the autoignition characteristics of the six fuels was as follows. Six elevated combustor pressure-temperature inlet conditions were selected, based on maximum rig heater power and air flow conditions (see Figure I.4.8). Once the air flow was established and steady, the fuel was then introduced into the injector at a very low (~0.15) equivalence ratio. After allowing the fuel system to equilibrate, the fuel flow was doubled in a single-step manner, so that the injector equivalence ratio was 0.3. This fuel flow rate was held for approximately five seconds and the PMT sensors and video camera were used to determine if ignition had occurred. In the event that a "sputtered" ignition (i.e., unsteady or pulsing light emissions) was observed, the test condition was repeated several times.

Rig test conditions	
P (psia)	***T (F)***
450	**1100**
550	**1135**
620	**1140**
700	**1150**
750	**1170**
800	**1180**

Figure I.4.8. *Matrix of Inlet Air Pressure and Temperature Conditions (all at 5% Pressure Drop).*

Initial Testing Results

Once this matrix of test conditions was completed for each fuel, a ranking chart of each fuel's autoignition characteristics was made and is shown below in Figure I.4.9. As indicated, each test was conducted at target pressure drops of five percent and final fuel-air equivalence ratios of 0.3. The red boxes denote test conditions in which no ignition was recorded, and green boxes indicate conditions at which ignition always occurred. The yellow boxes were the regions of the "sputtered" ignitions and which both ignition and non-ignition results were recorded.

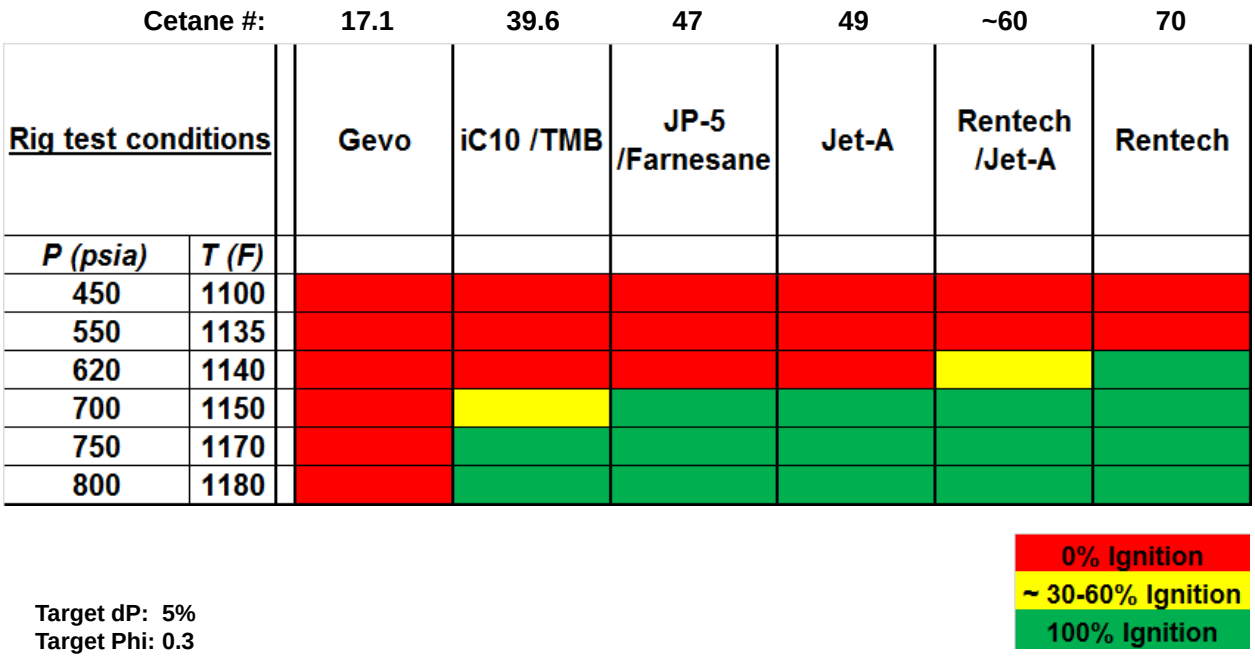

Figure I.4.9. *Autoignition Testing Results.*

In Figure I.4.9, each fuel's Cetane number is given above the fuel's name. As shown, there is a strong correlation between ignition and Cetane number. Specifically, Gevo, the lowest Cetane number fuel, did not autoignite under any test condition (in fact, Gevo was the only fuel not to exhibit the "purge flash" behavior under any experimental condition.) In contrast, Rentech had the highest Cetane number and ignited at four of the six test points. The four remaining fuels' ignition results were between these two fuels and their results scaled with Cetane number, as shown in Figure I.4.9.

Analysis/Simulation of Initial Test Results

Given the above data, the next step was an attempt to qualitatively explain these results using our suite of kinetics and modeling tools. Based on UTRC correlations of fuel droplet SMDs versus air flow conditions, the above test conditions yielded an initial fuel droplet SMD of 5 microns. Since this value is quite small and our existing vaporization-ignition code is currently configured for only one fuel (n-heptane), the subsequent simulations assumed that the fuel-air mixtures were premixed and prevaporized. To test this assumption, the ignition-vaporization code was used to access the impact on ignition times between prevaporized and five micron flows. The resulting ignition times were essentially identical at the above six test conditions for n-heptane. Thus, the assumption of prevaporized fuel-air mixtures appears justified.

Since the experimental results indicated that the fuel Cetane number was an important characteristic for the fuel's autoignition behavior, the ability to capture this impact in the simulations was addressed as follows. Although there is currently no detailed kinetic model that incorporates low-temperature chemical reactions for surrogate fuel compounds that would adequately represent the above fuels, Lawrence Livermore National Labs has published a detailed low-temperature kinetic model for primary reference fuels (PRFs). For PRFs, the important characteristic ignition property is Octane number. Intuitively, one would expect that an inverse relationship between a fuel's Octane and Cetane number would exist. Indeed, that does appear to be the case and Southwestern Research Institute has published correlations between fuels' Octane and Cetane numbers. Thus, to effectively capture the

impact of the above fuels' Cetane numbers, both the LLNL PRF mechanism was used in conjunction with the SwRI Octane-Cetane relationship to estimate the above six fuels ignition characteristics for the six experimental conditions. Figure I.4.10 illustrates the respective ignition times for the six fuel blends as a function of equivalence ratio for the 800 psia/1180 F test condition.

As indicated, the ignition times for these fuels range from approximately ten to one milliseconds. These values are in good agreement with the estimated residence time within the injector tube: ~0.75 milliseconds. Thus, a ratio of ignition time to residence time (i.e., Damkohler number) for each fuel at each test condition can also be made and the companion figure to Figure I.4.10 is shown in Figure I.4.11.

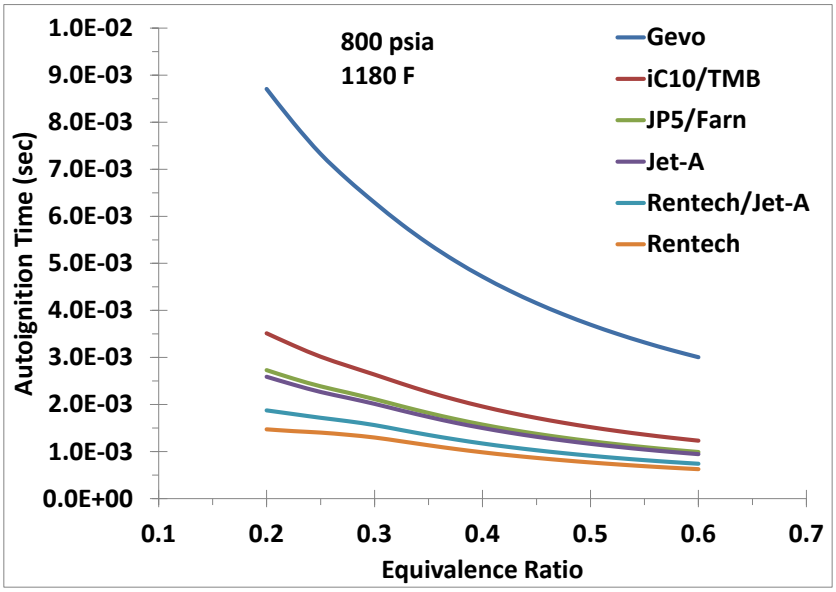

Figure I.4.10: *Autoignition Times for the Six Tested Fuel Blends at 800 psia/1180F.*

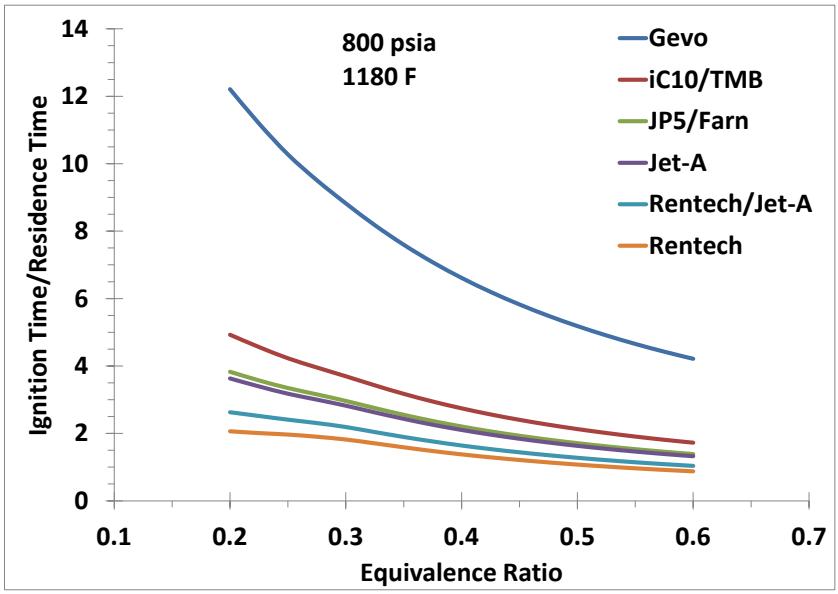

Figure I.4.11. *Ratio of Autoignition and Injector Residence Times for the Six Tested Fuel Blends at 800 psia/1180F.*

For conditions in which this ratio is much greater than one, it would be expected that the fuel-air mixture would not be able to ignite within the injector simply because the residence time in the injector is less than the ignition time and there is insufficient time to initiate and establish a reaction zone within the injector. Based on the experimental results at this test point, the iC10/TMB mixture successfully ignited within the tube. At an equivalence ratio of 0.3, the characteristic time ratio for this fuel is 3.7. Since the residence time for all of the test conditions in the matrix is essentially 0.75 milliseconds and assuming this test point is a limit value, then the proportionality constant for all experimental test conditions for all fuels would be 3.7 then a scaled plot of characteristic times would then allow for the determination of ignition. That is, if the fuel's scaled ratio is less than one it would have sufficient time to ignite within the tube, but if the ratio was greater than one it would not. An example of the scaled characteristic times for the fuels at the 700 psia/1150 F condition is shown in Figure I.4.12. As illustrated, the Gevo and iC10/TMB mixture values are above one and would not ignite. The Rentech and the Rentech/Jet-A fuels are well below and would ignite. The JP5/Farnesane and Jet-A fuels are near one, but should light. This description is quite reasonable compared to the results in Figure I.4.9.

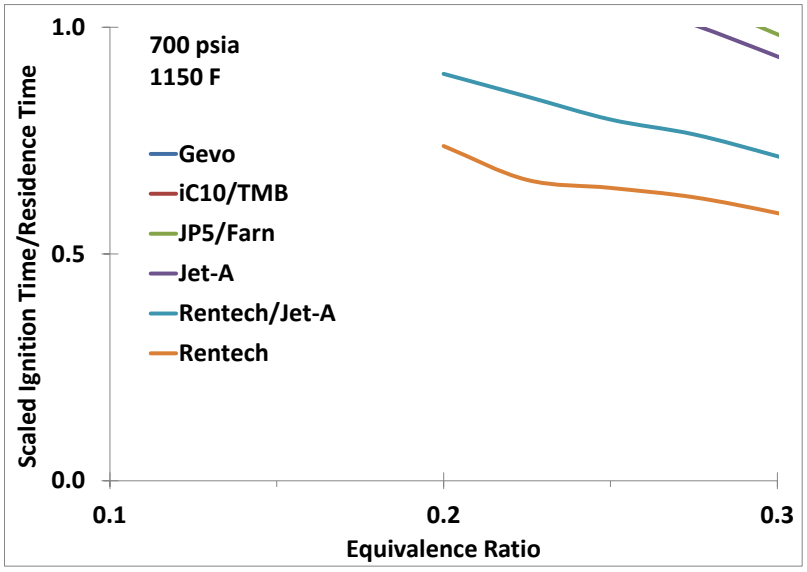

Figure I.4.12. *Scaled Ratio of Autoignition and Injector Residence Times for the Six Tested Fuel Blends at 700 psia/1150F.*

Simulation			17.1	39.6	47	48.8	~60	70
Rig test conditions			**Gevo**	**iC10 /TMB**	**JP-5 /Farnes ane**	**Jet-A**	**Rentech /Jet-A**	**Rentech**
P (psia)	***T (F)***							
450	**1100**							
550	**1135**							
620	**1140**							
700	**1150**							
750	**1170**							
800	**1180**							

Figure I.4.13. *Autoignition Simulation Results.*

Proceeding in a similar manner for the remainder of the matrix, a simulation results matrix similar to the experimental one shown in Figure I.4.9 can be made and is shown in Figure I.4.13. As can be seen, the agreement to Figure I.4.9 is quite good.

Final Testing Methodology – Minimum Phi at Ignition

The purpose of these tests was to ascertain the impact of the various chemical and physical fuel properties on autoignition characteristics in a more quantifiable manner than the previous "light/no-light" test. Those tests impulsively doubled fuel flow rate from an equivalence ratio of 0.15 to 0.30 to determine whether or not ignition occurred. In the present tests, the same fuel flow rate yielding an initial equivalence ratio of 0.15 was generated. However, instead of an impulsive doubling of the fuel flow, a more gradual, linear, and repeatable increase in fuel flow was admitted to the injector. The fuel flow rate is increased until either ignition occurs (as indicated by PMT signal) or the injector equivalence ratio approached 0.75. If no ignition were observed by that phi, the fuel flow was cut off to prevent any potential hardware overheating. An example time history of this fuel delivery is shown in Figure I.4.14.

As indicated in the figure, the JP-5/Farnesane blend, at inlet conditions of 500 psia and 1100 F, autoignited at approximately a phi of 0.48-0.49 based on PMT signal response. The full matrix of test conditions for this experiment is given in Table 1.4.1. The last entry in the matrix – 800 psia/1175 F/4% pressure drop is meant to simulate a maximum expected take-off cycle condition.

Table 1.4.1: Matrix of Inlet Test Conditions.

P (psia)	T (F)	dP (%)
500	900	5
500	950	5
500	1000	5
500	1100	5
700	900	5
700	950	5
700	1000	5
700	1100	5
800	1175	4

The equivalence ratios at which ignition was observed for the six fuels are shown in Figure 1.4.15 for the conditions illustrated. Evidently, the ignition phi values inversely scale with the fuel's Cetane number. That is, for given inlet conditions, as the fuel's Cetane number decreased, the corresponding equivalence ratio for ignition increased. In fact, for the Gevo fuel (C-1) at 500 psia and 1000 F, ignition was not observed before an equivalence ratio of 0.75 was reached, whereas the other five fuels all successfully ignited at ratios below 0.75 for this test point. A similar inverse relationship for inlet conditions on ignition phi was observed for the fuels. That is, for a given fuel, as the inlet pressure increased, the equivalence ratio at ignition decreased and as the inlet temperature increased, the equivalence ratio at ignition also decreased.

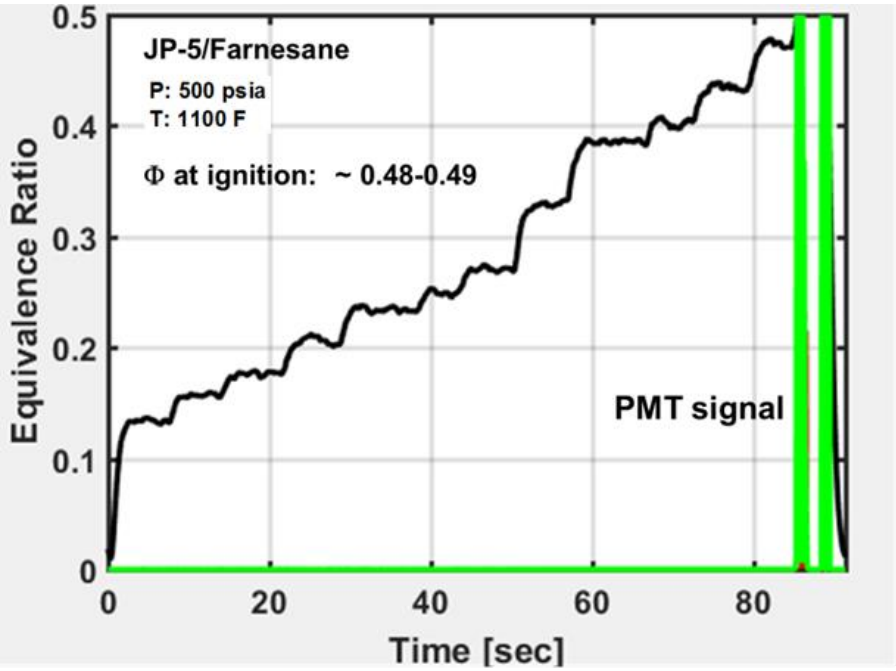

Figure 1.4.14: *Equivalence Ratio Sweep for JP-5/Farnesane Blend at Inlet Conditions Shown.*

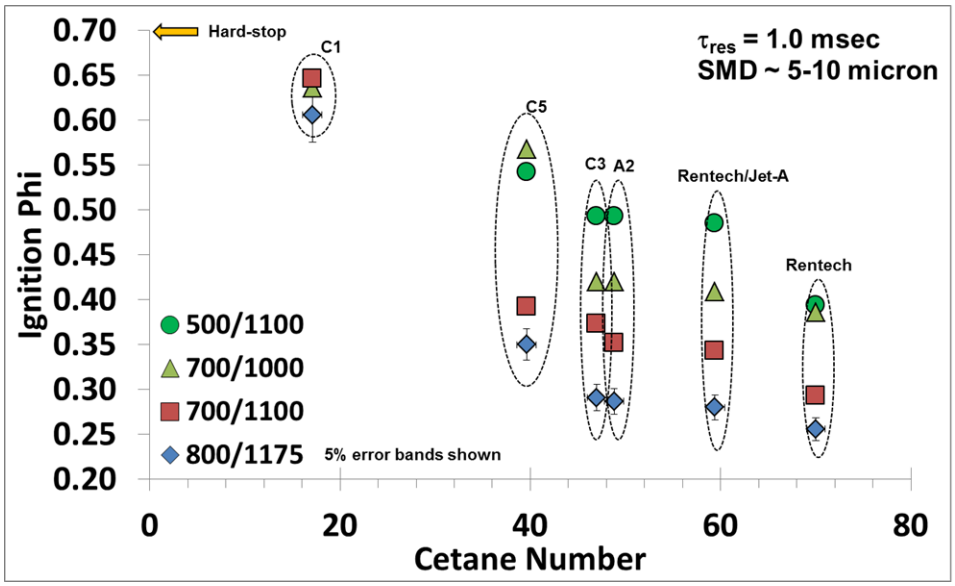

Figure I.4.15: *Ignition Phi Results for the Six Tested Fuels at the Indicated Test Conditions.*

Utilizing these results, a preliminary statistical analysis was conducted to correlate these ignition equivalence ratios with the physical and chemical fuel properties discussed above. Pearson correlation coefficients for these properties were generated based on the experimental ignition equivalence ratios. The results are summarized in Table 1.4.2. As indicated, the fuel parameter that had the highest impact on ignition equivalence ratio was the fuel Cetane number. It was the only parameter that yielded a correlation coefficient greater than 0.9 at all the analyzed test points. The next highest parameter was fuel density and its correlation coefficient value ranged between 0.5 and 0.3 over the analyzed conditions.

Table I.4.2: Pearson Correlation Coefficients of Fuel Physical and Chemical Properties on Recorded Ignition Equivalence Ratios.

Phi at Ignition	800/1175	700/1100	700/1000	500/1100
Cetane Number	-0.908	-0.932	-0.911	-0.974
Density	-0.512	-0.403	-0.548	-0.314
Surface Tension	-0.430	-0.316	-0.463	-0.255
Viscosity	-0.227	-0.158	-0.554	-0.302
Flash Point	-0.114	-0.014	-0.282	-0.070
Smoke Point	-0.070	-0.140	-0.308	-0.335
Molecular Weight	0.045	0.068	-0.357	-0.137
H/C Ratio	0.492	0.433	0.230	0.231

Analysis and Simulation of Results

An *a priori* assumption was made with regard to simulating the experimental results, based on the above discussion and preliminary analysis. Specifically, it was assumed that the most significant fuel property controlling these autoignition tests would be the fuel's Cetane number. (As discussed above and shown in Table I.4.2, this assumption was borne out upon completion of these minimum phi ignition tests.) This assumption allowed for the utilization of a **single fully detailed kinetic mechanism**, self-contained and self-consistent, that would be capable of simulating the ignition times of all six fuels based solely on the fuel's Cetane number.

A correlation developed by Southwest Research Institute was used to convert the fuel's Cetane number to Octane number. With knowledge of the fuel's Octane number, the fully detailed Lawrence Livermore National Labs "Primary Reference Fuel" kinetic mechanism could then be used to estimate the fuel's relevant autoignition time. The generality of this approach lies in the fact that once the fuel's Octane number is known, it can be represented as a distinct blend of two hydrocarbons: iso-Octane and n-Heptane. These are the two parent hydrocarbon species that comprise the LLNL primary reference fuel mechanism. The importance of this mechanism can be understood by referring to Figure I.4.16.

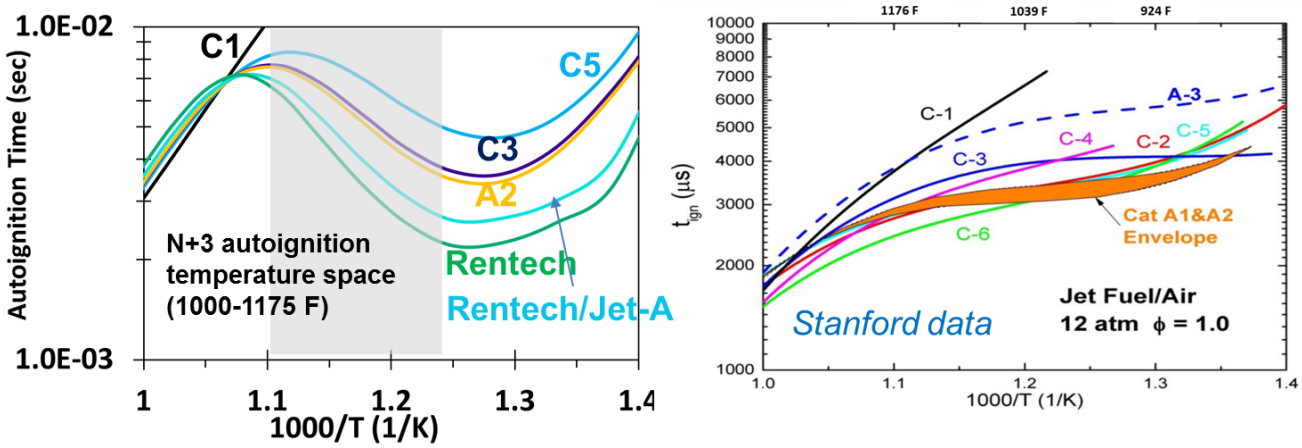

Figure I.4.16: *Comparison of REAL Fuel Stock Tube Ignition Delays (Right) and Binary Fuel Blend Simulation Ignition Delays (Left) for NJFCP Fuels at Conditions Indicated.*

The grey band shown in the leftmost panel of Figure I.4.16 denotes the experimental inlet temperature region of these N+3 autoignition experiments. It can be seen that the test region lies within the real fuels' NTC chemistry regions. Thus, it was imperative to capture this chemistry region in a systematic manner. Use of the LLNL mechanism allows for the realistic representation, in a systematic manner, of this kinetic region.

Another important aspect shown in Figure I.4.16 is that though each NJFCP fuel is a multispecies fuel, the representation of a given fuel as a binary blend of iso-Octane and n-Heptane dependent on the fuel's Cetane number yields calculated ignition delay times that are in reasonable agreement with the experimental shock tube ignition delay times. Note that the abscissa and ordinate axes of both plots are identical. Quantitatively, the simulations are approximately 2x longer, with the worst agreement (>2x) occurring for the Gevo (C1) fuel; qualitatively, the simulations reasonably capture the shock tube ignition delay times. Thus, this modeling approach affords a similar analysis method to gain insight into the results of the minimum phi at ignition tests as follows.

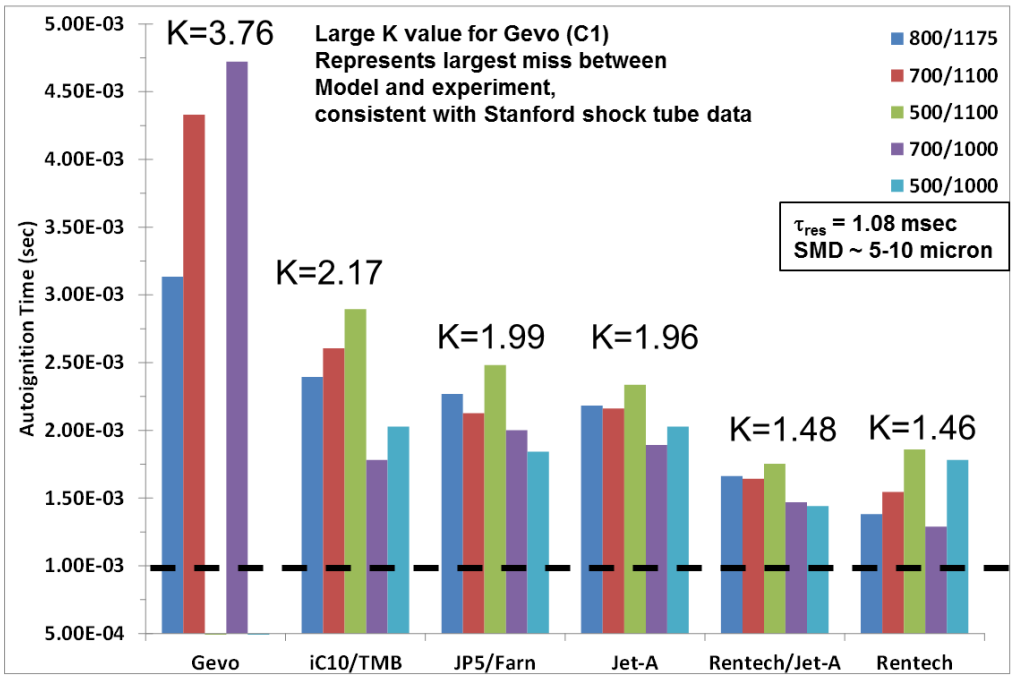

Figure I.4.17: *Computational Autoignition Times associated with the Experimental Minimum Equivalence Ratios at Ignition for the Various Fuels at Indicated Inlet Conditions.*

Based on the **experimental** equivalence ratios for the various fuels and inlet conditions given in Figure I.4.15, the corresponding **computational** ignition delay times were calculated. The results of these multiple calculations are given above in Figure I.4.17. As can be readily observed, for a given fuel (but different experimental combinations of pressure, temperature, and equivalence ratio), the resulting ignition delay times are remarkably consistent. For example, over the five different inlet conditions, the JP5/Farnesane blend computed ignition delay times were all close to 2 msec. These results are not surprising if it is remembered that all the experiments were conducted for identical injector tube residence times (~ 1 msec; indicated by the dashed black line).

Furthermore, if the ~ 2x agreement shown in Fig. I.4.16 is considered here, it would appear that all the experimental ignition delay times are also of the order of 1 msec. Thus, it appears entirely consistent that, given the respective inlet conditions, the **minimum** equivalence ratio necessary for autoignition of a given fuel would be the ratio whose ignition time is essentially the injector residence time. (Expressed another way, the ratio of the characteristic ignition time to residence time, the critical Damkohler number, is unity at ignition.)

The various "K values" shown in Figure I.4.17, associated with each fuel, reflect the average proportionality constant between the simulated ignition delay time and the experimental ignition delay time. These values are entirely consistent with the "light-no light" testing results as well as with the comparison to the Stanford shock tube ignition delay data given in Figure I.4.16.

Additionally, the lower Cetane number fuels have higher fractions of iso-Octane. From Figure I.4.16, the fuel that had the highest discrepancy with the shock tube data was the C1 (Gevo) fuel, which had the highest fraction of iso-Octane. The trends given in Figure I.4.17 are consistent with this finding.

Given the K factors for each fuel that have been benchmarked against the experimental data, we can calculate ignition delay times at other representative combustor inlet conditions. Using these K values, we can scale the simulation ignition delay times to actual conditions to assess realistic autoignition probabilities. Shown in Figures I.4.18 and I.4.19 are comparisons of scaled ignition delay times as functions of equivalence ratio for the six tested fuels versus injector residence time for operating conditions corresponding to "Max Takeoff" for N+3 and "Max Takeoff" expected for any future cycle, respectively. As shown in Figure I.4.18, up to stoichiometric conditions all fuels' ignition delay times exceed injector residence time. Accordingly, no tested fuel should autoignite within the injector.

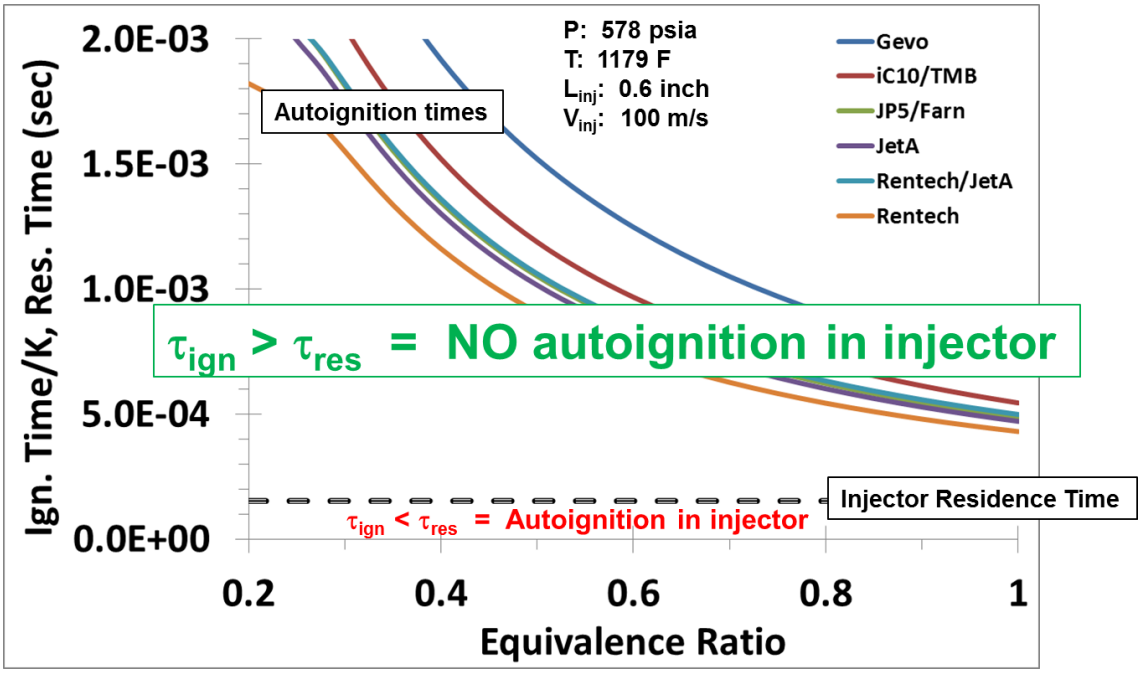

Figure I.4.18: *Scaled Computational Autoignition Times associated with Tested Fuels for Realistic Engine Operating and Design Conditions for N+3 Max TO Point.*

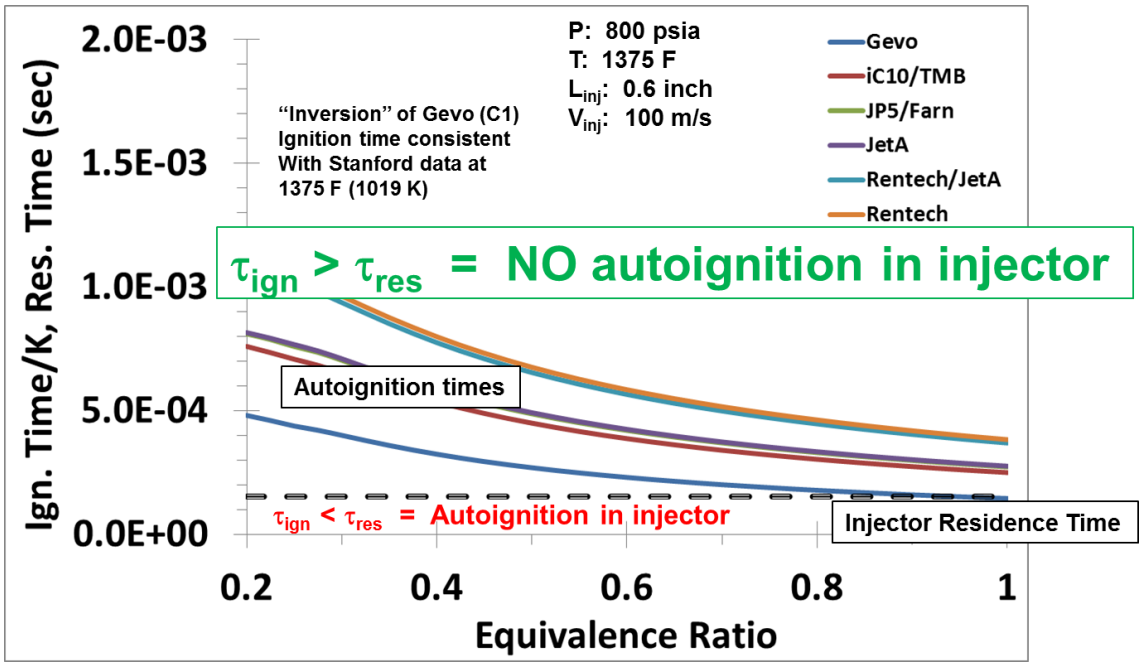

Figure I.4.19: *Scaled Computational Autoignition Times associated with Tested Fuels for Realistic Engine Operating and Design Conditions for Maximum Expected "Max TO" point for future cycles.*

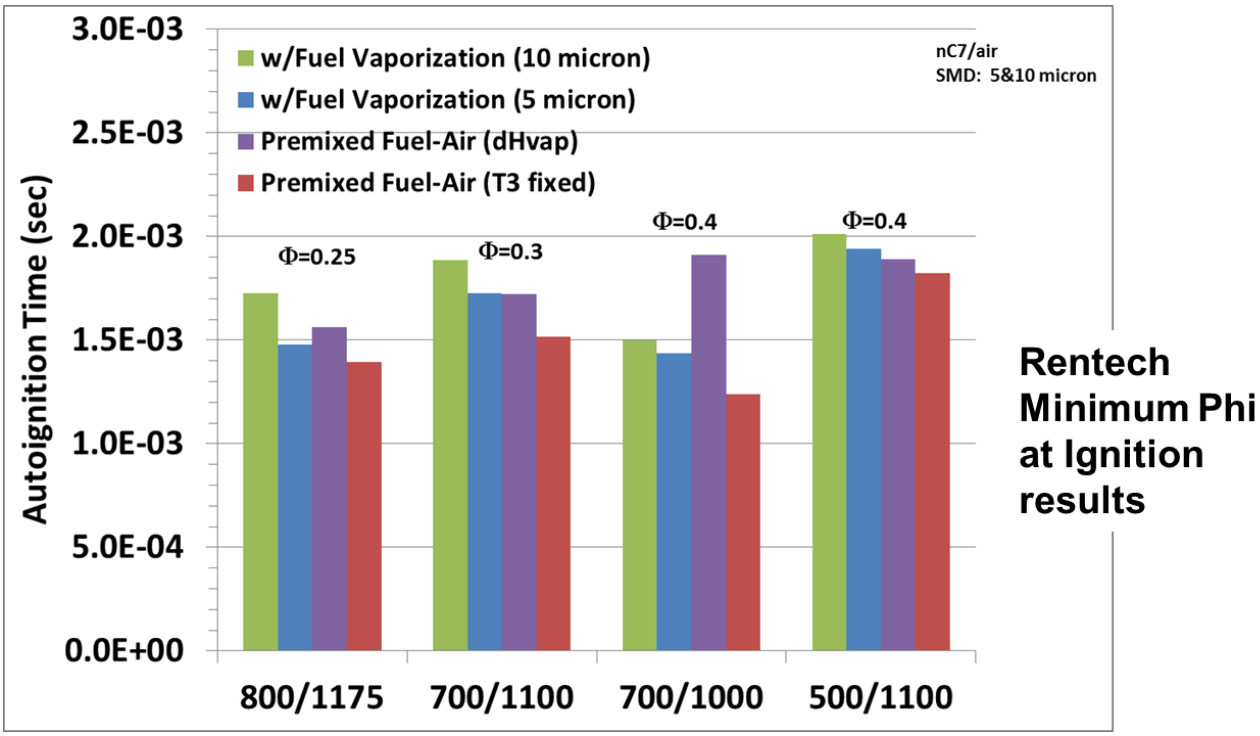

Figure I.4.20: *Sensitivity of Ignition Delay Time to Fuel Evaporation/Spray Effects at Ignition Minimum Phi Values for Inlet Conditions Shown (Based on Rentech Simulations).*

Figure I.4.19 reveals the same conclusion at the "Max Takeoff" operating condition for any expected future cycle. However, it can be seen that the ignition delay time margin has been reduced and the values are closer to the residence time than they were for the N+3 "Max TO" condition. Interestingly,

Figure I.4.19 indicates that at for this operating point, Gevo is the fuel with the lowest time scale margin. In fact, at equivalence ratios above approximately 0.8 (greater than the design injector fuel-air ratio), the ignition delay and residence times are essentially identical, indicating a potential issue. This finding of Gevo having a lower ignition delay time than the other fuels is consistent with the results of the Stanford shock tube data given in Figure I.4.16. That figure indicates that at temperatures greater than 1000 K (1375 F ~ 1020 K), the Gevo ignition delay slope markedly increases relative to the other fuels. The results in Figure I.4.19 are consistent with that observation.

Lastly, the above calculations have all been made assuming the fuel-air mixture is premixed, prevaporized and its initial temperature is the combustor inlet temperature (i.e., the fuel's latent heat has not lowered the mixture temperature). Figure I.4.20 illustrates the sensitivity of ignition delay to fuel vaporization, both via droplet SMD and fuel latent heat effects. Indeed, as expected, aspects of fuel droplet evaporation lead to slightly longer ignition delay times due to the time lag associated with generating fuel vapor and the simultaneous system temperature decrease due to vaporization. However, these increased times are not dramatically longer than the "ideal" premixed, prevaporized conditions. Furthermore, since these "ideal" times are indeed the shortest, they represent the most conservative estimates for design and safety analysis considerations.

The above autoignition study of alternative fuels was presented and published at the 2019 American Institute of Aeronautics and Astronautics (AIAA) Propulsion and Energy Forum in July 2017, as AIAA Paper Number AIAA-2017-4985 (Zeppieri, Smith, and Colket, 2017).

Ambient Flow Testing and Verification of UTRC N+3 Combustor Rig Components

Prior to assembly and installation of the N+3 combustor rig in UTRC's high-pressure single-nozzle test facility, sub-component testing was performed at ambient conditions to evaluate and verify basic flow quantities and flow splits. Ambient testing for this purpose included Flow Number (FN) checks of the main fuel nozzles to confirm flowrate versus fuel pressure drop, and effective area (Acd) checks of airflow circuits including bulkhead cooling, pilot swirler, and main swirlers to confirm airflow versus pressure drop. Specifically for the airflow circuits, pressure drop versus flowrate was measured to calculate effective flow area or Acd for each airflow component. For the pilot and main swirlers the actual (measured) effective areas were slightly smaller than design intent, by roughly 10 to 20%. Based on inspection of the metal swirlers, in addition to comparison to measurements of the same swirler designs using plastic fabrication (which measured closer to target values), it was concluded that the small Acd values for the metal swirlers is likely due to imperfections resulting from the Direct Metal Laser Sintering (DMLS) fabrication technique. These imperfections include surface roughness, inexact vane thicknesses, and excess material at edges and corners near the vanes. In the future, it is expected that these swirlers could be made closer to tolerance with improvements and refinements in the fabrication process. In the meantime, for these prototype swirlers the measured effective areas were deemed acceptable for combustion testing because airflow splits were not significantly impacted.

Task 5 – Downselect leading concept for single-sector testing

Summary of Mixer Design Studies, as Input to Task 5 Downselection Activity

The N+3 combustor effort identified fuel-air mixing as a primary driver to achieving NASA's aggressive N+3 emissions goals. Accordingly, the effort included detailed studies of potential mixer designs, their scalability and achievable mixedness levels, and the physics and design parameters that determine their performance. Briefly, the studies show that an annular mixer design comes closest to ideal mixing and provides the greatest range of scalability as a result of its greater degrees of freedom, and specifically by

holding the annular gap at a constant dimension when scaling. Design constraints in the study included minimum fuel pressure drop requirements (to evenly distribute the fuel) and minimum fuel orifice sizes (to prevent clogging), meaning that fuel can be injected from only a few sites within the mixer. The mixer must also operate within the pressure-drop requirement of the combustor liner, typically around 3% to 4%. These limitations mean that even for an optimized mixer that makes best use of shear-induced turbulence, fuel can be dispersed only a limited distance from its injection site. The result is that "round" mixers are limited in diameter to roughly less than 1-inch before mixing performance becomes unacceptable for meeting N+3 emissions levels. Larger diameters require moving to an annular-mixer approach.

Downselection Review & Scope

The downselection task (milestone) was completed in Q1 2016, enabling detailed hardware design and fabrication to begin at that time for the N+3 combustor. The downselection occurred following a final review with UTRC and P&W combustor stakeholders, including the Combustor Technology Manager and the Combustor Aero Chief from P&W, Combustion Fellows from both UTRC and P&W, and principal combustor designers and project leaders from both organizations. The downselection was also reviewed with NASA during the March 15th, 2016 monthly teleconference (project status update meeting). The downselection scope was limited to ACS (Axial Controlled Stoichiometry) combustor configurations consistent with the engine-implementable ACS combustor configuration successfully demonstrated in ERA Phase-2. After reviewing the N+3 combustor design studies from Task 2, along with NASA and P&W objectives for N+3, the downselection recommendation was to place first priority on a configuration utilizing round main injectors in a configuration comprising 14 sectors in a complete, annular combustor for a 2.0 core-size engine in the selected N+3 cycle. This configuration was deemed most likely to succeed and deliver the targeted low emissions levels.

Task 6a – Detailed design & fabrication for UTRC tests

Design of N+3 combustor rig for testing in UTRC high-pressure single-sector facility

The UTRC combustor rig was designed to assess the aero-performance of the small core ACS combustor by measuring its emissions and thermo-acoustic stability performance. The baseline hardware set includes the three main sub-assemblies; the insert sub-assembly, the main sub-assembly, and the pilot sub-assembly. The insert sub-assembly defines the rig cross sectional area and provides access for the emissions probe and rig igniter. The main sub-assembly defines the main swirlers and nozzles as well as their mounting fixtures. The pilot sub-assembly defines the pilot swirler, fuel nozzle, and bulk head cooling flows. All of the parts were designed to take full rig conditions (1000 psia, 4500 R) even though these full rug conditions are not expected to be experienced during the N+3 program. The insert frames are made out of 4130 steel and the required strength demonstrate that there is a large safety factor for all of the loads. The inserts are also made out of 4130 steel and are water cooled. The insert uses a cover-plate manufacturing method (design) to create multi-path water cooling features. This provides for water-cooling of the combustor sidewalls during N+3 combustor testing at UTRC.

Instrumentation Details

The instrumentation layout for the UTRC high pressure/temperature rig includes upstream static temperature (T3), static pressure (P3), and ITP (combustion dynamics) measurements for both the pilot and the main swirlers. There are additional thermocouple measurements upstream of both for health and safety of the hardware (checking for fuel leaks/burning upstream). Three instrumentation ports pass through the studs of the bulkhead to allow for a static temperature (health and safety), static pressure (P4), and an ITP measurement downstream of the bulkhead. There is an additional ITP port

that passes through the east insert to allow for a second axial location to measure the combustor thermo-acoustics. The last instrumentation is the three emissions probes. There is additional facility instrumentation to measure all air, fuel, water, and emissions flow rates.

Assembly and Installation

Photographs of the actual combustor liner hardware during installation into the rig are shown in Figure I.6a.1. The first view (on the left) is looking into the combustor from the OD (outside diameter), i.e. looking toward the engine centerline. As shown in the right-hand photograph in Figure I.6a1, the sidewalls are water-cooled. The bottom wall (visible in the left-hand photos) is also water-cooled, as is the top wall (not shown). Figure I.6a.2 shows a photograph of the emissions sampling probes, as well as a depiction of their location within the rig.

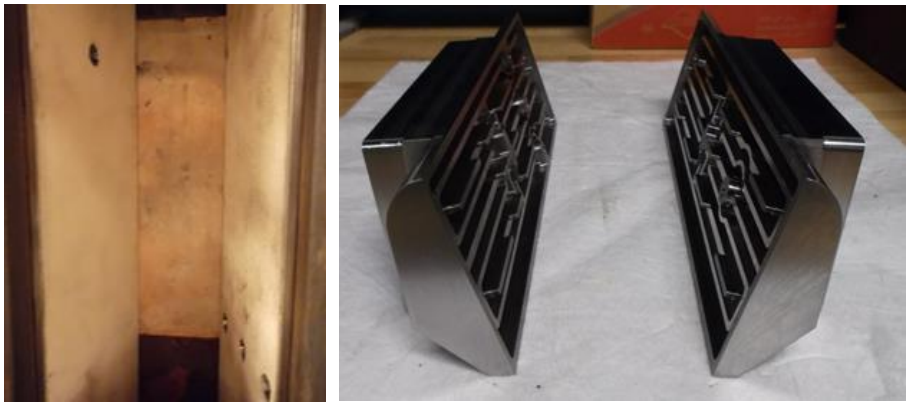

Figure I.6a.1. *Photographs of single-sector small-core N+3 combustor rig during various stages of assembly. Left photo: View from combustor OD showing more of the combustor length – in this view the torch igniter penetration is still visible on the left-hand sidewall, and the three (3) emissions probe penetrations are visible on the right-hand sidewall. Flow is from top to bottom in this photograph. Right photo: Photograph of sidewalls during fabrication, showing internal water-cooling passages.*

Task 6b – Detailed design & fabrication for NASA tests

Overview – Design of N+3 Combustor Rig for NASA CE-5

The primary difference between the N+3 combustor rigs intended for UTRC versus NASA testing is that the UTRC rig is water-cooled (it does not include combustor liner cooling air) whereas the NASA rig will be air-cooled and therefore all combustion process air (including liner cooling air) will enter the combustor and participate in combustion. All UTRC-acquired data are "corrected" for this missing air when calculating overall fuel-air ratio (FAR4).

A design review for the CE-5 hardware and facility installation was held with NASA on November 6th 2017, and a follow-up review to address action items was held on November 27th 2017. Following these reviews material was ordered and fabrication was initiated for the CE-5 N+3 combustor hardware.

As compared to the N+3 combustor rig tested at UTRC, the N+3 combustor rig for CE-5 retains some key features, but also differs in important respects. Features which are the same include:

- Single-sector size.
- Cross-sectional shape/dimensions that simulate the combustor sector shape, and allow straightforward fabrication.
- Dome (bulkhead) height to match expected combustor height in N+3 core-size engine.
- Air-cooled dome (bulkhead).

Features in the CE-5 rig which are different from the UTRC rig include:

- Air-cooled combustor liner (top, bottom, and side walls). Note that the side walls will be only impingement-cooled (with unheated high-pressure air provided by the CE-5 facility), with the cooling air exiting via a slot at the combustor aft end. In contrast, the top and bottom (OD and ID) walls will include effusion or film cooling, so that the top and bottom wall cooling air will be included in the combustion process as in an engine application.
- Air feed to the pilot and main injectors from a single plenum, with flow splits established by effective areas (Acd's) of each component.
- Sloped bottom (ID) wall at the combustor aft end, to more closely simulate an engine installation in which the combustor exit height must match the turbine inlet height (span).

All of the components for the NASA N+3 combustor were fabricated, instrumented and assembled before delivery to NASA in July 2018. In addition, cold-flow tests of airflow versus pressure drop (for calculation of effective area) were performed at UTRC on the components and sub-assemblies before final instrumentation and delivery to NASA. A photograph of the completed N+3 combustor for NASA CE-5 testing is shown in Figure 1.6b.1.

Figure I.6b.1. *Photograph of N+3 combustor hardware for NASA testing, during preliminary assembly.*

Note that in the installation the CE-5 test-section windows can be installed (as illustrated in Figure I.6b.2), but they do not view the interior of the combustor itself. Instead, the windows view the outside of the combustor rig to monitor for fuel leaks during operation of the rig. The N+3 combustor rig (the test article) is aft-mounted, being cantilevered forward from the mounting flange at the exit of the test section. Thus, the inlet piping directly supplies air from the facility compressors and heaters to the test-section volume, which serves as an inlet plenum for the N+3 combustor rig. In this manner, cooling air is provided to the air-cooled OD (top) and ID (bottom) walls of the combustor, from the same source as the primary combustion air, as in an engine. Cooling air from the OD and ID walls enters the combustor and participates in combustion, also as in an engine. For the sidewalls which define the single sector, and which do not exist in an engine, high-pressure ambient-temperature air is used to provide impingement cooling which is then directed downstream to exit via aft-facing slots adjacent to the combustor exit, so that this air does not participate in the combustion process. The NASA emissions probes traverse vertically and horizontally at the exit-plane of the combustor, as shown in Figure I.6b.2.

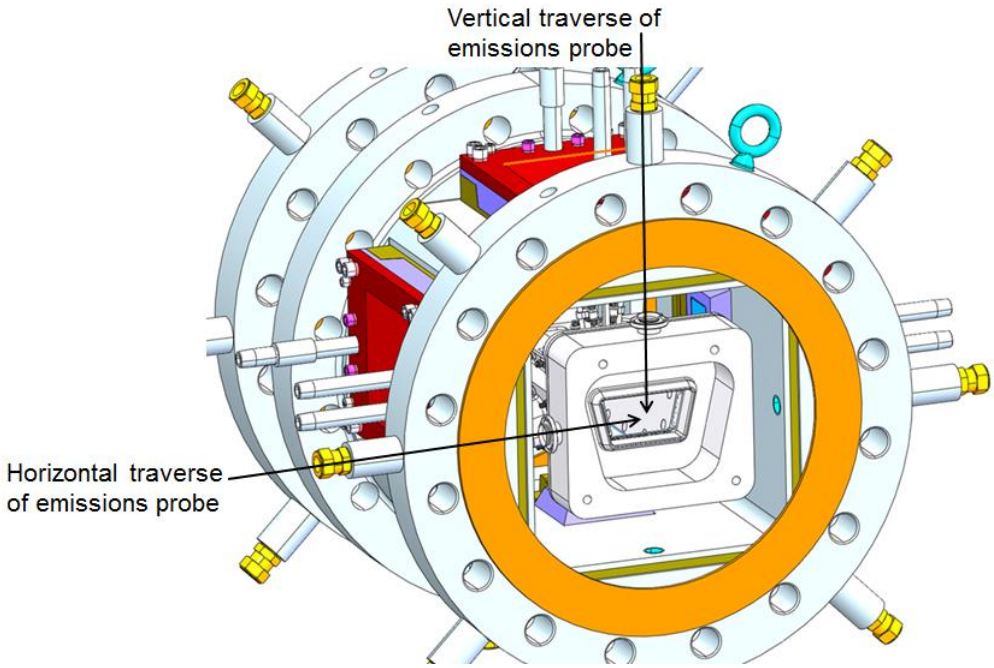

Figure I.6b.2. *Aft-looking-forward (ALF) view of N+3 combustor rig installed in CE-5, with the mounting-flange hidden (made invisible) to show the spacer-block and emissions probe traversing paths. The NASA single-point traversing emissions probe has two available traversing paths, as shown: a vertical (up-down) path, and a horizontal (left-right) path. The combustor is positioned (mounted) in the test-section with the center of the combustor-exit on the CE-5 test-section centerline, so that both probe traversing paths can acquire data across the center-region of the combustor exit.*

Flow checks, Instrumentation, and Final Assembly of N+3 Combustor for NASA CE-5 Testing

After completing the fabrication of all components for the N+3 combustor rig, but before final instrumentation and shipment of the rig to NASA, cold-flow tests were performed to assess the airflow partitioning ("flow splits") and total pressure drop ("effective area") of the combustor. A photograph of the effective-area or "Acd" test setup at UTRC is shown in Figure I.6b.3. This cold-flow rig includes an air-plenum (as annotated in the figure) into which various components can be mounted from the flange located on the top of the plenum (the flange can be customized to test various components). Air enters the plenum from the bottom, passes through the component under test, and exits to the room (ambient) at the top of the rig. Airflow rate and pressure drop are measured, and effective area is calculated from these measurements. The rig's flow metering and pressure transducers were calibrated prior to Acd testing of the N+3 combustor components, and a Coriolis meter was added as a secondary airflow measurement for improved accuracy.

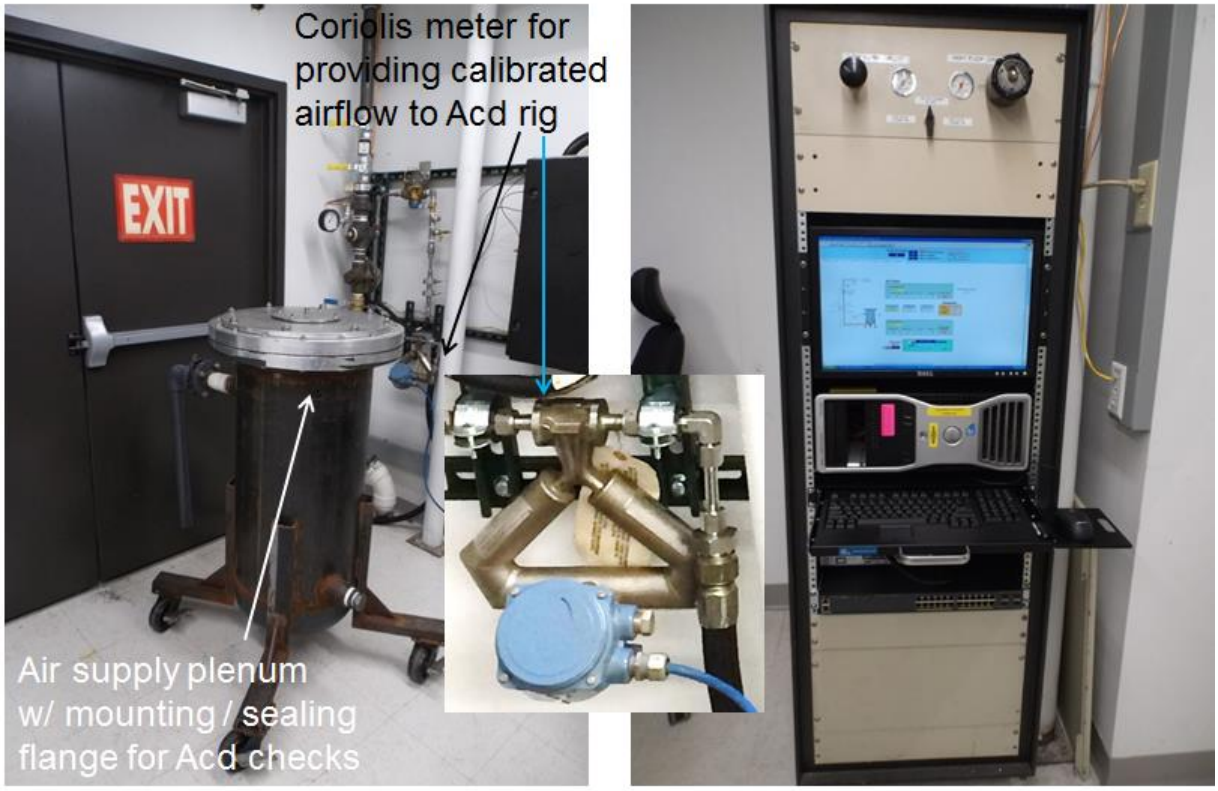

Figure I.6b.3. *Photograph of UTRC cold-flow testing lab, for measuring effective area of combustor components. N+3 combustor components were mounted inside the test-plenum shown.*

Task 7 – Characterize (test) N+3 combustor in UTRC and NASA rigs

NOx Correlation & EPAP Calculation for N+3 Combustor Configuration Selected for CE-5

Emissions data were acquired in UTRC's test rig for several candidate configurations for the N+3 combustor, with variations in both pilot type and combustor geometry. Pilots tested included high-shear pilots similar to those used in Pratt & Whitney's Talon-X combustor, as well as airblast- and hybrid-type pilots. Emissions data were obtained over the full range of N+3 combustor operating conditions, including full pressure and inlet temperature. In addition, emissions data were acquired for Jet-A fuel and for an alternative fuel (a 50/50 blend of Jet-A and Rentech fuel) showing no significant change in emissions with fuel type. Based on the UTRC N+3 combustor rig results, a selection was made for the final configuration to be tested in NASA's CE-5 facility. With selection of the final N+3 combustor configuration completed, a final NOx correlation for the N+3 combustor was generated based on the data acquired for the configuration targeted for NASA (CE-5), and was used to evaluate N+3 NOx emissions performance against CAEP/6 standards and NASA's N+3 emissions goals.

The quality of the fit between the final NOx correlation and the N+3 NOx emissions data, over a wide range of operating conditions, is indicated in Figure I.7.1 which plots these two parameters against each other, together with a linear regression fit and its associated R^2 value. As shown, there is very little variation (scatter) about the fit line and the R^2 value is 0.9955 which indicates a good fit.

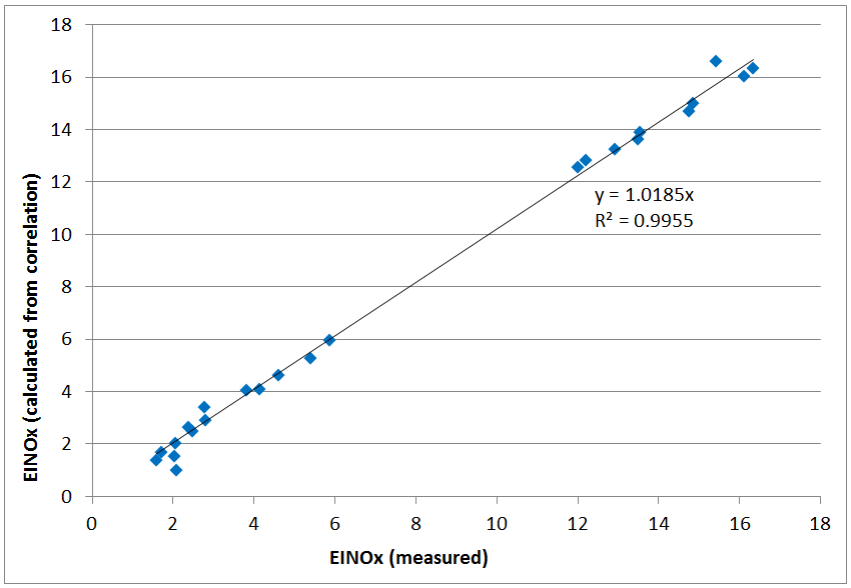

Figure I.7.1. *Plot of measured NOx emissions versus calculated NOx emissions using the final N+3 NOx correlation, for the final selected CE-5 N+3 combustor configuration.*

Finally, an LTO (Landing-TakeOff cycle) NOx EPAP (EPA Parameter) value was assigned to the N+3 combustor using the final NOx correlation of Figure I.7.1 with the N+3 cycle deck. As shown in Table I.7.1, the thrust-weighted NOx emissions for the duration of the LTO cycle is estimated to be 12.0 grams NOx / kN thrust (Dp/Foo), which is 15.3% of the CAEP/6 regulated level for this engine cycle. This is less than the targeted value for the N+3 combustor (less than 20% of the CAEP/6 regulated level) and meets NASA's N+3 LTO NOx goal. The cruise NOx goal was also met, as illustrated by the data acquired and plotted in Figure I.7.2.

ICAO Thrust Setting	*Time at condition (min)*	**NOx (g / Foo) in LTO cycle**
100%	0.7	**0.9**
85%	2.2	**1.3**
30%	4.0	**5.9**
7%	26.0	**3.8**
	Dp / Foo =	**12.0**
	% of CAEP6 =	**15.3%**

Table I.7.1. *Calculation of LTO NOx for N+3 combustor, using updated correlation for N+3 NOx emissions based on final selected combustor configuration. The calculation shows that LTO NOx emissions for the N+3 combustor are less than 20% of CAEP/6, meeting the LTO NOx performance target for this combustor development effort.*

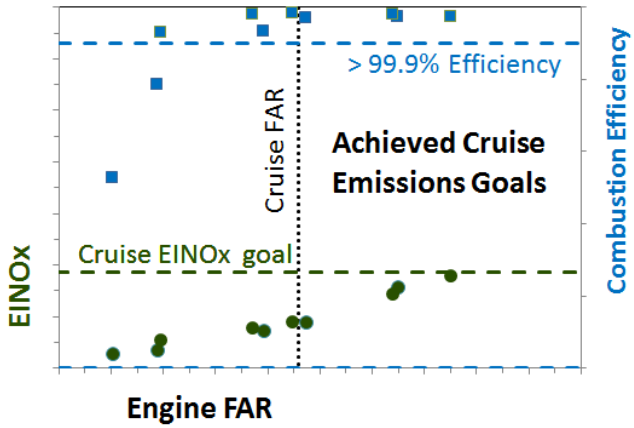

Figure I.7.2. *N+3 combustor data acquired at UTRC, versus cruise NOx goal.*

The above results from testing in UTRC's water-cooled N+3 combustor rig can be compared to the results obtained by NASA in their CE-5 testing of the air-cooled N+3 combustor rig, which UTRC provided as described in Section I.6 (the Task 6 discussion section of this report). NASA tested the N+3 combustor over a range of conditions within the capability of the CE-5 facility (up to 250 psia and 1080 F inlet conditions) to generate a NOx emissions correlation for assessment of NOx performance against CAEP/6 standards. The range of conditions tested at CE-5 are as follows (T3 is inlet temperature and P3 is inlet pressure to the combustor):

- N+3 cycle points, scaled to a maximum CE-5 pressure of 250 psia
- Low power parameter variation (pilot-only operation)
    - T3 scaling at P3=207 psia, at 650 F, 779 F, 850 F
    - P3 scaling, T3=779 F, at 88 psi, 150 psi, and 207 psi.
- High power parameter variation (pilot and mains in operation)
    - T3 scaling at P3=250 psi, at 1080 F, 1000 F, 900 F, and 800 F.
    - P3 scaling at T3=1080 F, at 250 psi, 200 psi, and 150 psi.
    - Pilot to main fuel splits, at constant total ⌀, and pilot ⌀ of 0.6 to 1.

Based on NASA's N+3 combustor measurements from the CE-5 facility, and the resulting NOx correlation, and also based on NASA's modeling of an N+3 engine cycle, NASA calculates that the N+3 combustor provides an 82% reduction from CAEP/6 LTO NOx emissions. In general the results from NASA and UTRC are close, and both show greater than 80% reduction in emitted NOx levels compared to the ICAO CAEP/6 standard, thus meeting NASA's goals for an N+3 small-core combustor technology.

Task 8 – Evaluate combustor dynamics in UTRC tests with choked exit

Combustor testing under Task 8 made use of the variable choked-exit capability (the VRASC facility, or Variable Resonance Acoustic Screening Capability) in UTRC's Jet Burner Test Stand, where the N+3 combustor was tested.

Acoustic analysis of N+3 combustion dynamics tests

In order to understand how the combustor dynamic response is related to the acoustic modes in the combustor as a function of the plunger stroke, spectral analysis was performed for transient data sets of dynamic pressures where the plunger stroke was translated from 6 to 54 inches over 190 second interval. The continuous data set of pressure response versus plunger position was found to provide a

rich set of data that clearly illustrates the variation of the longitudinal modes and dynamic pressure amplitude.

Figure I.8.1 shows a waterfall plot of bulkhead dynamic pressure (P7) amplitude spectra versus plunger stroke for a cruise condition (with higher main fuel-to-air than the cycle point). Each spectrum corresponds to a 5-second record segment and plotted at the average stroke location over that record segment. The magenta lines correspond to spectra computed from the 30-second records for a fixed plunger stroke location which agree well with the transient spectra, thus validating the transient data analysis. The waterfall plot of P7 clearly shows a large periodic variation of amplitude with stroke position at a mean value of about 900 Hz.

Figure I.8.2 shows a corresponding waterfall plot of the pressure ratio P8/P7 where P8 is an aft test section dynamic pressure at the branch to the VRASC. Again, the magenta lines are from analysis of 30 secondary records with a fixed plunger stroke location which agree well with the transient data analysis. The waterfall plot shows a series of bumps and valleys that move to lower frequencies at the larger stroke locations. This topology is directly due to the longitudinal modes in the combustor and VRASC as will be illustrated later with the aid of an acoustic model of the rig. The black lines correspond to an approximate calculation of the quarter-wave mode and harmonics (2x, 3x, and 4x the quarter wave frequency) using an approximate T4 temperature and longitudinal length equal to the length of the plunger stroke plus the width of the test rig (length justified later). The trending of the bumps and valleys correlate well with the approximate longitudinal mode frequencies.

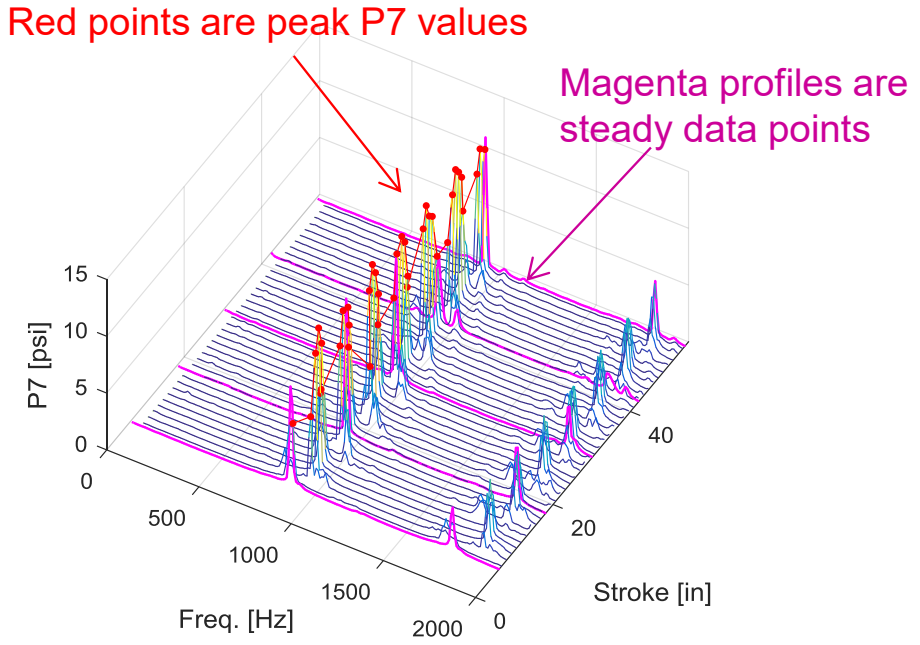

Figure I.8.1. *Waterfall map of bulkhead dynamic pressure (P7) spectra versus plunger stroke position.*

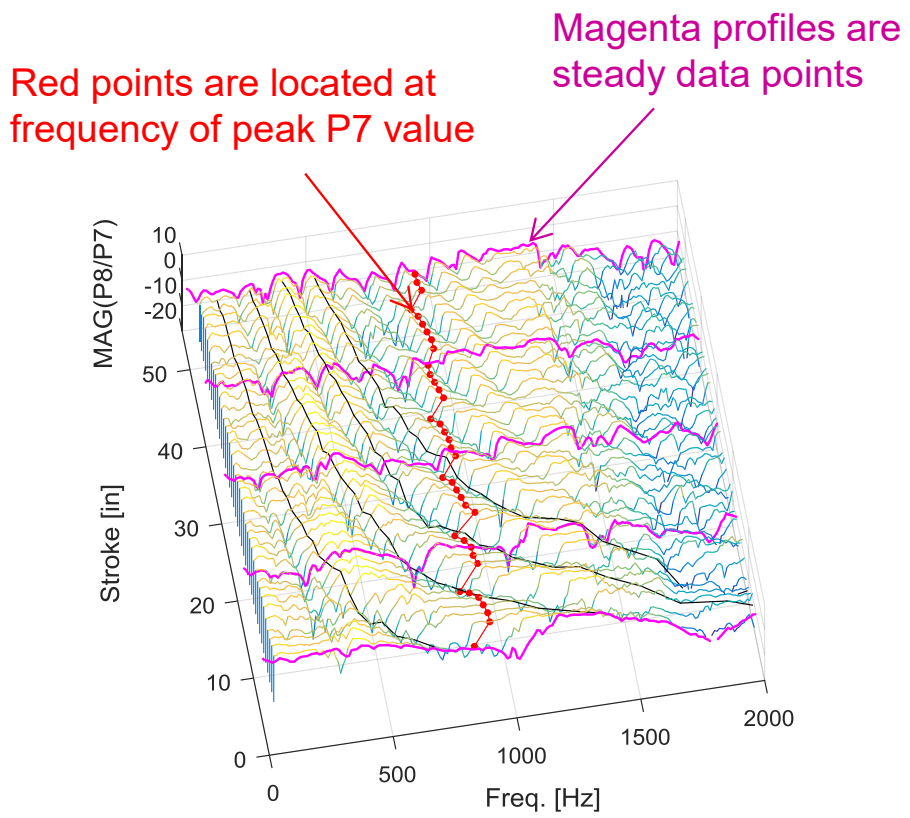

Figure I.8.2. **Waterfall map of pressure ratio (P8/P7) versus plunger stroke position.**

The frequency and pressure ratio magnitude (P8/P7) corresponding to the peak amplitude of P7 are plotted versus stroke in Fig. I.8.3 (this is also illustrated on the waterfall plots of Figs. I.8.1 and I.8.2 as the red data points). The corresponding data for the steady data fixed plunger points are shown at solid red squares which are in excellent agreement with the transient data. Comparing the P7 amplitude (middle plot) with the P8/P7 magnitude (bottom) shows a strong correlation of the peak P7 amplitude with the pressure ratio peak, while the frequency at the peak amplitude is nearly constant at 930 Hz.

This observation is different than the expectation that the frequency of the peak amplitude would directly vary with plunger stroke. Instead it appears that there is a preferred combustor frequency that gets amplified when mode shape presents favorable conditions. It is interesting how this favorable condition occurs repeatedly from the fundamental mode for the short plunger stroke to the 6th harmonic for the largest plunger stroke. Since each harmonic has significantly different spatial variation in the combustor, expect at the boundary conditions, it suggests that it is the pressure amplitude and phase near the pilot (bulkhead) which is the important feature to create the favorable Rayleigh condition (unsteady heat release in phase with the acoustic pressure).

To help understand the acoustic characteristics of the combustor rig, a FEA model in COMSOL has been developed. The geometry is shown in Fig. I.8.4 which models all the significant piping including the piping behind the plunger (which communicates to the combustor side of the plunger via a gap around the plunger circumference). The models of the fuel injector/swirlers were tuned and validated with flowing impedance bench tests performed in the prior quarter and inserted into the test rig model.

Forced response solutions were obtained using a spherical volume source (representing the approximate location of the pilot flame) shown in Fig. I.8.4.

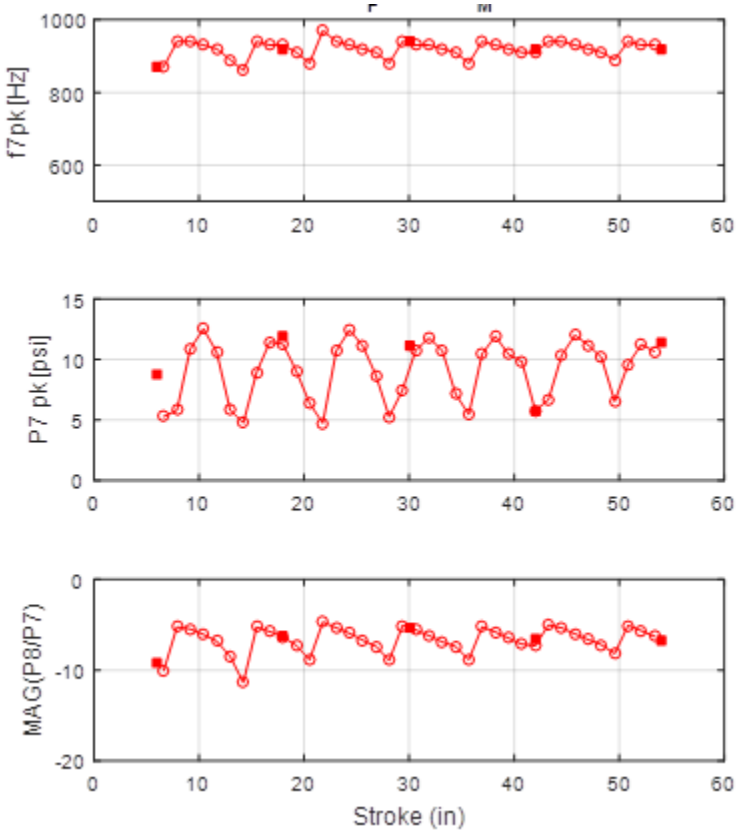

Figure I.8.3. *Frequency, amplitude and pressure ratio at peak dynamic pressure (P7) versus plunger stroke position.*

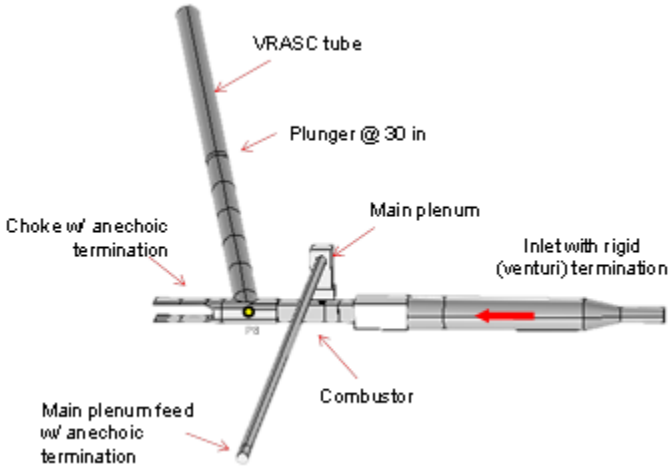

Figure I.8.4. *FEA model of N+3 combustor rig.*

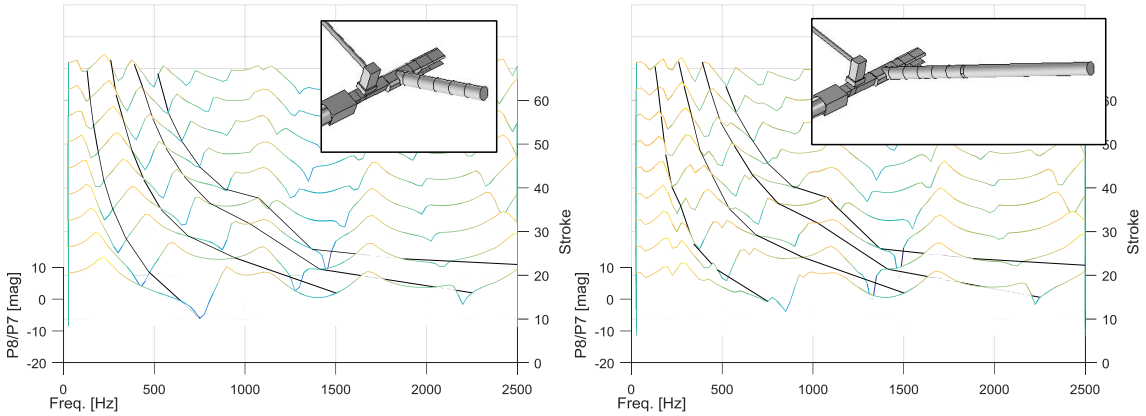

Figure I.8.5. *FEA model predictions of pressure ratio (P8/P7).*

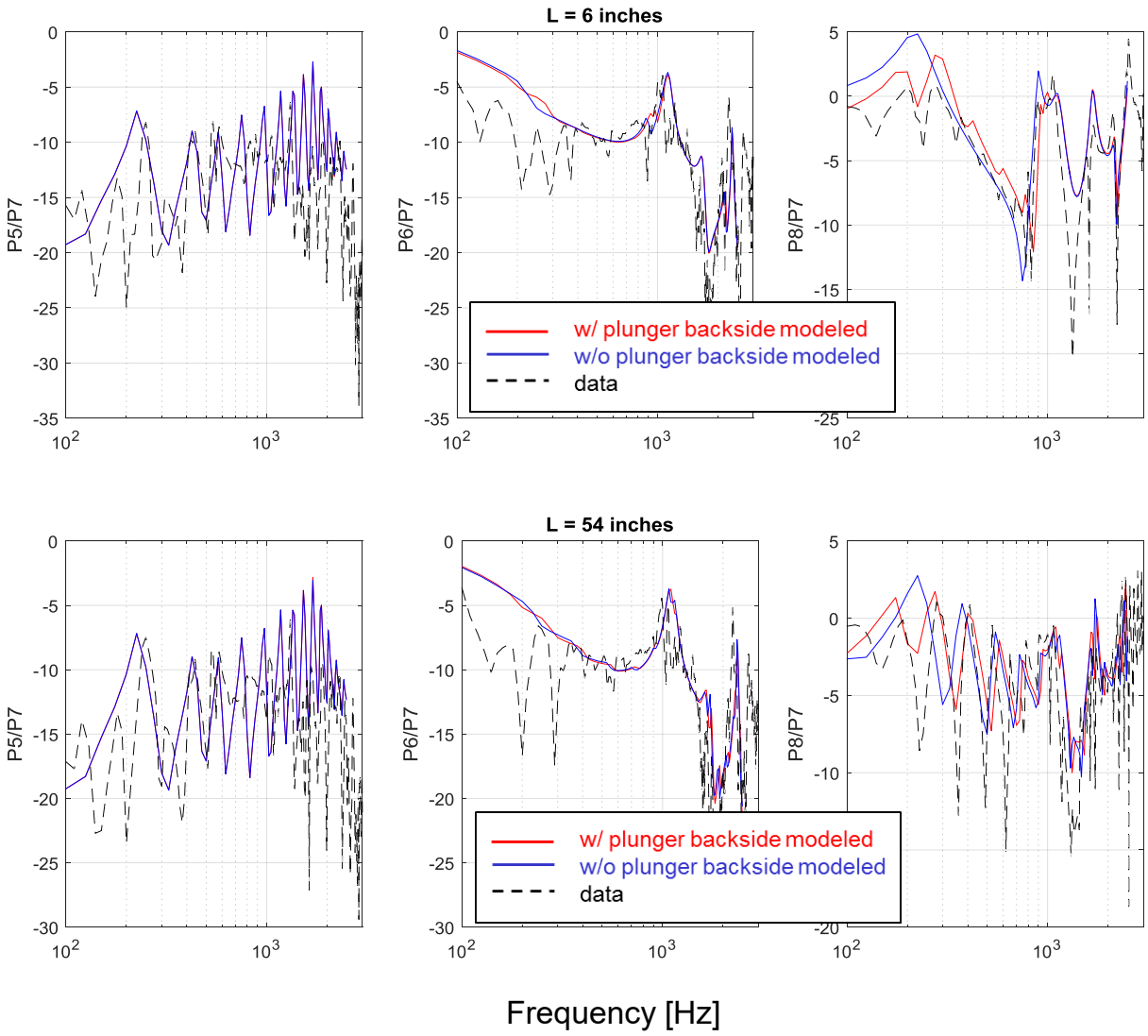

Figure I.8.6. *Comparison of FEA model prediction of pressure ratios versus data.*

The solutions for a range of plunger strokes is shown in Fig. I.8.5 in terms of the pressure ratio P8/P7 without (left image) and with (right image) the backside of the plunger modeled. Both results show the bumps and valleys that move with stroke like the data. The addition of the plunger backside introduces "wrinkles" into the bumps and valleys below 1000 Hz. Figure I.8.6 shows an overlay of the measured pressure ratios. The pilot and main plenum pressures to bulkhead pressure (P5/P7 and P6/P7, respectively) are in good agreement with data for both models and invariant with plunger stroke position. The aft-to-bulkhead pressure ratio (P8/P7) shows better agreement with the data for the model with the plunger backside. In summary, an acoustic model has developed that reasonably captures most of the observed response and can be used to provide modal understanding of the combustor rig.

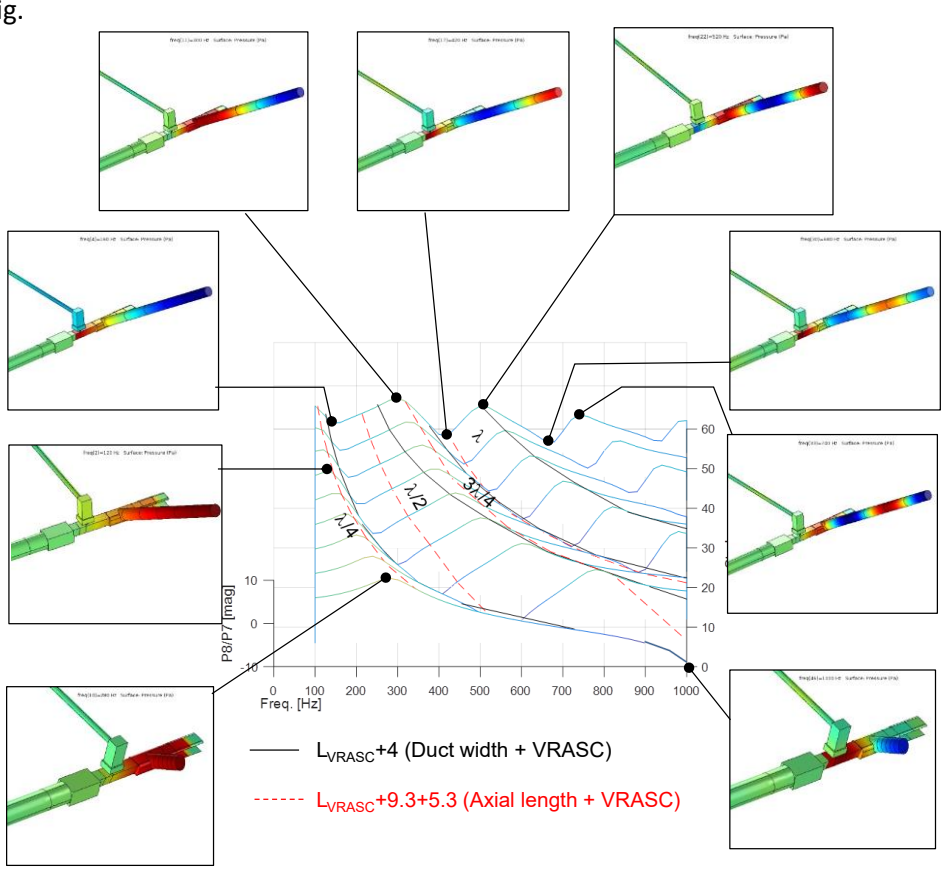

Figure I.8.7. *Pressure mode shapes predicted by FEA model.*

For simplicity, the mode shapes from the model without plunger backside will be examined. Figure I.8.7 shows the P8/P7 pressure ratios, and the associated mode shapes, out to 1000 Hz. Two longitudinal lengths listed at the bottom of the figure were considered for computing the frequency of longitudinal modes using the estimated T4 temperature. The most intuitive length would be to sum the axial length from the bulkhead to the VRASC branch and the stroke of the plunger (LVRASC). The corresponding quarter, half, three-quarter, and full wavelength frequencies are overlaid on the pressure ratio map as red, dashed lines. The quarter-wave frequencies closely map with the first bump for all plunger positions and images of the pressure distribution are consistent with a quarter wave mode shape (rigid, high pressure at plunger and release, zero pressure at bulkhead). At the shortest plunger position, the half wavelength dashed line aligns well with a valley and the corresponding image shows a half-wavelength pressure field, as expect. However, at the longer strokes locations, the bump associated with the high modes don't line up with the red dashed lines. Instead, a longitudinal length that sums

the rig cross-sectional dimension with the plunger stroke appears to better map on to the peaks and value. Examining the images of the mode shapes at the peaks (where the P7 magnitude approximately peaks), the mode appears to mainly exist between the plunger and the opposite wall of the test section, which explains why this length scale maps better in this region. Observing the corresponding pressure at the pilot and mains tends to indicate a velocity anti-node (greenish color), which suggests the airside velocity fluctuations at the injector(s) (and hence fuel-to-air ratios) could be the primary feedback mechanism.

Combustion dynamics testing: Summary of results

Plots of the average acoustic pressure amplitude at P8 (over a sweep of the tunable rig's side-branch plunger) were analyzed for all of the N+3 combustor configurations tested for combustion dynamics. The results showed notable differences in the propensity for the various configurations to excite combustion dynamics.

Results of N+3 combustion dynamics testing on Jet-A versus Rentech (alternative fuel)

Figure I.8.8 shows representative dynamics results comparing Jet-A to alternative fuel (Rentech), for one of the configurations tested. In Figure I.8.8, data are shown for various plunger positions in the tunable UTRC rig (corresponding to different resonant frequencies of the rig) at two different air-inlet operating conditions, idle and approach, but at similar fuel-air-ratios. Amplitude and frequency of the dynamic response is plotted for both fuels. In some cases, the Alternative fuel showed higher amplitudes, and in other cases the Jet fuel showed higher amplitudes. Frequency was not affected by fuel type.

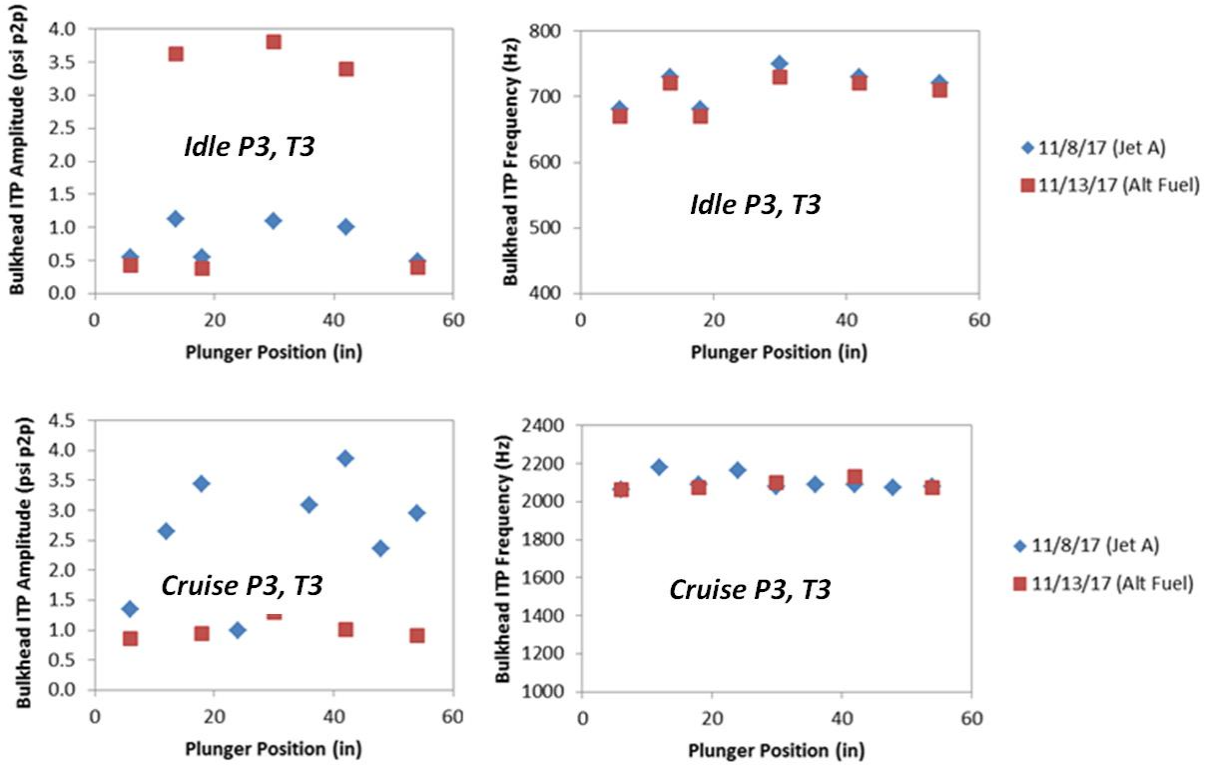

Figure I.8.8. *Dynamics response of UTRC N+3 combustor rig in tunable choked-exit facility, for two different fuels (Jet-A and Rentech alternative fuel). Plunger position was moved to tune the rig.*

Task 9 – Characterize (test) N+3 combustor in NASA CE-5 rig

N+3 Combustor Installation and Testing at NASA CE-5 Site

In addition to fabricating the N+3 combustor rig for NASA CE-5 testing, UTRC also worked with NASA facility personnel during FY2018 to plan and prepare for combustor installation and testing, including discussion of mold design for the CE-5 facility's castable ceramic, instrumentation and interfaces including service lines for the combustor rig in CE-5, and detailed test planning including operating conditions. Note that the CE-5 rig is not capable of the full pressure associated with all of the N+3 cycle points, so the test plan provides reduced-pressure simulation of the test points where necessary. The CE-5 rig can, however, reach the full cycle inlet temperatures for all of the N+3 cycle points to be tested, as well as the full fuel-air ratios (FARs). Additional information regarding the CE-5 combustor hardware and installation was provided in Section I.6 (the Task 6 discussion above). The CE-5 testing and results were discussed in Section I.7 (the Task 7 discussion above).

Task 10 – Management & Reporting

	Program Tasks with Milestones	Schedule																
		2014	2015				2016				2017				2018			
		Q4	Q1	Q2	Q3	Q4	Q1	Q2	Q3	Q4	Q1	Q2	Q3	Q4	Q1	Q2	Q3
Task 1	**Define & specify combustor requirements for N+3 engine**																	
Milestone A:	*Define N+3 engine cycle & combustor envelope*		A															
Task 2	**Layout & design studies for small-core combustor concepts**																	
Milestone B:	*Complete preliminary design of scaled-down ASC combustor for N+3*			B														
Task 3	**Assess alternative-fuel and high-OPR effects on combustor design & performance**																	
Milestone C:	*Select/define alternative fuel(s) for design & testing, & specify relevant chem. & phys. properties*				C													
Task 4	**Sub-component testing at UTRC**																	
Accomplish.:	*Ongoing tests to guide & validate preliminary & detailed design*	<---------->																
Task 5	**Downselect leading concept for single-sector N+3 combustor testing**																	
Milestone D:	*Downselect leading N+3 combustor concept for fabrication*						D											
Task 6	**Detailed design & fabrication of N+3 combustor hardware for UTRC and NASA tests**																	
Milestone E:	*Complete detailed design of N+3 combustor & rig hardware, for UTRC rig tests*								E									
Milestone G:	*Complete detailed design of N+3 combustor & rig hardware, for NASA rig tests*														G			
Milestone F:	*Leading concept designed & fabricated for testing of N+3 combustor at UTRC, at full pressure*										F							
Milestone J:	*Leading concept designed & fabricated for testing of N+3 combustor at NASA, w/ multiple fuels*															J		
Task 7	**Characterize N+3 combustor in UTRC rig at full engine P3 & T3, with 2 fuels**																	
Milestone H:	*Tests of leading concept (N+3 combustor) including measurement of LTO NOx at relevant engine operating conditions, completed in UTRC rig at full cycle P3 & T3*												H					
Milestone I:	*Demonstration of fuel flexibility for emissions and performance on Jet-A and a 50% alternative fuel blend suitable for aircraft use, in UTRC tests of N+3 combustor*													I				
Task 8	**Evaluate combustor dynamics in UTRC tests with variable choked exit, with 2 fuels**																	
Milestone K:	*Dynamics testing completed in UTRC rig with tunable choked exit & 2 fuels*														K			
Task 9	**Characterize air-cooled N+3 combustor in NASA CE-5 tests with multiple fuels**																	
Milestone M:	*Delivery of the leading low emissions concept (N+3 combustor) to NASA, with test matrix*															M		
Milestone N:	*Tests of the N+3 combustor in NASA's CE-5 rig completed with multiple fuels*																	N
Task 10	**Management & reporting**																	
Milestone Q:	*Recurring milestone: Reports completed at the required times (Quarterly, Annual, Final)*		Q	Q	Q	Q	Q	Q	Q	Q	Q	Q	Q	Q	Q	Q	Q	
Milestone R:	*Recurring milestone: Presentations for reviews completed at the required times (Annual, Final)*					R				R				R				R
Task 11	**Combustor transition duct tool development for small core, high OPR engines**																	
Milestone L:	*Complete aero conceptual design for combustor & transition duct in small-core, high-OPR engine*														L			
Task 12	**Design & Fabricate Hardware for Preliminary Testing in NASA's CE-5 Facility**																	
Milestone V:	*Complete & deliver drawings/models of hardware assembly & installation into CE-5 rig*						V											
Milestone W:	*Complete & deliver hardware for preliminary testing in CE-5 rig*								W									
Task 13	**Annular Combustor Test with Vane Pack in P&W's X960 Facility**																	
Milestone X:	*Complete testing of annular ACS combustor in X960 with vane-pack at combustor exit*											X						
Task 14	**Additional Pilot Injector Investigations for N+3 Combustor**																	
Milestone Y:	*Select pilot configuration for N+3 combustor testing in NASA's CE-5 rig*														Y			

Figure I.10.1. *Planned project schedule, for 5-year effort from Oct. 2014 through Sept. 2019.*

Figure I.10.1 above provides the latest task schedule plan for the N+3 combustor effort, including the addition of Tasks 12 and 13 during FY 2016, and the addition of Task 14 during FY2017. At this time (end of Fiscal Year 2019) UTRC has completed all of its milestones for this effort, including delivery of the N+3

combustor rig for testing in NASA's CE-5 facility. The milestones met include the following: A. the N+3 combustor envelope and engine cycle were defined, B. a scaled-down ASC combustor design for N+3 was defined with projections that the N+3 emissions goals could be met, C. alternative fuels were selected and tested for autoignition behavior at UTRC, D. & E. the detailed N+3 combustor configuration was downselected and designed for rig fabrication, F. fabrication of the baseline rig was completed, G. design of hardware was completed for N+3 combustor testing in NASA's CE-5 facility, H. & I. the UTRC combustor rig was installed and tested in UTRC's high-pressure rig using both Jet-A and alternative fuel (a 50-50 blend of Jet-A with Rentech fuel), J. fabrication was completed for all components in the N+3 combustor rig that was delivered to NASA for CE-5 testing, K. combustion dynamics testing on both Jet-A and alternative fuel was performed, L. the cost-share activity to evaluate modeling tools for transition ducts (diffusers) was completed, M. the N+3 combustor rig for NASA was delivered for CE-5 testing along with a test matrix, N. NASA testing of the N+3 combustor was performed, V. & W. main-mixer hardware was fabricated and delivered to NASA for mixing evaluation in CE-5, X. combustion dynamics testing of an annular ACS combustor with vane-pack at Pratt & Whitney was completed, and Y. combustion dynamics testing of alternative pilots for the N+3 combustor was completed. In addition, all technical progress reports and presentations were provided to NASA (milestones Q and R).

Task 11 – Combustor transition duct tool development for N+3 engines

Introduction

Pratt & Whitney funded Task 11 as cost-share toward the overall N+3 combustor development program. The Task 11 objective was to evaluate an improved CFD methodology for diffuser design, i.e. for the transition duct from compressor to combustor. The study began with modeling a Pratt & Whitney Advanced Demo Diffuser Rig (ADDR). A full ADDR data set was selected to evaluate CFD models, and the conclusion from the ADDR study was that LES performs very well for such advanced diffuser while RNS or DES performs very poorly. After this initial study, the PW and UTRC team decided to further evaluate CFD models by modeling canonical diffuser problems published in the literature. These evaluative studies of canonical cases are presented here.

Modeling of Canonical Diffuser Studies

For the FY2018 studies, two canonical cases are considered as described here. The first case involves an annular diffuser with two different blockage parameters, defined as the ratio of boundary layer momentum thickness to the gap height, see Figure I.11.1. The solution domain is a 20 degree sector to reduce computation cost and align with typical combustor modelling practice. The conditions are summarized in table I.11.1. The second case is the experiment conducted by Ashjaee and Johnston, 1980, see reference 1. The experiment setup is shown in figure I.11.2. Detailed diffuser inlet geometry is shown in figure I.11.3. Because the contraction geometry is not available, the modeling domain is starting from the end of the contraction section. The airsolid of the modeling domain is shown in figure I.11.4. The impact of not modeling contraction part to the profile at station 1 is thought to be negligible due to large contraction ratio of roughly 13 and the existence of tripping strip. Flat velocity profile at inlet will be used with turbulence intensity of 0.25%, consistent with the contraction ratio. The magnitude of the velocity at inlet is determined by matching the measured center velocity of 46.6m/sec at station 1. The exit plenum with pressure outlet is also included in the domain with relatively coarse mesh. Diffusers with angle 4,8,10, 12, and 18 are modeled, covering well-behaved, transitory stall and stall regions. The conditions are summarized in table I.11.2.

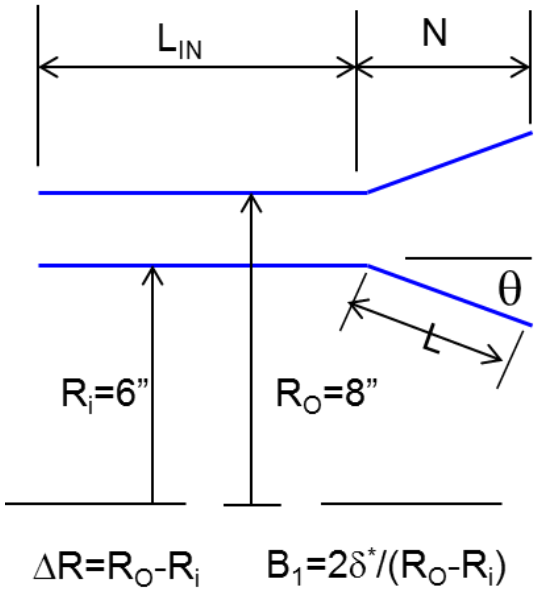

Figure I.11.1 Annular Diffuser

Condition B1=0.0079				Condition B1=0.05		
u	74.86	m/sec		u	74.86	m/sec
Lin	2.4	inch		Lin	20.4	inch
T	70	F		T	70	F
T	294.26	K		T	294.26	K
vis	1.8186E-05	kg/ms		vis	1.8186E-05	kg/ms
P	14.7	psia		P	14.7	psia
density	1.20	kg/m^3		density	1.200	kg/m^3
Re	3.010E+05			Re	2.559E+06	
a	343.85	m/sec		a	343.9	m/sec
M	0.22			M	0.22	

Table I.11.1 Conditions for Annular Diffuser

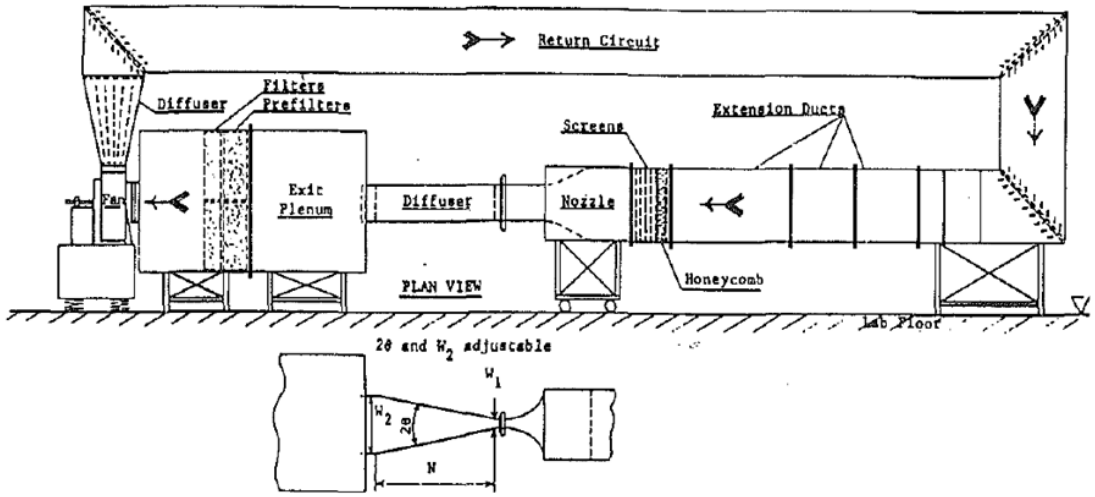

Figure I.11.2. *Ashjaee and Johnston Diffuser Test Setup*

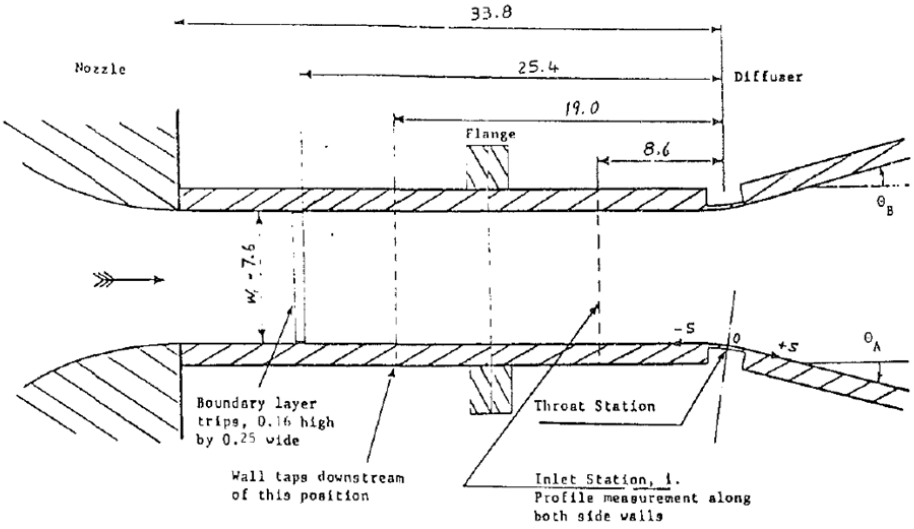

Figure I.11.3. *Ashjaee and Johnston Diffuser Test Setup*

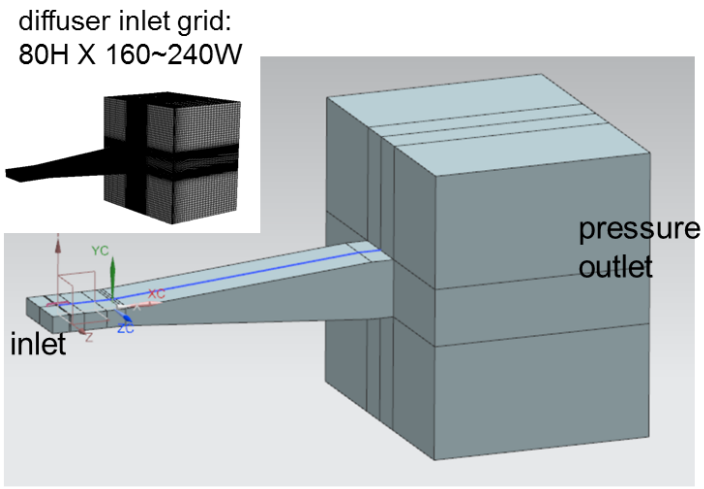

conditions

U free-st1.	46.6	m/sec
w1	7.6	cm
T	88.3	F
vis	1.85E-06	kg/msec
P	14.7	psia
density	1.164	kg/m^3
Re	2.23E+06	

u_τ =2.09m/sec

Figure I.11.4 2D Diffuser

Table I.11.2 Conditions for 2D Diffuser

Modeling Results

For the annular diffuser cases, only well-behaved diffuser are considered, therefore, only realizable k-e model is used. The calculated inlet profiles with various diffuser angles are plotted in figure I.11.5. Table I.11.3 lists the calculated blockage parameter B1, defined as the ratio of the momentum thickness to annular gap height. We can see that the predicted B1 various slightly as diffuser angle changes, due to local flow acceleration at diffuser inlet. The reference B1 values are from the boundary layer correlation for flat plate.

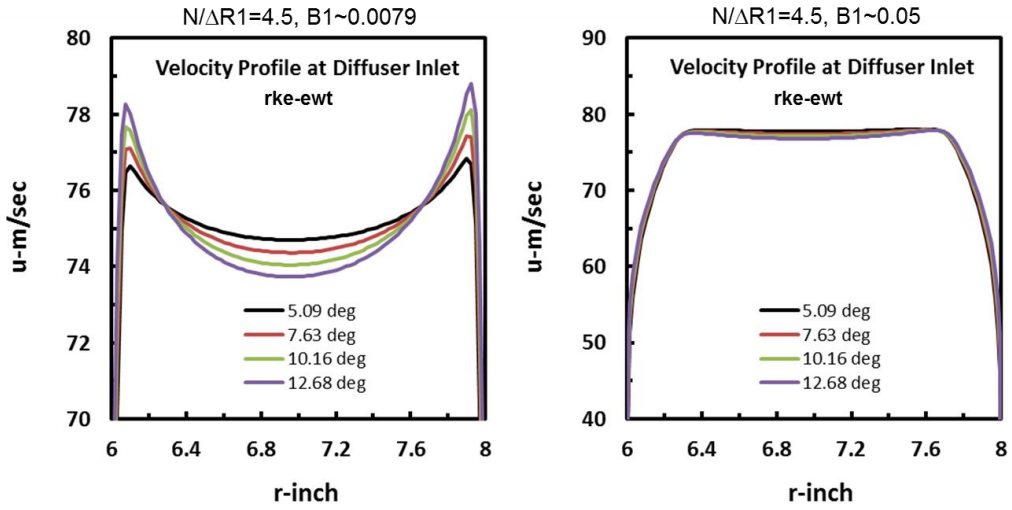

Figure I.11.5 *Velocity Profiles at Diffuser Inlet*

B1-correlation	0.0079
5.09 degree	0.0082
7.63 degree	0.0074
10.16 degree	0.0067
12.68 degree	0.0061

B1-correlation	0.05
5.09 degree	0.04
7.63 degree	0.038
10.16 degree	0.035
12.68 degree	0.033

Table I.11.3 *Calculated Blockage Parameters*

Figure I.11.6 shows the pressure recovery together with the results from Stanford report of Cocanower et. al., 1965, reference 2. Because B1 various slightly, Stanford results for both B1=0.03 and 0.05 are plotted. We can see that CFD agrees with Stanford report very well.

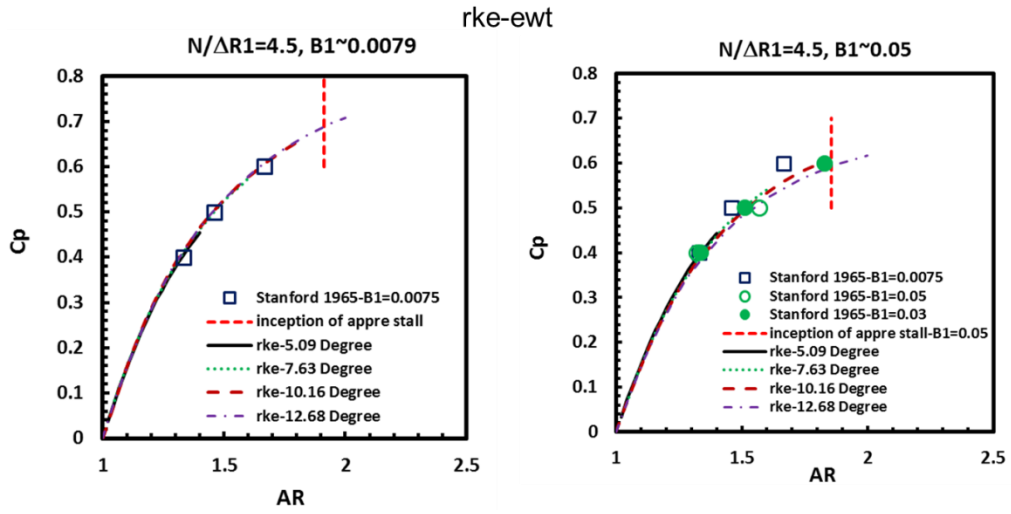

(a) B1~0.0079 (b) B1~0.05

Figure I.11.6 *Pressure Recovery of Well-Behaved Annular Diffuser*

For the second case, i.e. 2D diffuser, Figure I.11.7 shows the typical mesh with boundary layer mesh. At the beginning, mesh targeting y+<1 is constructed. However, it is found that because of y+1 requirement and mesh size limit, grids with very large grid aspect ratio exist along the diffuser walls, which results in convergence and solution issues. Therefore, mesh following Fluent grid guideline for enhanced wall-treatment is constucted, i.e., y+ around 50 (300>y+>30) for the attached flow, y+<5 for separation region, and grid aspect ratio around 20 (<100). Generally speaking, y+ is lower in the separation region so that y+<5 is usually satisfied. If y+<5 in the separation region is not satisfied, grid adaption can be applied. The other choice will be re-gridding. However, re-gridding is not preferred because grid aspect ratio may become an issue again. Figure I.11.8 shows the adapted grid. The impact of grid to pressure recovery, Cp, for 12 degree case is shown in figure I.11.9. Before adaptation, some area in the separation zone has y+ value greater 30, where wall function is not valid. We can see that there's some improvement due to grid adaptation to reach y+<5 in the separation region.

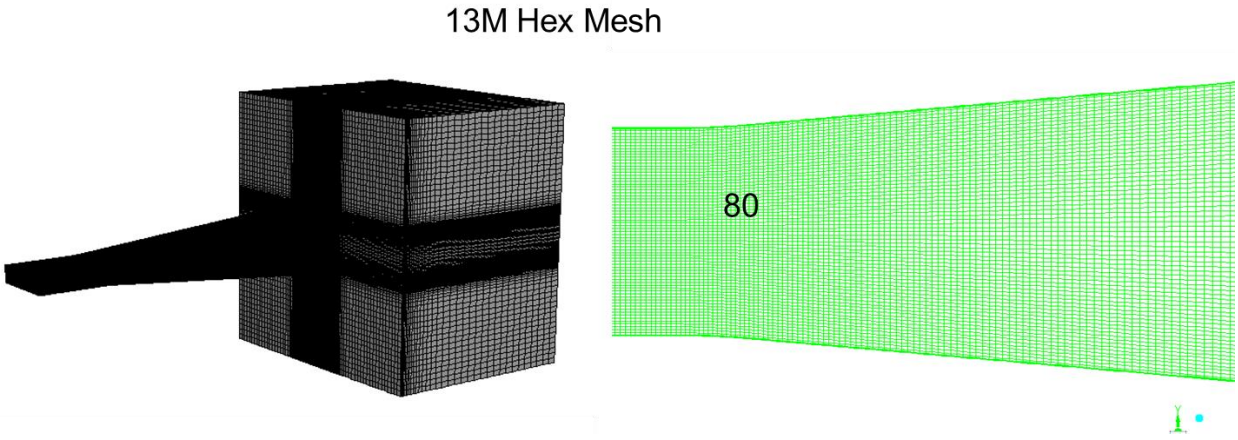

Figure I.11.7. *Mesh for Ashjaee and Johnston Diffuser Test Case*

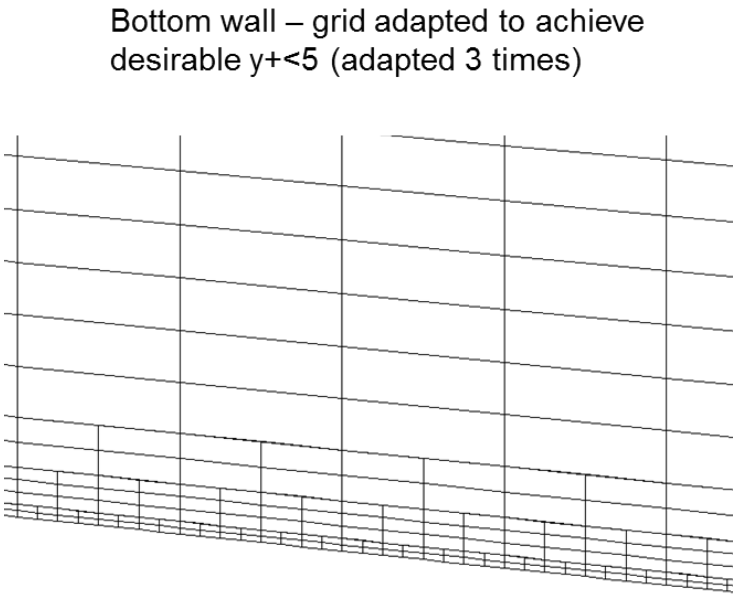

Figure I.11.8. *Mesh for Ashjaee and Johnston Diffuser Test Case*

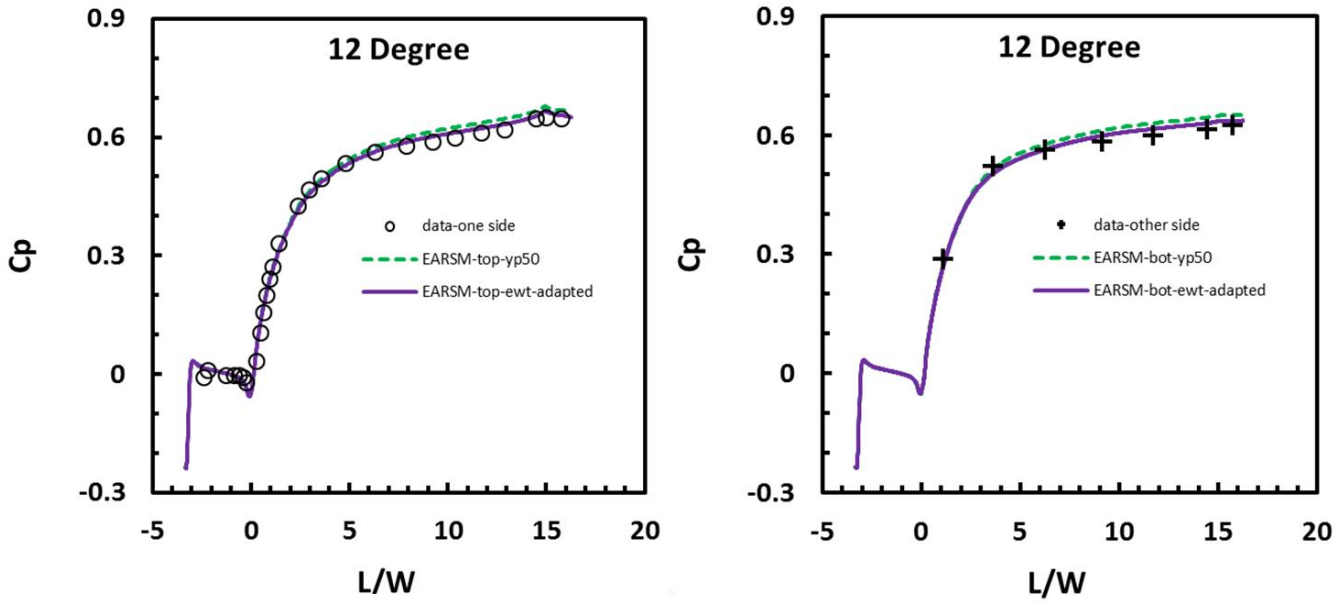

Figure I.11.9. *Impact of Grid Adaptation to Pressure Recovery*

Figure I.11.10 shows the diffuser inlet profile at station 1.0, which is located at 3.4 inch upstream of the diffuser inlet. Generally speaking, profiles with grid following Fluent guideline of enhanced wall treatment (ewt) matches with the data better.

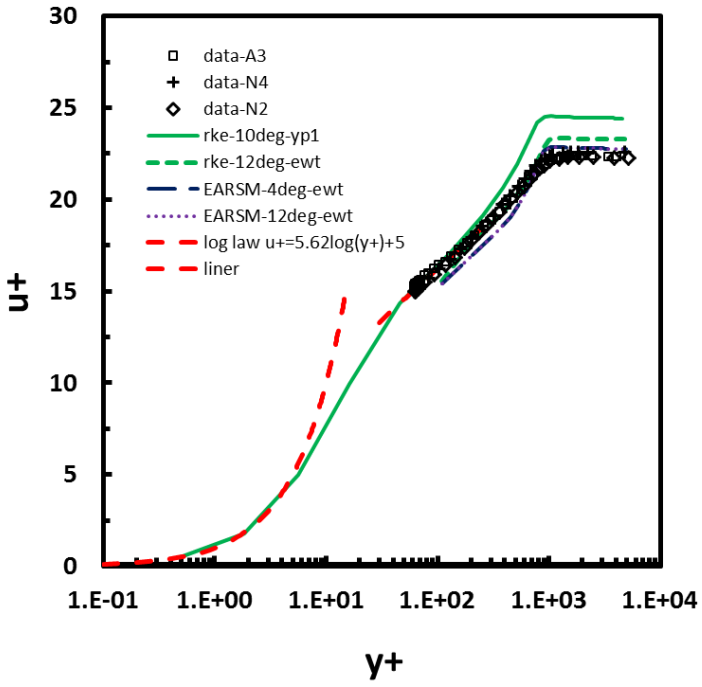

Figure I.11.10. *Comparison of Predicted to Measured Profile at Station 1.0*

Figure I.11.11 shows the comparison of predicted to measured pressure recovery Cp for 4 and 8 degree cases. Pressure recovery is defined as the static pressure difference from station 1 divided by dynamic head at the edge of the boundary layer at station 1. We can see both rke and EARSM match with the measurement well, with EARSM slightly better. Figure I.11.12 shows the pressure recovery for 2D diffuser with transitory stall. Due to fail to predict separation, rke overpredicts Cp from L/W~3 to the end, see in figure I.11.13 and I.11.14. EARSM matches with the measured Cp very well. The predicted separation points by EARSM are at L/W=12 and 6 for 10 and 12 degree, respectively, which are close to the measured separation points at L/W=8 and 5 for 10 and 12 degree, respectively, considering the uncertainty of the measurements, see figure I.11.15 and I.11.16. Figure I.11.16 shows the pressure recovery for 2D diffuser with stall. For the 18 degree stall case, rke still over predict Cp due to fails to predict separation while EARSM performs reasonably well, see figure I.11.17 and figure I.11.18. From roughly L/W=0 to 5, EARSM slightly under predict Cp for the 18 degree case because the detail flow structure inside the separation zone is difficult to predict accurately. Velocity data is needed to address this issue. For the 24 degree stall case, only rke is converged while EARSM using refined grid failed to converge, which needs further investigation to see if grid aspect ratio is still too high for the refined grid. rke slight over predicts Cp with right tred. rke it is able to predict a separation zone, see figure I.11.19 and I.11.20.

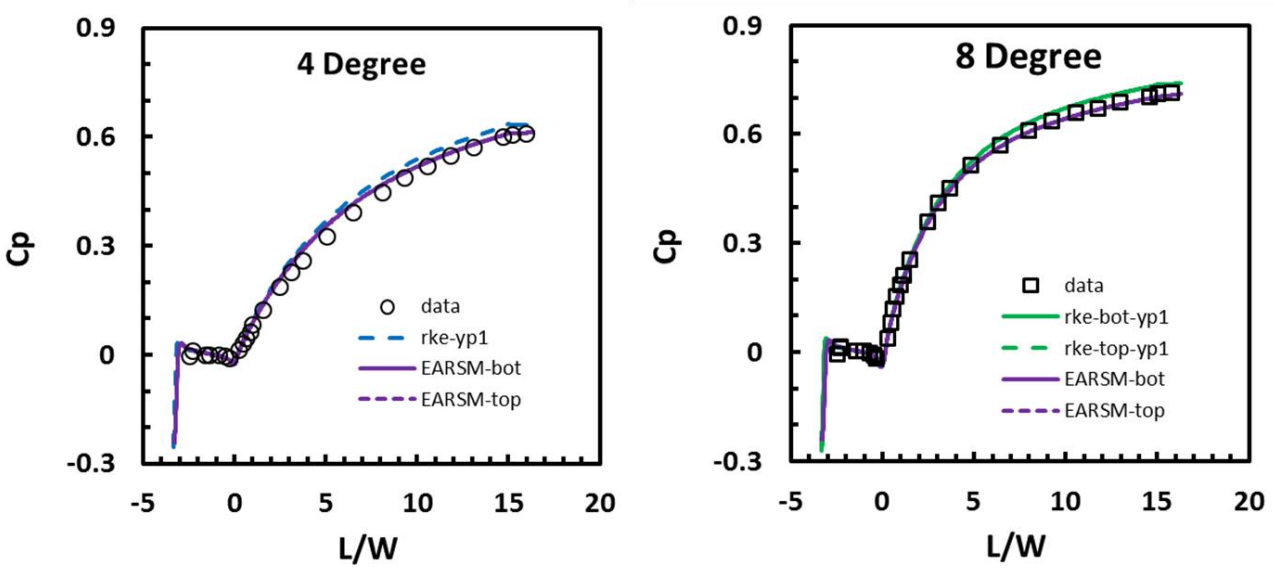

Figure I.11.11 Cp of Well-behaved 2D Diffuser

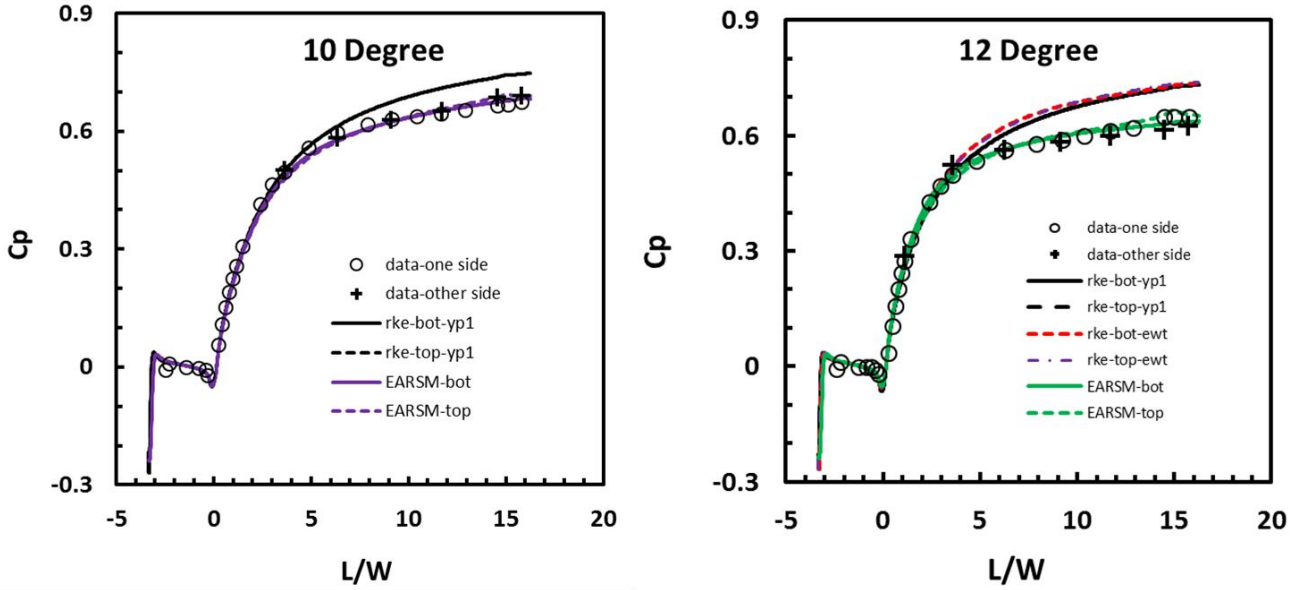

Figure I.11.12 Cp of 2D Diffuser with Transitionary Stall

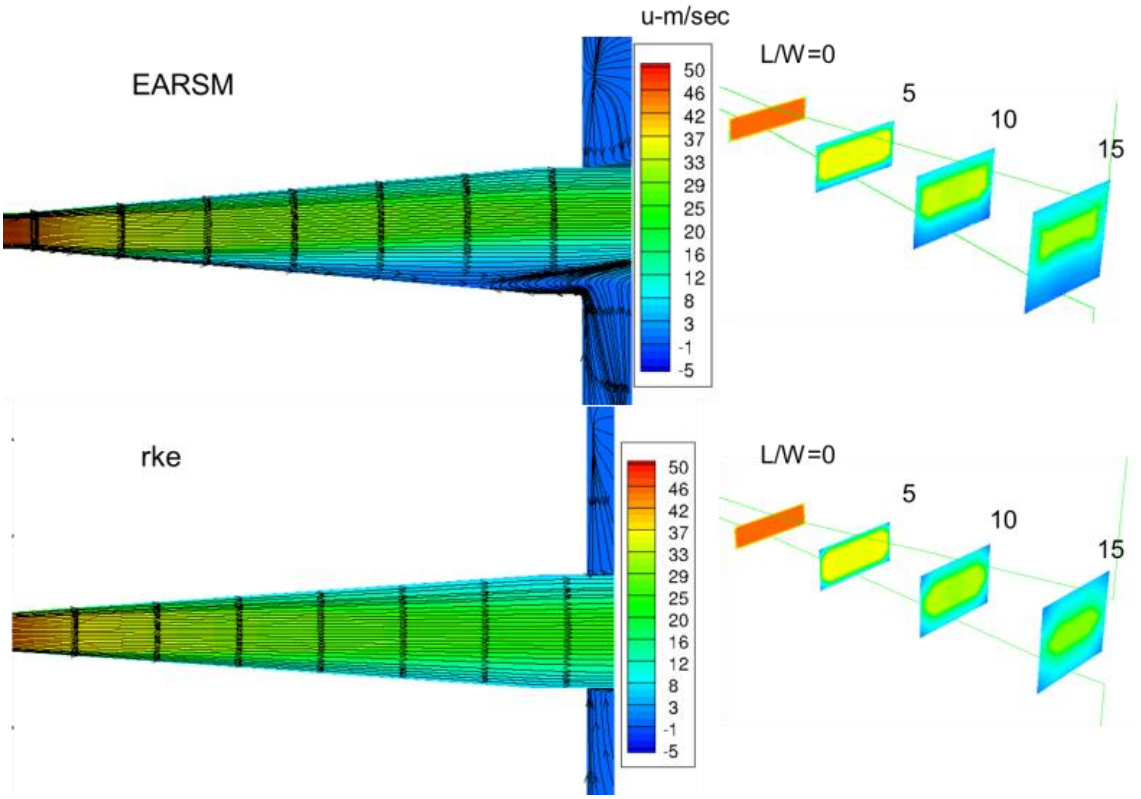

Figure I.11.13 Velocity Plot of 2D Diffuser with 10 Degree Full Angle

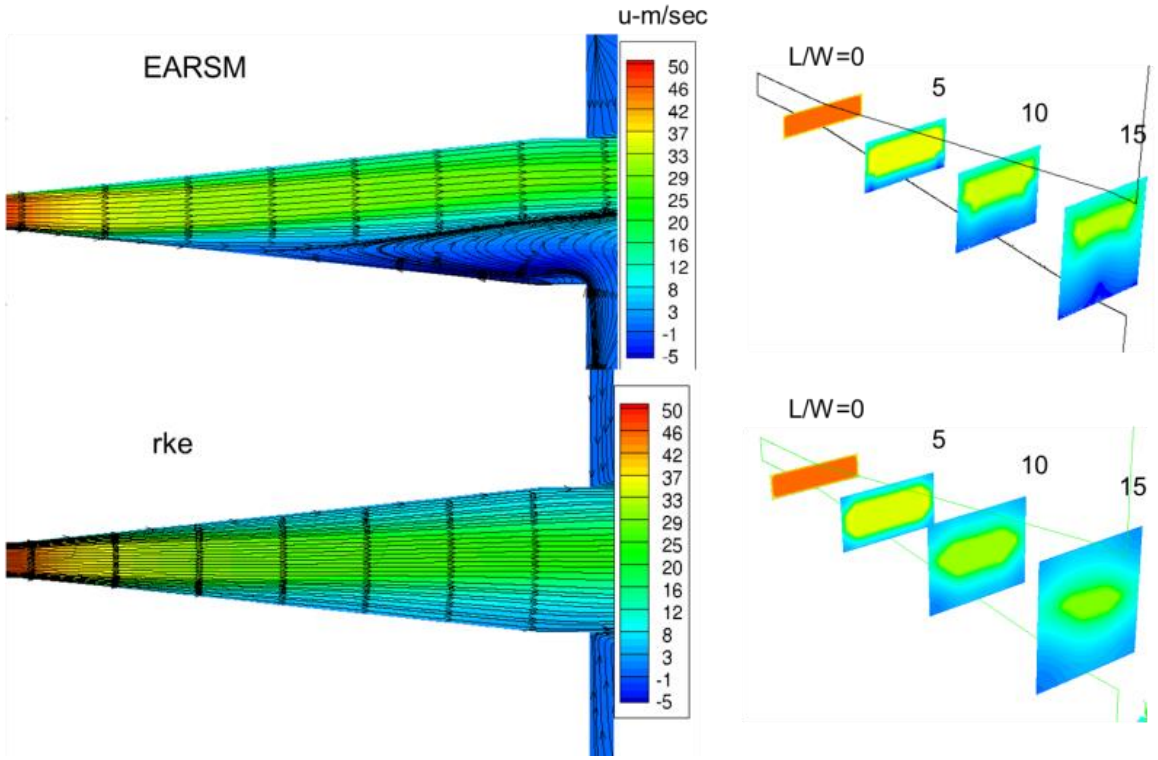

Figure I.11.14 Velocity Plot of 2D Diffuser with 12 Degree Full Angle

EARSM

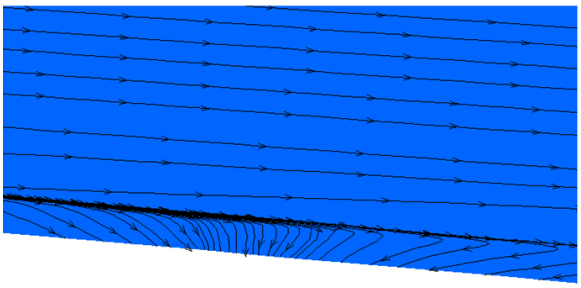

Separation point ~Ls/w=12 (midplane)

Data

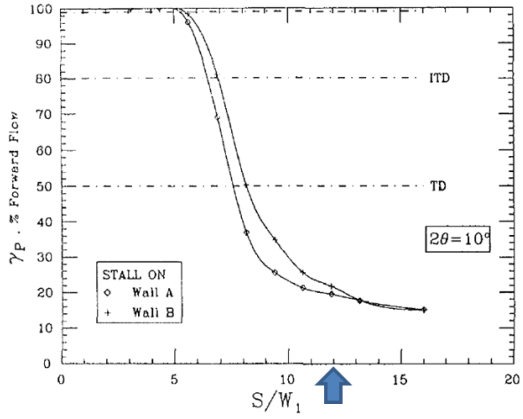

Figure I.11.15 Separation Point for 10 Degree Case

EARSM

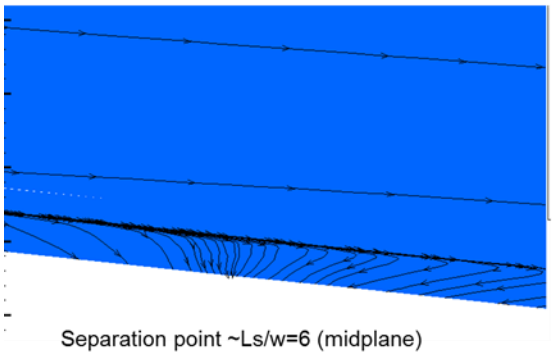

Separation point ~Ls/w=6 (midplane)

Data

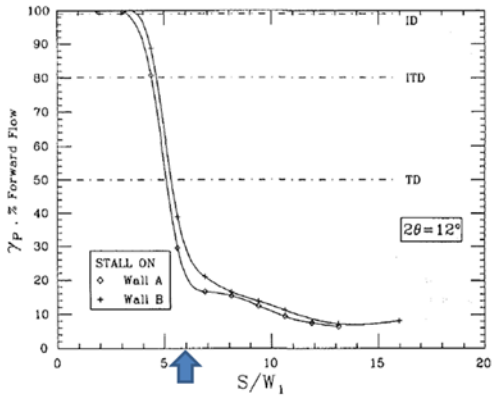

Fig. 9 Flow direction intermittency along diffuser wall, 2θ = 12 deg. Uncertainty in γ_p = ± 1 percent (20:1 odds).

Figure I.11.16 Separation Point for 12 Degree Case

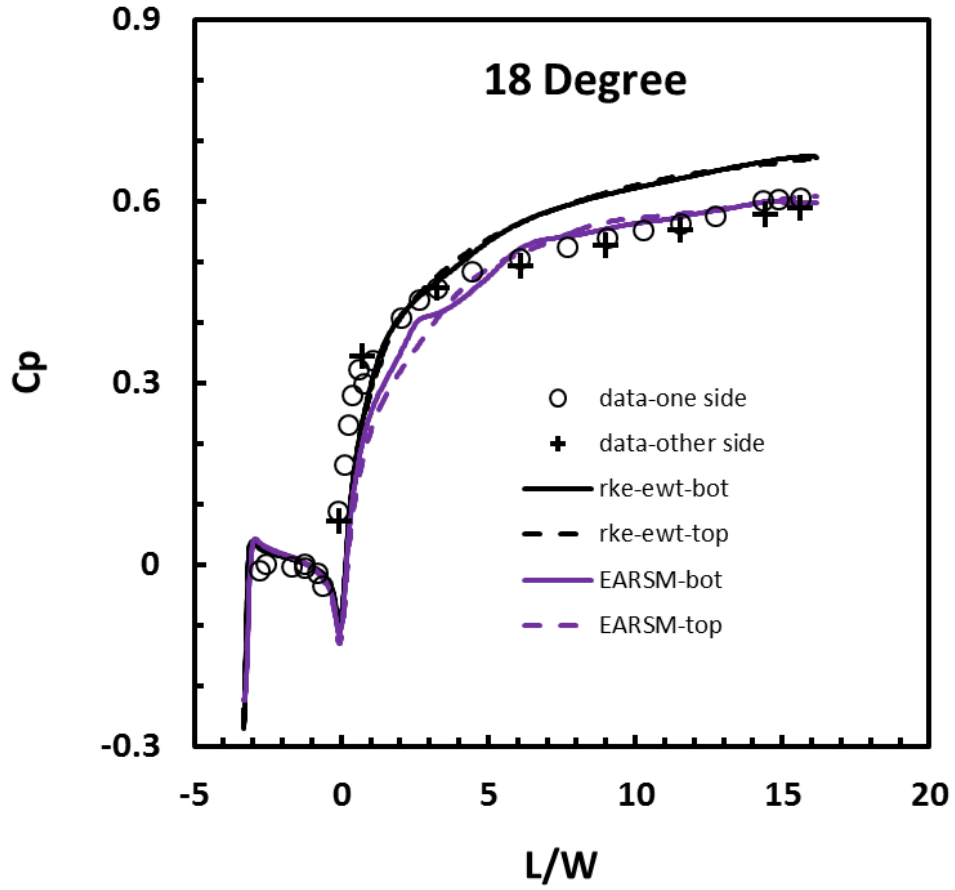

Figure I.11.17 Cp of 2D Diffuser with 18 Degree Full Angle

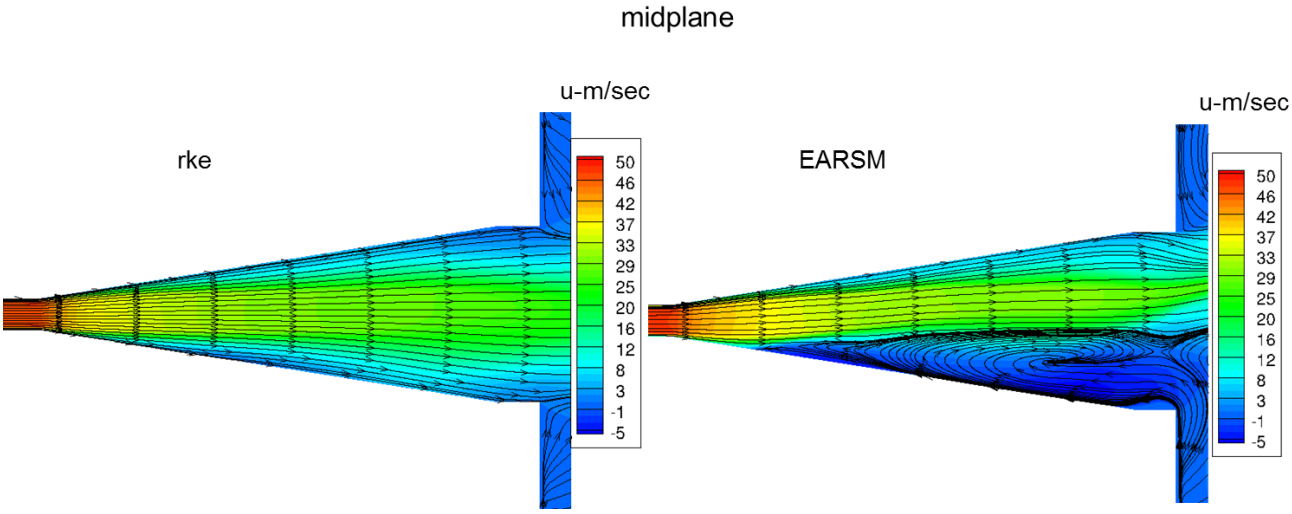

Figure I.11.18 Velocity Plot of 2D Diffuser with 18 Degree Full Angle

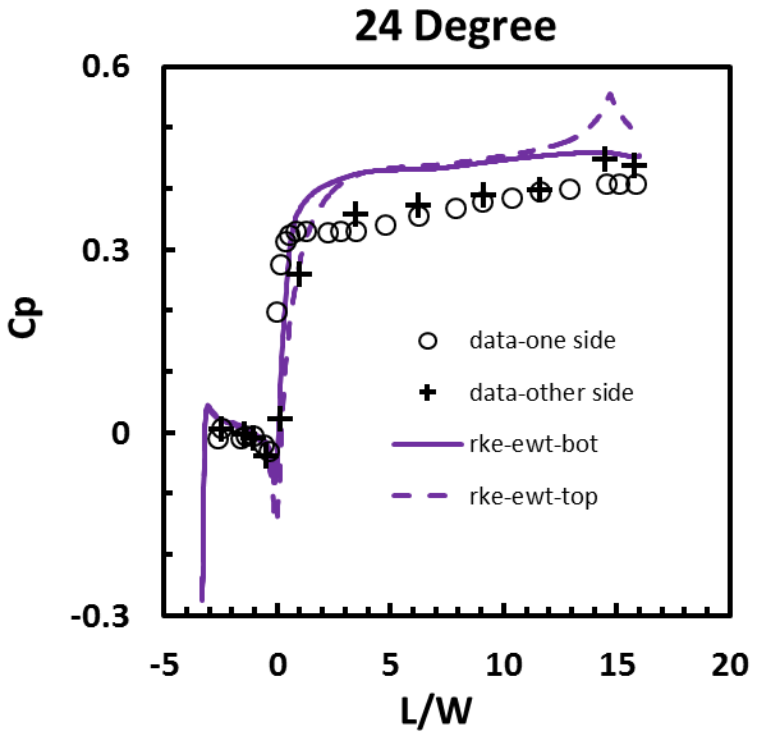

Figure I.11.19 Cp of 2D Diffuser with 24 Degree Full Angle

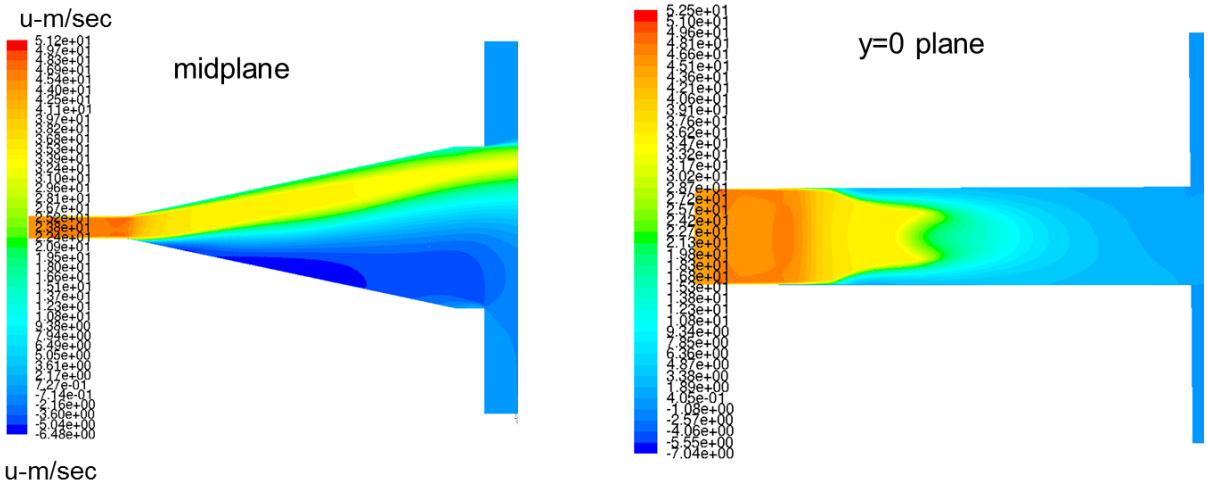

Figure I.11.20 Velocity Plot of 2D Diffuser with 24 Degree Full Angle

Summary

Based on the modeling studies of P&W diffusers, it was found that the RNS-LEVM (linear eddy viscosity model, e.g., rke, kw-sst) performs reasonable well for well-behaved diffusers, including PW well-behaved combustor diffuser. RNS-LEVM performs poorly for PW aggressive combustor diffuser design (ADDR) with high prediffuser angle. ADDR LES modeling (wall function/wall modeled) with 3.1 probe support matches with the measurements very well. Based on the modeling studies of canonical diffusers reported here (in this report) the rke model over-predicts Cp for 2D diffusers with transitory stall and full stall. Explicit Algebraic Reynolds Stress Model (EARSM) performs well for well-behaved 2D diffusers, 2D

diffusers with transitory stall and full stall. It is recommended to follow Fluent grid rule for enhanced wall treatment (ewt), i.e., y+ ~50 (300>y+>30) for attached flow region, y+<5 for separation region, and grid aspect ratio~20<100.

Finally, during 2018 a technical paper reporting the results of this task (as funded by Pratt & Whitney) was written and submitted to AIAA (the American Institute of Aeronautics and Astronautics) for publication and presentation at the AIAA SciTech conference in January 2019. The title of the paper is "Evaluation of a CFD Design Tool for Gas Turbine Diffusers," and the paper reports results from evaluations of multiple candidate CFD methods for efficient prediction of diffuser performance. The goal was to identify a tool capable of providing accurate and timely predictions useful for advanced gas turbine combustor system diffuser designs, and to verify that tool against literature data from canonical diffuser experiments (depicted in Figures I.11.1 through I.11.4).

Task 12 – Design and Fabricate Hardware for Preliminary CE-5 Testing

During Calendar Year 2016 a cost proposal and statement of work was submitted to NASA, for additional UTRC tasks to support CE-5 testing in 2016 (adding to the scope of the original contract). The proposal was accepted and the contract was modified and signed on December 15, 2015 to add Task 12 to the original scope of work for the N+3 combustor effort. The added scope included design, fabrication, and delivery of test hardware for NASA testing in 2016, as well as engineering support for NASA testing of this hardware, including test planning and preparation, and data analysis. This task supported stand-alone testing in NASA's CE-5 rig of main combustor fuel-air mixers at a size relevant to N+3, for capturing data at the mixer exit including fuel evaporation and mixedness using CE-5's laser diagnostics capabilities.

During the first half of 2016, UTRC designed and fabricated the hardware, and delivered it to NASA in June 2016 for testing. From the data acquired at NASA we observed several qualitative trends, which were consistent with our expectations and predictions:

- Mixing is improved at higher mixer (swirler) pressure drop.
- Evaporation is improved at higher inlet temperature.
- Mixing appears to be weakly affected by total pressure.

The results provided input and validation of our approach for main-mixer design for the N+3 combustor.

Task 13 – Annular Combustor Test with Vane Pack in P&W's X960 Facility

During FY 2017 testing was completed for the full-annular ACS combustor with a vane-pack in Pratt & Whitney's X960 annular combustor test facility. The data were analyzed to positively identify the acoustic modes, and were examined and reviewed with Pratt & Whitney to extract learning and highlight any phenomenon of particular interest.

Executive Summary

In support of combustor development for N+3, an existing ACS (Axially Controlled Stoichiometry) full annular combustor was tested for combustion dynamics in Pratt & Whitney's X960 facility. This combustor was previously designed and fabricated by Pratt & Whitney and UTRC with NASA support under the ERA Phase-II low NOx combustor program, and was tested for emissions performance under that program. For the testing reported here, an existing Pratt & Whitney engine vane-pack was placed at the combustor exit, and acoustic instrumentation was added to the combustor and facility. The X960 facility's emissions probes were removed since they were not compatible with the vane-pack, and since

the focus of the tests reported here was combustion dynamics, not emissions. The complete test assembly included an inlet diffuser, diffuser/combustor case, combustor, and vane-pack, and thus provided an accurate representation of an engine's combustor geometry and acoustic boundary conditions.

Combustion tests of this configuration showed significant combustion dynamics (excited acoustic tones) when only the pilot was fueled, and also when both the pilot and main stages were fueled. Measured amplitudes at the frequency peaks were as high as 13.2 psipp (pilot only) and 10.6 psipp (pilot and mains). For pilot-only operation the dominant tone's frequency was near 600 Hz (with amplitudes up to 13.2 psipp), and there was also some acoustic excitation in the 400 - 450 Hz frequency range (with amplitudes closer to 1 psipp or less). For operation with fuel to both the pilot and main stages, the frequency characteristics were generally opposite: the dominant tone's frequency was near 400 Hz (with amplitudes up to 10.6 psipp), and there was also some acoustic excitation in the 550 - 600 Hz frequency range (with amplitudes closer to 1 psipp or less); in addition, a small (~1 psipp) tonal peak near 800 Hz (a harmonic of the 400 Hz mode) was sometimes evident when the main stage was fueled.

The measured 600 Hz tone was identified as a tangential mode, which can only truly exist in an annular combustor test such as this one. The measured 400 Hz tone was identified as a bulk mode, which is specific to an engine's entire combustor-section module, which was accurately replicated in this test from diffuser inlet to vane exit. Thus, the test results reported here provide a unique and valuable data set that are relevant to a real engine application of the ACS combustor. In general, the major learning from these tests was as follows:

1. The pilot, as designed for this ACS combustor, was dynamically unstable on its own (i.e. without fuel from the main-stage contributing to the acoustic oscillations).
2. Acoustic amplitudes due to combustion were significant, especially at frequencies associated with the 1st tangential mode in the combustor (as enabled by this full annular test configuration).
3. Multiple acoustic frequencies were excited, with the peak frequencies being dependent upon operating condition.
4. To reduce risk for N+3 combustor development, and to reduce risk for future engine testing of the ACS combustor, further investigation of ACS combustion dynamics including the pilot is recommended.

Separate combustion dynamics tests of the N+3 ACS combustor are planned for UTRC's single-sector facility in late 2017. The single-sector rig cannot exactly replicate the tangential and bulk acoustic modes of an engine, but with its tunable side-branch ("trombone") it can replicate the frequencies associated with these modes. The X960 ACS test results summarized above will provide valuable guidance about which acoustic modes are of most interest, and which frequency bands should be targeted in the UTRC combustion dynamics tests.

Motivation & opportunity for annular rig tests of combustion dynamics

Pratt & Whitney and UTRC have been developing Axially Controlled Stoichiometry (ACS) lean-burn combustor technologies with the support of NASA since 2010, when NASA awarded its Phase-I ERA (Environmentally Responsible Aircraft) low-NOx combustor development contract. The Phase-I effort provided proof-of-concept demonstration of the ACS combustor, showing its potential for achieving ultra-low emissions in jet-fueled aircraft. Details are provided in the Phase-I final report to NASA for contract NNC10CA11C. A follow-on ERA Phase-II effort further developed the ACS combustor for N+2 aircraft applications, providing demonstration of a full annular combustor designed to fit an existing Pratt & Whitney engine envelope (see the Phase-II final report for contract NNC10BA12B, Task Order

NNC13TA45T). Both the Phase-I and Phase-II demonstrations focused on combustor emissions, and did not specifically explore combustion dynamics, i.e. combustion-induced pressure oscillations. However, because combustion dynamics are often associated with lean-burn combustion devices such as the ACS combustor, this remained an open risk item at the end of the ERA program.

The present N+3 combustor project is using the ACS concept developed under ERA as a basis for developing a small-core, low-emissions combustor for future N+3 aircraft. This effort is also advancing ACS combustor technology by working to further reduce pollutant emissions, and by addressing technology risk items such as combustion dynamics. UTRC's single-sector N+3 combustor rig will be used to test for combustion dynamics at pre-selected acoustic resonant frequencies. However, without acoustic data from an engine-like ACS combustor, the selection of frequencies (acoustic modes) for single-sector testing would have no experimental basis, and would be guided by only limited information about the underlying physics.

A better approach is to acquire test data for an annular ACS combustor under acoustic conditions that exactly replicate an engine installation, and then use that data to inform the selection of test frequencies for the single-sector rig. For this purpose, NASA provided funding under the N+3 combustor project to install and test the existing ERA Phase-II full annular combustor in the X960 test facility, coupled for the first time to a turbine vane pack provided by Pratt & Whitney, to determine which acoustic modes are prone to combustion dynamics. The results of these tests are reported here.

Existing full-annular rig components (ERA Phase-II ACS combustor, and P&W vane pack)

The full annular combustor from the ERA Phase-II program was used for the testing reported here. The ERA Phase-II annular ACS combustor was tested at Pratt & Whitney's X960 facility under the ERA program without a vane-pack. For those tests, instead of a vane-pack, the X960 rotating emissions rake was inserted into the combustor exit to obtain emissions measurements. For the combustion dynamics testing reported here, however, the full annular combustor was attached to a first-stage turbine vane-pack supplied by Pratt & Whitney. Fitting of an existing vane-pack at the combustor exit was possible because the ERA Phase-II ACS combustor was designed, by intent, to be compatible with installation in a Pratt & Whitney engine, including mating to the engine's vane-pack.

The exit area between the vanes' trailing edges establishes the minimum flow area for the combustor exhaust gases: here the flow velocity approaches Mach one in an engine, and this choked condition largely establishes the flow versus operating pressure characteristic of an engine. In addition, the small flow area and high Mach number cause the vane-pack to reflect acoustic energy back into the combustor, thus making the combustion chamber a resonant acoustic cavity (susceptible to combustion dynamics). With the vane-pack installed, these same phenomena occur in both engines and rigs, so that combustion rig testing provides a good simulation of engine operation both in terms of combustor operating conditions (flow versus pressure) and in terms of acoustic properties of the combustion chamber (and therefore combustion dynamics).

Finally, it is worth noting that the upstream features of the existing annular ACS combustor rig from ERA Phase-II are also representative of an engine installation, and capture engine-like acoustic boundaries. The existing ERA Phase-II rig includes the prediffuser, case, inner shrouds, as well as the combustor. With the vane-pack installed for the tests reported here, the complete annular ACS rig as installed at X960 provides an accurate representation of engine combustor acoustics, and provides a valuable platform for testing ACS combustion dynamics.

Combustor Instrumentation

Under ERA Phase-2, limited acoustic instrumentation was installed on the annular ACS combustor and was only provided for the purpose of health and safety monitoring, since the focus of the ERA Phase-2 testing was to evaluate combustor emissions. Therefore, in preparation for combustion dynamics testing under the current effort, the annular ACS combustor was returned from the P&W test site to UTRC for installation of additional instrumentation. The added instrumentation included ITP (Infinite-Tube Probe) sense-lines for measuring dynamic pressures, thermocouples for monitoring combustor panel temperatures (since heat transfer loads can increase when combustion dynamics induce oscillatory flows near the panels), and proof-of-light thermocouples to monitor the presence of combustion (in the absence of the rotating thermocouple rake that was used together with the emissions rake during emissions testing under ERA Phase-II).

Six ITP pressure-taps were installed on the ACS annular combustor itself, two ITP pressure-taps were installed on the combustor case, and one ITP pressure-tap was installed aft of the vane-pack to monitor the facility exhaust path. In addition, a Kulite transducer was mounted in each of the fuel circuits (four total) to monitor dynamics pressures in the fuel system. In the combustor, four of the ITP taps were axially in-line at the same circumferential location, to provide information about acoustic amplitude and phase at different axial locations, thus enabling identification of axially-propagating acoustic modes. Similarly, three of the ITP taps were circumferentially in-line at the same axial location, to provide information about acoustic amplitude and phase at different circumferential locations "around the wheel," thus enabling identification of circumferential acoustic activity such as tangential or spinning modes.

Before installation in the X960 facility, all of the ITP sensors were inspected, pressure-tested, refurbished as necessary, and calibrated at UTRC to relate input pressure signal to output electrical signal. The calibrations were then applied in the X960 data acquisition and storage system to provide dynamic pressure data in engineering units (psi). During data acquisition at X960, the ITP output electrical signals were anti-aliased by applying a 100 kHz analog filter prior to A-to-D conversion at 500 kHz. The resulting digital data were then downsampled to 10 kHz after applying a 4 kHz digital Butterworth filter, and were stored as alias-free 10,000-cut (10 kHz data sample rate) pressure data in psi units.

In addition to the newly-installed dynamic-pressure taps for the ITPs, multiple static-pressure taps remained installed following the ERA Phase-II testing. These static-pressure taps were used to monitor combustor liner pressure drops, airflow splits, and diffuser pressure recovery. Since combustor performance had been previously tested under EAR Phase-II, the primary purpose of this instrumentation during the dynamics testing was to confirm that combustor operation was consistent with previous experience.

Finally, in addition to the pressure instrumentation, the annular ACS combustor was also fitted with multiple thermocouples to monitor metal temperatures (e.g. the combustor liner) as well as to monitor the presence of combustion or "proof of light." Some of these thermocouples were installed prior to testing under ERA Phase-II, but additional thermocouples were added by UTRC for the tests reported here. Specifically, two each of the aft OD and ID panels were removed and type K thermocouples were applied directly to the metal, on the side facing away from the combustor to allow egress of the thermocouple wires. In addition, UTRC added 12 proof-of-light thermocouples by drilling through the aft panel studs and inserting type B thermocouples slightly into the combustion gas path.

Vane-Pack and Vane Instrumentation

Because the ACS annular combustor was designed to fit an existing engine, an existing engine vane-pack was able to be mounted at the combustor exit to provide an engine-like acoustic boundary condition. In addition, because this vane-pack had been previously used at X960 for testing another combustor, hardware to mount the vane-pack in the X960 rig already existed and was available for use. This hardware included the vane-pack itself, the TOBI (tangential on-board injection) mounted to the vane-pack ID, feather-seal hardware mounted to the vane-pack OD, an ID heat-shield immediately aft of the TOBI, and a water-cooled OD heat-shield immediately aft of the feather-seal hardware. Flow versus pressure-drop characteristics (effective areas) were measured for all of these components prior to testing at X960, to enable determination of airflow split between the combustor and the vane cooling passages (including the TOBI, which cools the first turbine blade row in an engine, as well as leakage paths and simulated BOAS or blade outer air seal air).

Prior to the ACS combustion dynamics testing, Pratt & Whitney refurbished and re-instrumented the vane-pack to ensure all cooling flowpaths were clear, the sealing surfaces were clean, and instrumentation was available to monitor pressure drops and flows in the vane-pack and surrounding components. For this purpose pressure taps were provided on the aft vane platform and also on the TOBI and ID heat-shield. On the OD aft vane platform, one of the pressure taps was dedicated to an ITP sense-line, to provide a measure of acoustic amplitude and phase downstream (aft) of the vane-pack.

Facility installation & fuel system

Both the combustor and vane-pack had been previously tested at X960 under separate prior programs, but they had not been previously tested together. Therefore a detailed solid-model was created of the complete assembly in the X960 rig, to ensure that all interface details were correct and that all needed components were identified, specified, and procured (and were tracked in a Bill of Materials document generated specifically for this test).

For testing of the ACS annular combustor, four fuel manifolds were provided, corresponding to four separately controllable fuel circuits. Three of these circuits provided fuel to the pilot injectors, in a staged arrangement that allowed fuel shifting for evaluating combustion dynamics response. Dynamic pressure sensors (Kulites, or microphones) were installed in each of the fuel circuits to monitor acoustic response of the fuel system to combustion dynamics.

Analysis

An unsteady pressure signal can be represented as the sum of a mean pressure and an unsteady pressure:

$$p = \bar{p} + p'$$

$p =$ pressure
$\bar{p} =$ mean pressure
$p' =$ unsteady pressure

The unsteady pressure, in turn, is a sum of tonal pressure waves of varying frequency

$$p' = \sum A_i \cos(\omega_i t + \phi_i)$$

$A =$ unsteady pressure amplitude
$\omega = 2\pi f =$ angular frequency (f = linear frequency)
$\phi =$ phase angle

In a resonant chamber such as a combustor, each tonal pressure wave represents an acoustic mode as determined by the geometry, boundary conditions, and sound speed (and Mach number for the case of high speed flows). Thus, identification of the frequency content of a signal is the first step in determining an acoustic mode, and in characterizing a combustion dynamics event.

To determine the frequency and amplitude of measured pressure oscillations, a sliding-window Fast Fourier Transform (FFT) with a Hamming window is implemented in Matlab on the acquired time-series data, as depicted in Figure III.1. The width of the time window is set as the number of FFT's specified divided by the sample frequency, Fs. The FFT is computed over the window width (Nfft=2048, Fs=10,000 for the data acquired here), the window is slid along the time series, and the average FFT is computed based on the series of windows, as shown in Figure III.1 for an example data set.

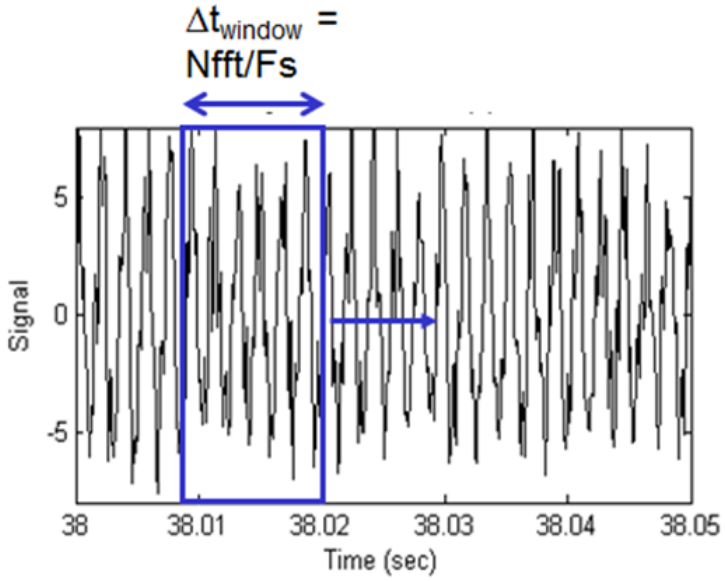

Figure III.1. *Computation of average FFT for time-series data.*

In theory (for simple geometries), characteristic frequencies for different acoustic modes can be obtained by solving the 2-dimensional wave equation, to give solutions in the form of Bessel functions:

$$p(r,\theta,z,t) = \sum_{m=0}^{\infty} \sum_{n=1}^{\infty} J_m\left(k_{r,m,n} r\right) e^{jm\theta} e^{j\omega t} \times \left(C_{1,m,n} e^{-jk_{z,m,n} z} + C_{2,m,n} e^{+jk_{z,m,n} z}\right)$$

$$\text{where} \quad J'_m(k_r r_0) = 0 \quad \text{and} \quad k_{z,m,n} = \left(k_0^2 - k_{r,m,n}^2\right)^{1/2}$$

$$J_m = \text{Bessel function} \quad \text{and} \quad \text{Re}(e^{jm\theta}) = \cos(m\theta)$$

Classical solutions for the frequencies of various fundamental mode shapes are shown in Figure III.2. These can be used to calculate approximate frequencies for the acoustic modes in a given combustor (of known dimensions). For the annular ACS combustor, circumferential modes are expected, and the analytical expression shows an expected frequency of approximately 600-700 Hz using the sound speed in the burned gas. For the annular ACS combustor the longitudinal mode frequencies are well over 1000 Hz and were not observed.

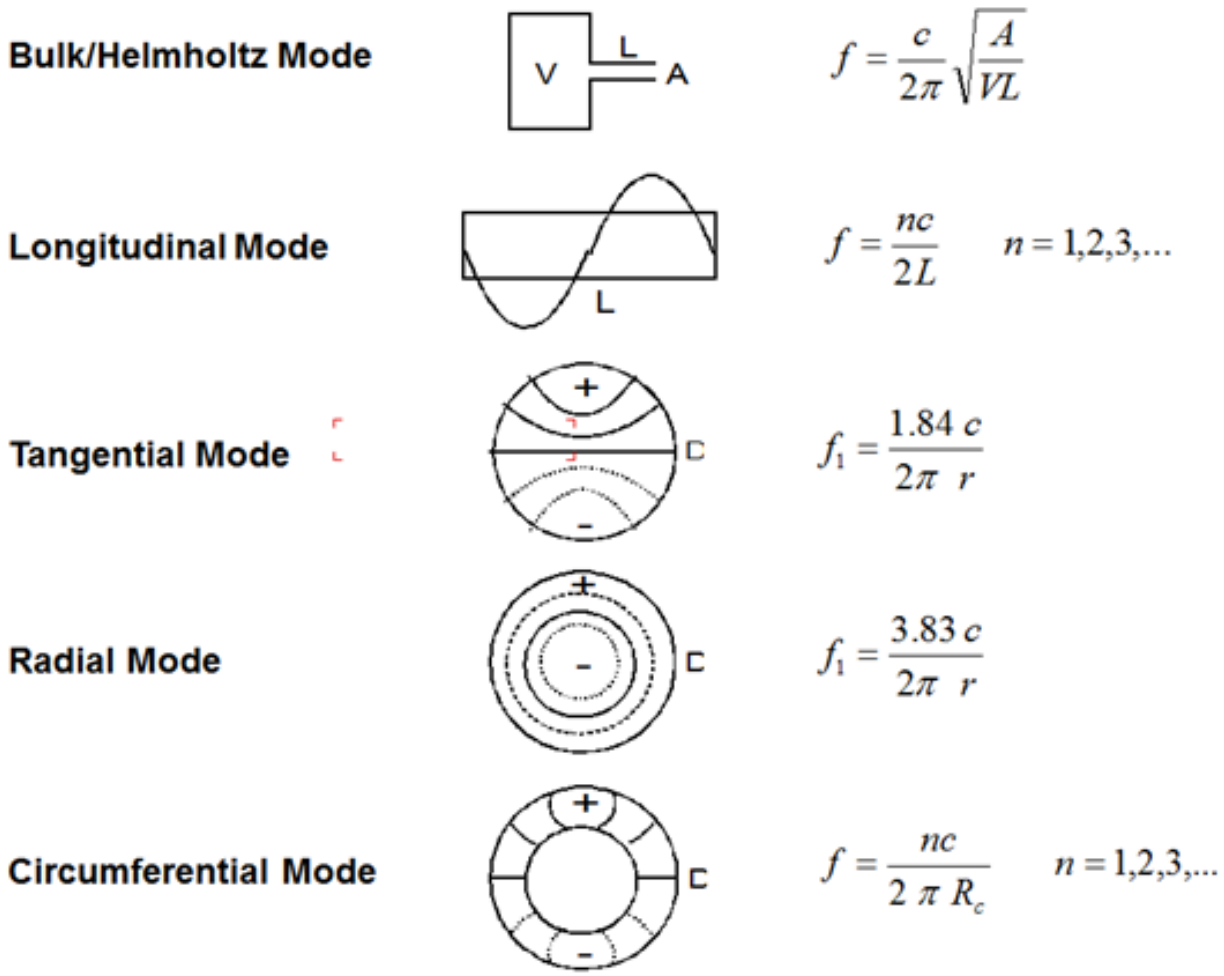

Figure III.2. *Classical solutions to the 2-D wave equation for various modes.*

Pilot-Only Dynamics

A summary of the combustion dynamics data from the reference combustor sensor (PDDIGNKI) acquired with fuel flowing only to the pilot zone is provided in Table IV.1, along with the combustor operating conditions. As shown in Table IV.1, peak dynamic pressures were as high as 13 psipp during some transient events, exceeding the allowable safety limits for the test facility. Table IV.1 also shows that for most of the pilot-only points, acoustic tones were observed and excited primarily at a frequency of roughly 600 Hz corresponding to a tangential or spinning acoustic mode.

Table IV.1. *Summary of flow conditions and peak unsteady pressures (reference ITP) for Pilot-Only operation. In the first column, ADR stands for "Analog Data Record number" and is the identifier for a data record.*

POINT ADR	MEAN P3 (psia)	T3 (F)	FAR	% Pri (of Pilot)	% Sec A (of Pilot)	% Sec B (of Pilot)	% Main (of Total)	DYNAMIC PDDIGNKI (REFERECE) Peak Freq (Hz)	Corrected Amp (psi-pp)
51	39	425	0.0151	100%	0%	0%	0%	605	2.3
55	56	450	0.012	100%	0%	0%	0%	640	0.4
56	58	529	0.0158	100%	0%	0%	0%	693	0.3
60	62	499	0.015	20%	51%	29%	0%	625	1.3
63	62	456	0.017	31%	44%	26%	0%	601	4.8
66	79	424	0.017	22%	44%	33%	0%	444	5.2
68	77	428	0.015	17%	52%	31%	0%	596	5.9
70	77	429	0.019	13%	54%	33%	0%	571	4.7
72	78	429	0.020	12%	54%	34%	0%	596	4.8
74	77	429	0.022	11%	55%	35%	0%	601	13.2

Acoustic spectra for representative pilot-only data points at low T3 (~430 F) are provided in Figure IV.1, in units of peak-to-peak amplitude (psipp). The blue lines show the measured data at the sensor location before correcting for pressure losses in the ITP sense-line, while the solid red dot shows the peak value at the ITP sense-line location after accounting for pressure losses in the line. (The corrected peak values are used for the summary data tabulated in Table IV.1.) For all cases shown in Figure IV.1 the dominant acoustic mode has a frequency of about 600 Hz which corresponds to a tangential acoustic mode in the combustor. The data also show that for these low-T3 cases the acoustic mode (frequency) is not affected by fuel/air ratio (FAR), but that amplitude does increase at high FAR.

For comparison to Figure IV.1, Figure IV.2 shows acoustic spectra for pilot-only data points at two different T3 values (two different combustor inlet temperatures) having similar fuel/air ratios. Clearly the higher inlet temperature case exhibits significantly reduced combustion dynamics (much lower acoustic amplitudes), providing an initial indication that dynamics may be reduced at higher inlet temperatures.

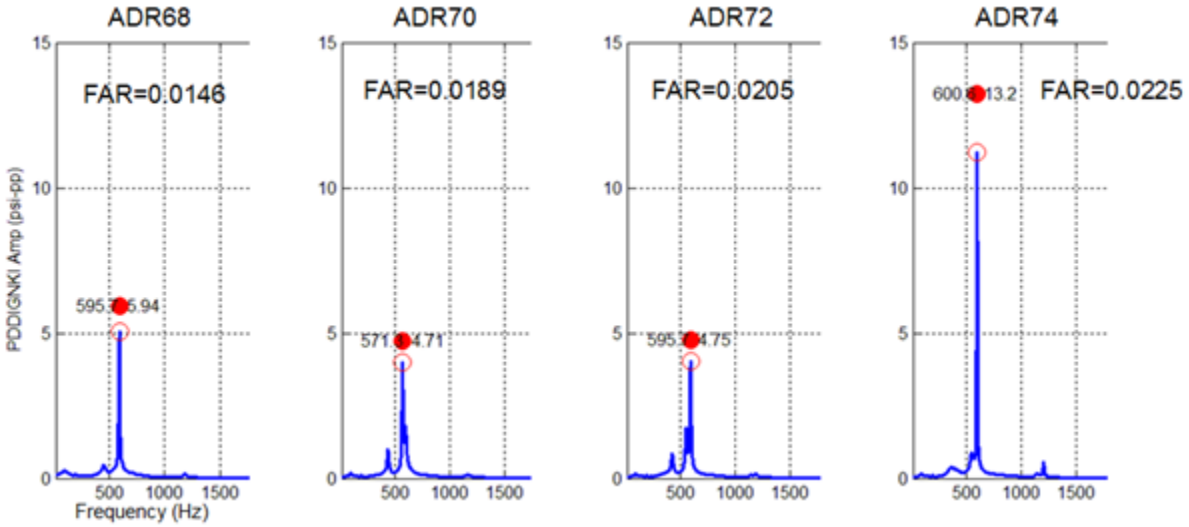

Figure IV.1. *Acoustic spectra for four data records (ADR 68, 70, 72, and 74) associated with pilot-only combustor operation (unfueled mains) at low combustor inlet temperature (T3 ~ 430 F). The plots show Power Spectral Density (PSD) of the dynamic pressure signal from sensor PDDIGNKI for pilot-only idle operation at various fuel/air ratios (FARs) all showing ~600-Hz dominant tone. The blue lines show the uncorrected PSD amplitude in psipp units, and the solid red dot shows the corrected peak value.*

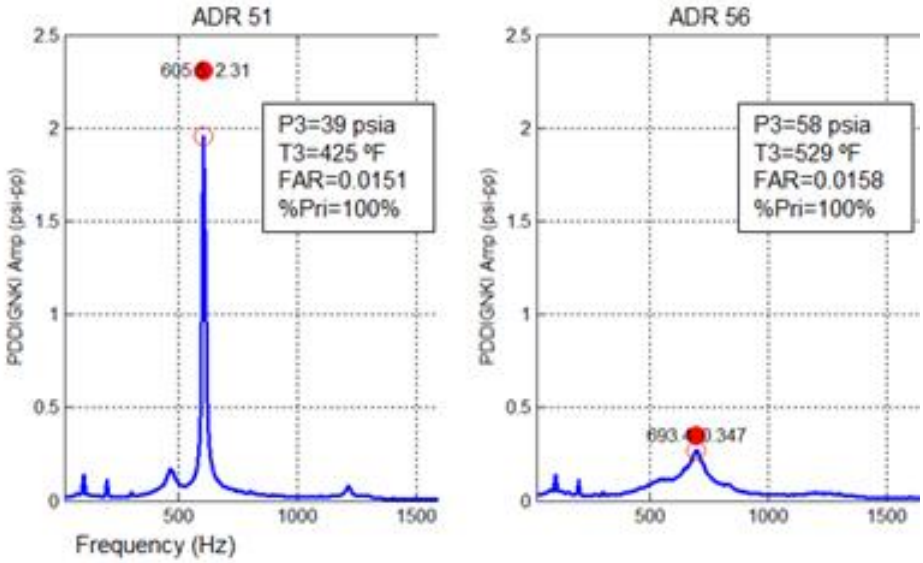

Figure IV.2. *Acoustic spectra for two data records (ADR 51 and 56) associated with pilot-only combustor operation (unfueled mains) at two different combustor inlet temperature (T3 ~ 425 F vs. T3 ~ 529 F) but similar fuel/air ratios (FARs). The plots show Power Spectral Density (PSD) of the dynamic pressure signal from sensor PDDIGNKI for pilot-only idle operation. The blue lines show the uncorrected PSD amplitude in psipp units, and the solid red dot shows the corrected peak value.*

Evaluation of the analytical equation for tangential acoustic modes in an annular combustor geometry yields a predicted frequency of approximately 600-700 Hz, depending on the T4 temperature (burned gas temperature) in the combustor. This is consistent with the dominant 600 Hz tone observed in the combustor when only the pilot zone was fueled. To further identify the acoustic mode, the phase relationship between different dynamic pressure sensors was analyzed. Three of the ITPs were placed in a circumferential array for identification of tangential acoustic modes. Unfortunately, only two of the three ITPs in the circumferential array were functional during the test (PDDCOM-G and PDDCOM-O), making identification of the tangential mode more challenging.

ADR 63 is shown in Figure IV.3 as a representative case for the pilot-only combustor test condition. The time series of the dynamic pressure signals were discretized into small time slices and the phase relationship and coherence between the signals computed. Sensor PDDCOM-G was located at 90 degrees from TDC (top dead center), and PDDCOM-O at 210 degrees. For a tangential mode, we would expect a phase difference of 120 degrees. As shown in Figure IV.4, the phase difference was found to be mostly in the range of +120-150 Hz. This is consistent with a +1T tangential mode. The positive sign indicates clockwise rotation in the combustor aft-looking-forward. A comparison of the amplitudes of the two dynamic pressure sensors (Figure IV.3., middle) shows that at some instances the amplitudes are comparable, while other instances the amplitude ratio varies. This suggests a tangential mode that is at some instances a standing mode and other times a spinning mode.

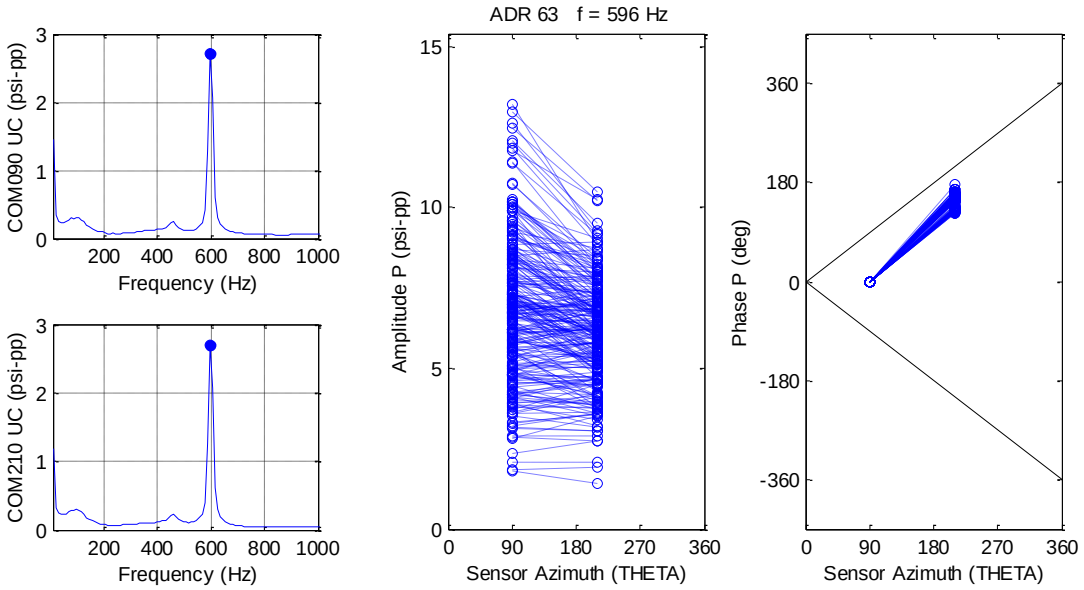

Figure IV.3. *Power Spectral Density (PSD) of the dynamic pressure signal from sensor PDDCOM-G "COM90" (top-left, uncorrected amplitude) and PDDCOM-O "COM210" (lower-left, uncorrected amplitude) averaged over 50-seconds for ADR 63. Corrected peak amplitude relationship for the two sensors at discrete time intervals is shown in the center plot. The right plot shows the change in phase angle between the two sensors for discrete time intervals. Sensor azimuth is defined from engine TDC (top dead center). The two sensors are located at +90 and +210 degrees. For a tangential mode, the dotted lines (data) would be expected to run parallel to the solid lines. The middle and right plots have been filtered to show only data in which the two sensors have coherence > 0.98, corresponding to periods when both sensors are responding to (measuring) the same acoustic mode.*

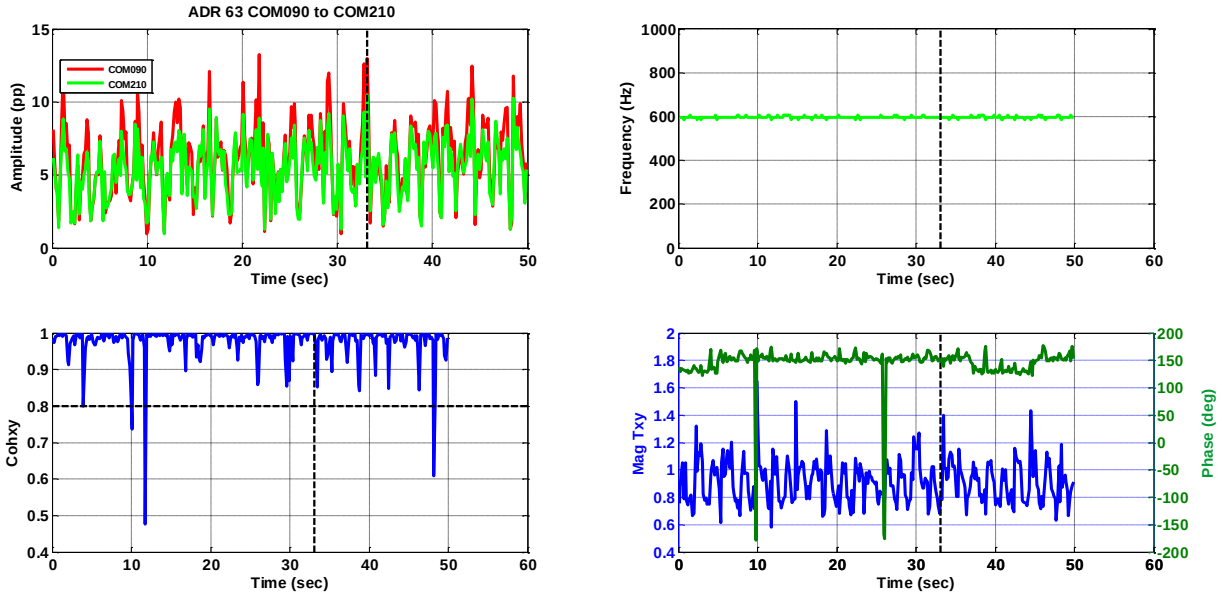

Figure IV.4. *Time series plots of dynamic pressure data for ADR 63, pilot-only configuration. Upper left: Corrected peak amplitude for PDDCOM-G (COM90) and PDDCOM-O (COM210); Upper right: Frequency of peak amplitude; Lower-left: Coherence between PDDCOM-O and PDDCOM-O sensors; Lower-right: Magnitude and phase of the transfer function for PDDCOM-G/PDDCOM-O.*

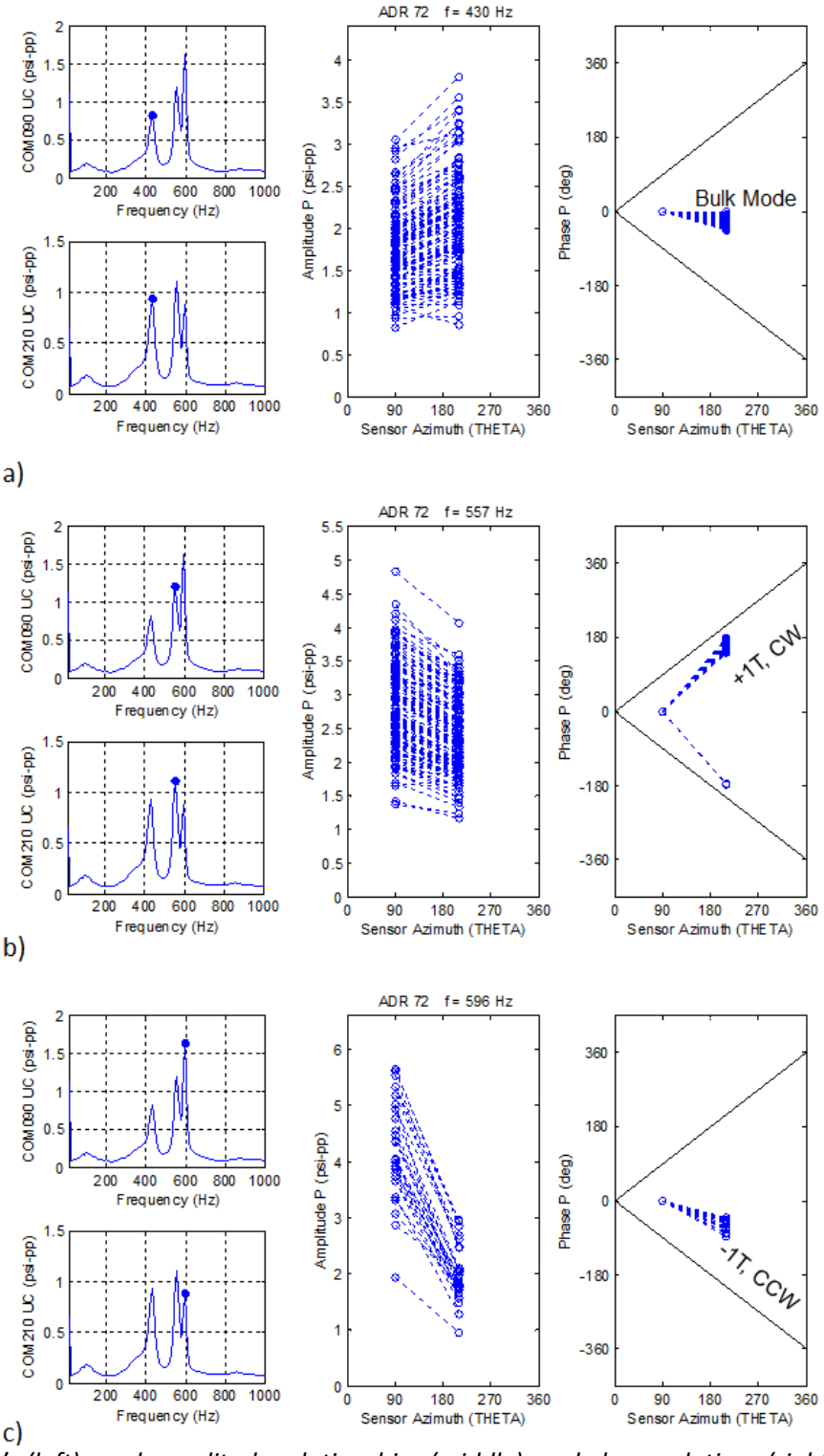

Figure IV.5. *PSD's (left), peak amplitude relationships (middle), and phase relations (right) for ADR 72: a) bulk mode 430 Hz, b) predominantly +1T (clockwise) tangential mode at 557 Hz and c) -1T*

(counterclockwise) tangential mode at 596 Hz. The middle and right plots have been filtered to show only data in which the two sensors have coherence > 0.98, corresponding to periods when both sensors are responding to (measuring) the same acoustic mode.

ADR 72 is a notable case because multiple distinct peaks are evident in the spectra (Figure IV.5), at 430 Hz, 556 Hz and 596 Hz. For this dataset, the acoustic data was post-processed with a narrow frequency band around each peak, and the phase relationship between the circumferential sensors was determined. From the plots in Figure IV.5, it is evident that the different peak frequencies exhibit much different phase relationships. The peak at 596 Hz appears to be a +1T tangential mode (clockwise, aft-looking-forward, the peak at 557 Hz appears to be a -1T tangential (counterclockwise, aft-looking-forward), and what is likely a bulk mode at 430 Hz with little phase difference between sensors.

Figure IV.6 shows the dynamic pressure peak amplitude versus axial position for all pilot-only test conditions. The axial position is referenced to the combustor span or length (0% span corresponds to the combustor bulkhead and 100% span corresponds to the leading edge of the vanes). It is observed that the mode shape is general flat axially inside the combustor. This is consistent with a tangential acoustic mode. Two exceptions are ADR 72 and ADR 74, which exhibited a spike in amplitude in the front-end of the combustor.

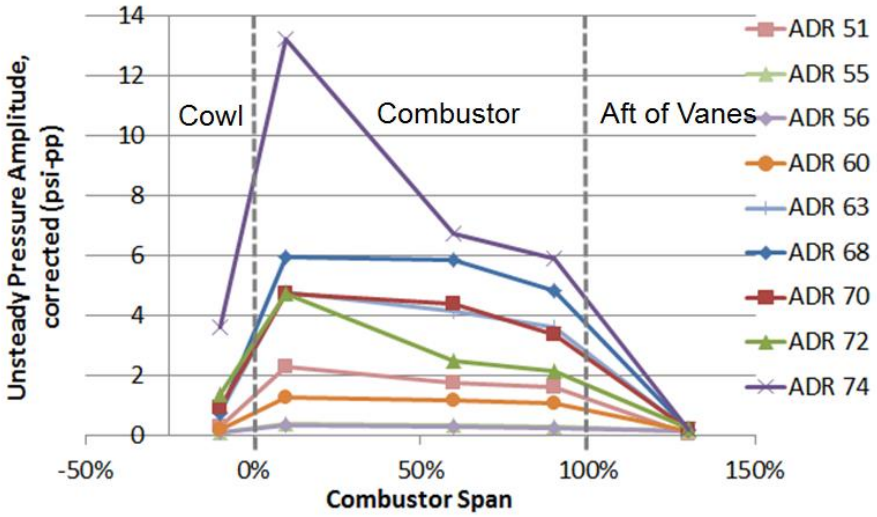

Figure IV.6. *Peak corrected amplitude of 600-Hz tone vs. sensor axial position for combustor operating low-power with fueled pilot zone only. Zero-span indicates the combustor bulkhead, 100%-span indicates leading edge of the vane pack. The dynamic pressure sensors are generally in the same circumferential position (within 30 degrees), from left-to-right PDDCDO-I, PDDIGNKI-I, PDDCOMM-G, PDDCOM-G, PDD410-I.*

Pilot-and-Main dynamics

A summary of the combustion dynamics data from the reference combustor ITP (PDDIGNKI) acquired with fuel flowing to both the pilot and main zones is provided in Table IV.3, along with the combustor operating conditions. In Table IV.3 we see that for operation with the mains fueled (“on” or “lit”) the excited frequency was generally 400 Hz which is believed to correspond to a “bulk” or “Helmholtz” mode in the combustor and case. Amplitude levels with the mains lit were high, with recorded events exceeding 10 psipp, which also transiently exceeded the allowable safety limits for the facility.

Table IV.3. *Summary of flow conditions and peak unsteady pressures for Pilot-and-Mains operation. In the first two columns, ADR stands for "Analog Data Record number" and is the identifier for a data record.*

POINT	MEAN							DYNAMIC	
ADR	P3 (psia)	T3 (F)	FAR	% Pri (of Pilot)	% Sec A (of Pilot)	% Sec B (of Pilot)	% Main (of Total)	PDDIGNKI (REFERECE) Peak Freq (Hz)	Corrected Amp (psi-pp)
78	101	429	0.0185	20%	33%	48%	24%	405	10.6
80	134	409	0.0190	25%	30%	44%	26%	400	8.4
82	134	408	0.0191	25%	30%	44%	27%	400	8.0

When fuel is supplied to the main injectors (the downstream injectors in the ASC configuration) there appears to be a shift in the dominant acoustic mode, with the 400 Hz mode now becoming most excited. This 400 Hz mode appears to be associated with a "bulk" or "Helmholtz" mode in the combustor and case. Figure IV.7 shows acoustic data (spectra) for operation of the combustor when fuel is supplied to both the pilot and the main fuel injectors. Note that this operating point does not correspond to an engine high power point, but instead corresponds to a low power "staged" condition (pilot and mains both on) at an off-idle condition at low inlet temperature and pressure. Also note that the 600 Hz mode is still visible, but is not significantly excited (the amplitude at 600 Hz is low). Further note that a smaller peak at about 800 Hz is visible, which was confirmed in the data to be exactly twice the ~400 Hz frequency and therefore corresponds to a harmonic (non-linearity) of the high-amplitude 400 Hz tone.

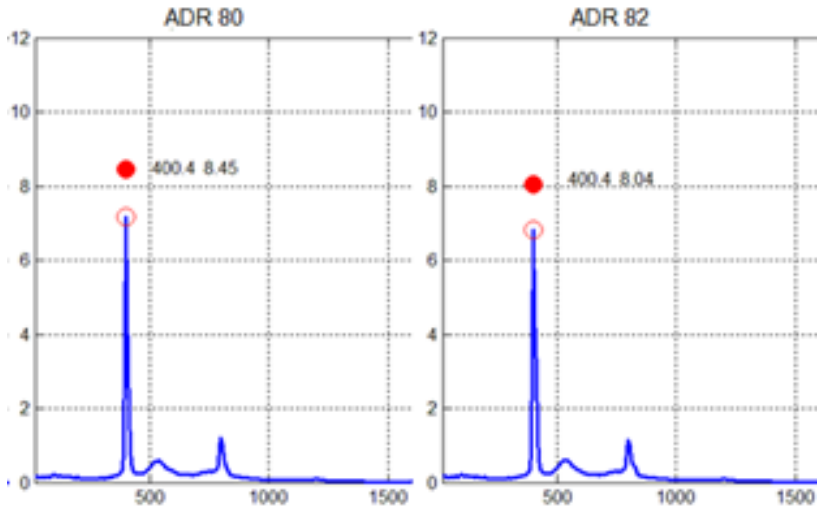

Figure IV.7. *Acoustic spectra for two data records (ADR 80 and 82) associated with combustor operation while fueling both the pilot and main injectors. The plots show Power Spectral Density (PSD) of dynamic pressure signal from sensor PDDIGNKI, which reveal a dominant mode around 400 Hz. The blue lines show the uncorrected PSD amplitude in psipp units, and the solid red dot shows the corrected peak value.*

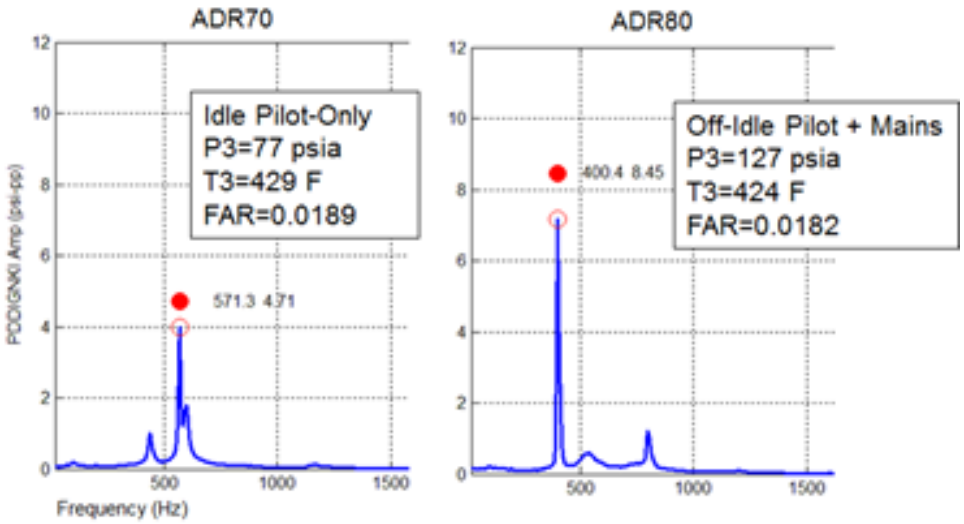

Figure IV.8. *Acoustic spectra for two data records (ADR 70 and 80) comparing pilot-only operation (ADR 70) to operation with fueling of both the pilot and mains (ADR 80). The plots show Power Spectral Density (PSD) of the dynamic pressure signal from sensor PDDIGNKI. The blue lines show the uncorrected PSD amplitude in psipp units, and the solid red dot shows the corrected peak value.*

A comparison of the spectra for operation with pilot-only to operation with fueling of both the pilot and mains is given in Figure IV.8. Although the fueling scheme is different for these two cases, the total FAR is similar, and both points are obtained at similar inlet temperatures (~424 – 430 F). Despite the similar overall conditions, it is clear that shifting fuel from the pilot to the mains causes a shift in the excited acoustic mode, from a mode at ~550 – 600 Hz to a mode at ~400 Hz. Interestingly, the 400 Hz mode is evident (but not dominant) during pilot-only operation, and conversely the ~550 Hz mode is evident (but not dominant) during operation with both the pilot and the mains fueled.

ADR 82 is shown in Figure IV.9 as a representative case for the combustor running with fuel to both the pilot and the mains. The time series of the dynamic pressure signals were discretized into small time slices and the phase relationship and coherence between the signals computed. Sensor PDDCOM-G was located at 90 degrees from TDC, and PDDCOM-O at 210 degrees. From Figures IV.9 and IV.10, it can be seen that there is little phase difference between the two circumferential sensors. This is consistent with either a bulk mode or a longitudinal mode. However, a longitudinal acoustic mode for this combustor would occur at a much higher frequency. Therefore, it is most likely that this 400 Hz mode is a “bulk” or “Helmholtz”-type mode. Figure IV.10 shows strong peak amplitudes and high coherence between the sensors.

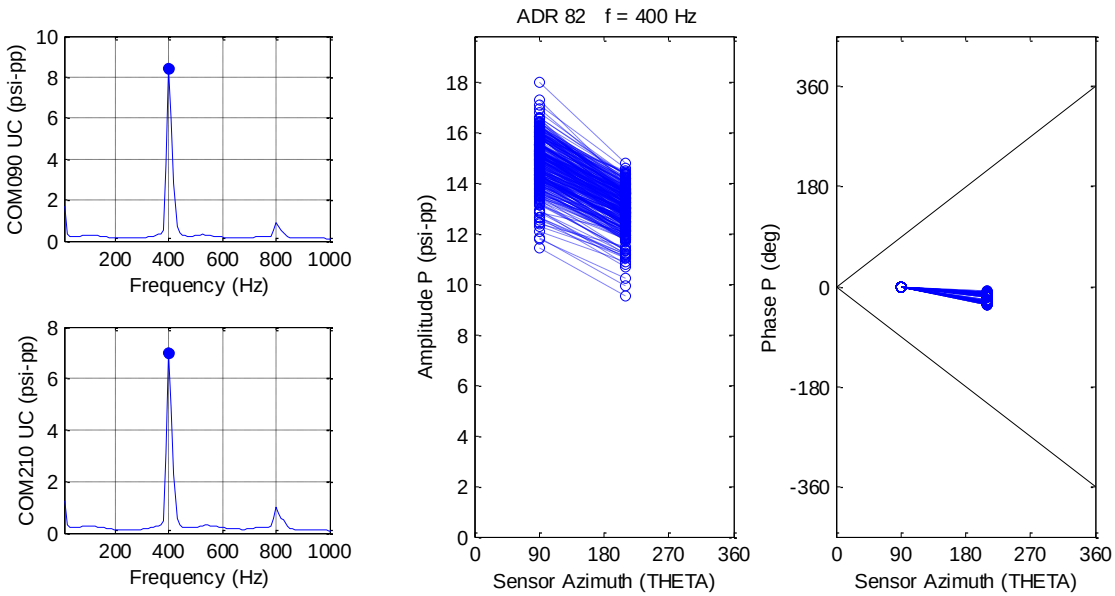

Figure IV.9. The left *plots show Power Spectral Density (PSD) of the dynamic pressure signal from sensor PDDCOM-G "COM90" (top-left, uncorrected amplitude) and PDDCOM-O "COM210" (lower-left, uncorrected amplitude) averaged over 50-seconds. The middle plot shows the corrected peak amplitude relations for the two sensors at discrete time intervals. The right plot shows the change in phase angle between the two sensors for discrete time intervals. Sensor azimuth is defined from engine TDC. The two sensors are located at +90 and +210 degrees. For a tangential mode, the dotted lines (data) would be expected to run parallel to the solid lines. For a bulk-mode, the phase difference would be expected to minimal or flat. The middle and right plots have been filtered to show only data in which the two sensors have coherence > 0.98, corresponding to periods when both sensors are responding to (measuring) the same acoustic mode.*

Figure IV.11 shows the dynamic pressure peak amplitude versus axial position for three test conditions with pilot and mains fueled. The axial position is referenced to the combustor span or length (0% span corresponds to the combustor bulkhead and 100% span corresponds to the leading edge of the vanes). It is observed that the mode shape is general flat axially inside the combustor, with a slight increase towards the aft of the combustor.

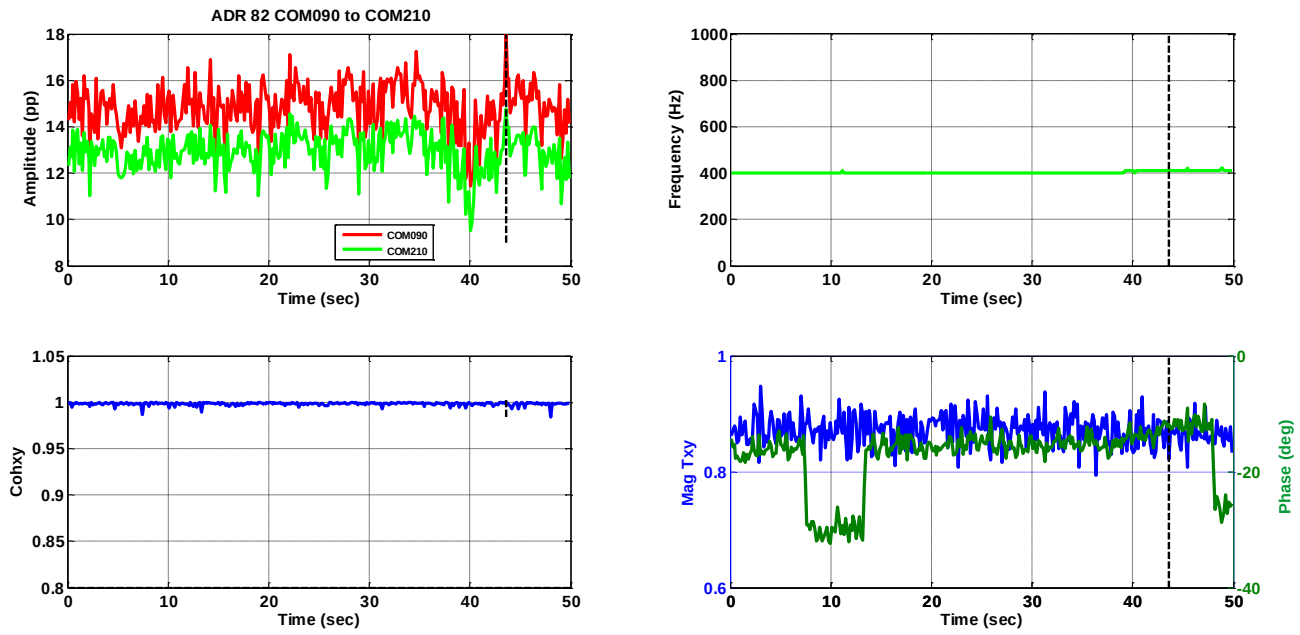

Figure IV.10. *Time series plots of dynamic pressure data for ADR 82, pilot and mains fueled. Upper left: Corrected peak amplitude for PDDCOM-G (COM90) and PDDCOM-O (COM210); Upper right: Frequency of peak amplitude; Lower-left: Coherence between PDDCOM-O and PDDCOM-O sensors; Lower-right: Magnitude and phase of the transfer function for PDDCOM-G/PDDCOM-O.*

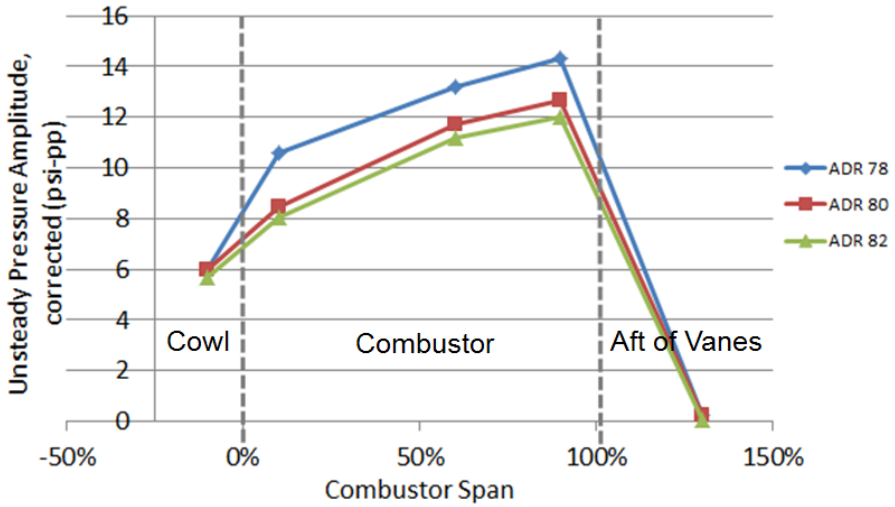

Figure IV.11. *Peak corrected amplitude of 400-Hz tone vs. sensor axial position for combustor operating low-power with fueled pilot and main zones. The dynamic pressure sensors are generally in the same circumferential position (within 30 degrees), from left-to-right PDDCDO-I, PDDIGNKI-I, PDDCOMM-G, PDDCOM-G, PDD410-I.*

Summary and conclusions from annular rig tests of combustion dynamics

A test of the ACS combustor with a vane-pack was completed at Pratt & Whitney's X960 facility to obtain learning on the acoustic response of the ACS design. Adding a vane pack to the combustor creates engine realistic acoustic boundaries, providing the most accurate prediction of the combustor's propensity for combustion dynamics short of an engine test. At pilot-only idle conditions, significant

tangential acoustics were observed. When the main fuel stage was added (fueled), the acoustic response shifted to a frequency range consistent with a bulk mode, but facility limits prohibited significant exploration of higher power points. This test provided significant learning early in the ACS development, clearly highlighting the need to understand the fundamental drivers of combustion dynamics in the ACS design before proceeding to engine testing.

Task 14 – Additional Pilot Injector Investigations for N+3 Combustor

Impedance Testing & Modeling

The N+3 baseline and alternative pilot swirlers, as well as the N+3 main swirlers, were tested for acoustic impedance with mean through-flow in UTRC's acoustics laboratory. The fuel injectors were tested under cold flow conditions in UTRC's impedance tube with flow. A COMSOL FEA model of the impedance tube with simplified injector representation was constructed and tuned (loss coefficient) to match the impedance data over a range of pressure drops. The impedance tube and COMSOL model are shown in Figure I.14.1. Several views of the impedance-tube experimental setup are shown in Figure I.14.2.

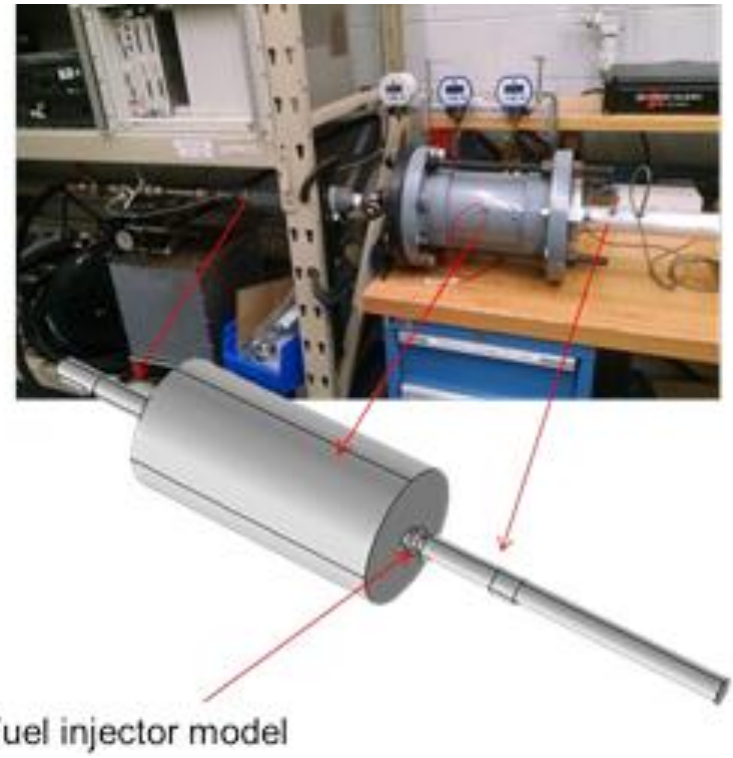

Figure I.14.1. *Injector impedance tube and COSMOL model (flow is left to right).*

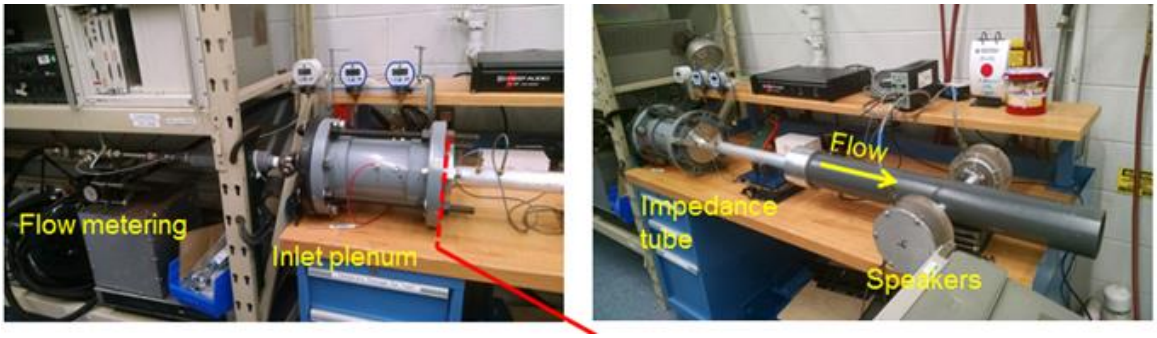

Figure I.14.2. *Additional views of the UTRC impedance rig and the tested N+3 swirlers.*

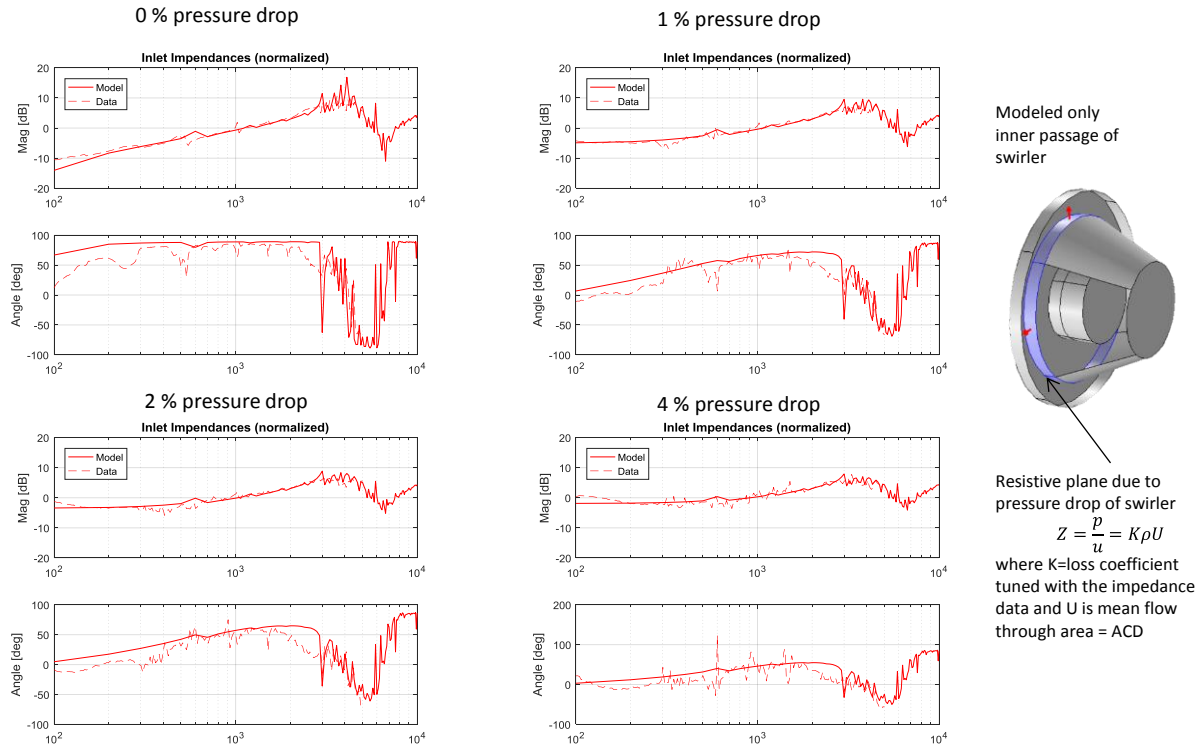

Figure I.14.3. *Measured and model impedance data for pilot injector.*

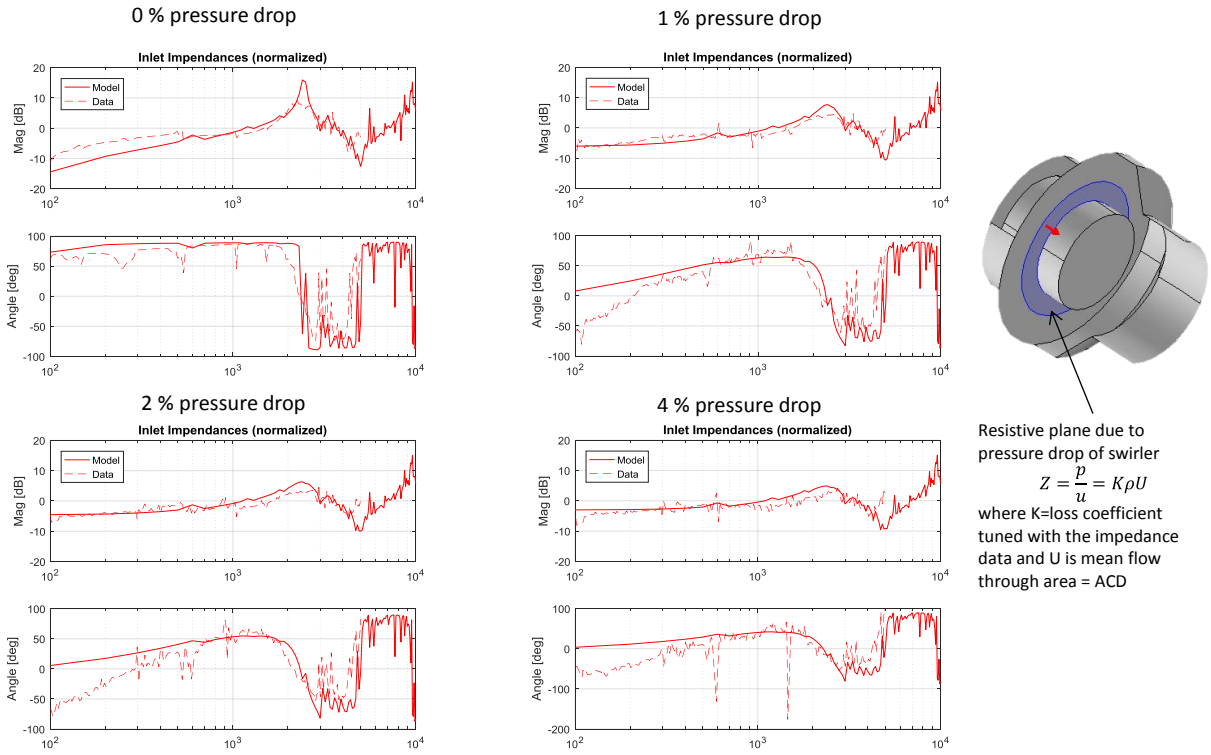

Figure I.14.4. *Measured and model impedance data for main injector.*

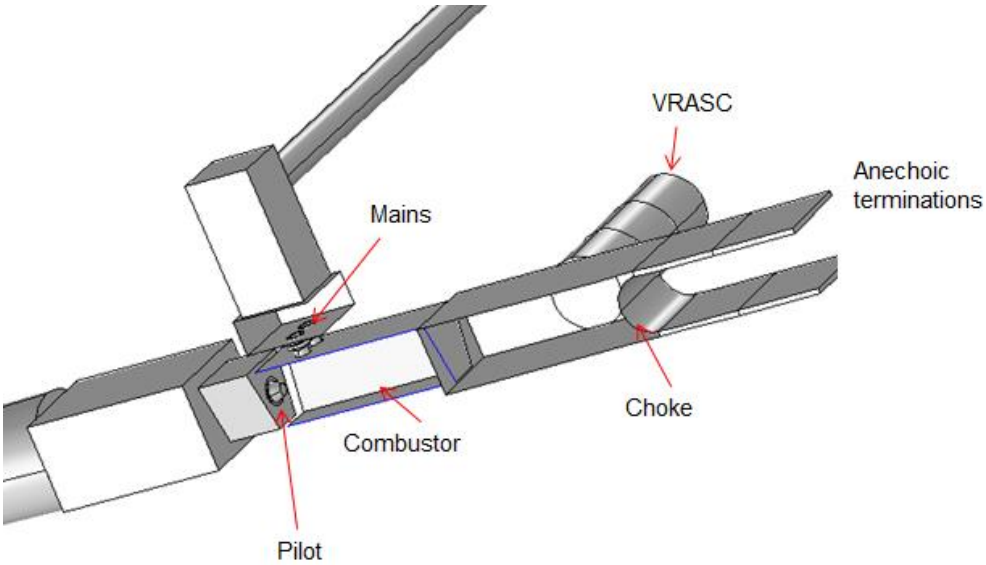

Figure. I.14.5. *N+3 combustor rig with COMSOL model, including choked exit boundary condition.*

The acoustic (impedance) data and model comparisons for the N+3 pilot and main injectors are shown in Figures I.14.3 and I.14.4, respectively. Figure I.14.5 shows the acoustic COMSOL model of the N+3 combustor rig with the choked exit installed. The boundary conditions of the FEA model are the venturi in the supply (nearly choked, rigid conditions) and the choked exit after the combustor, and the acoustic model includes all rig piping as well as the tuneable side-branch and the combustor and swirlers.

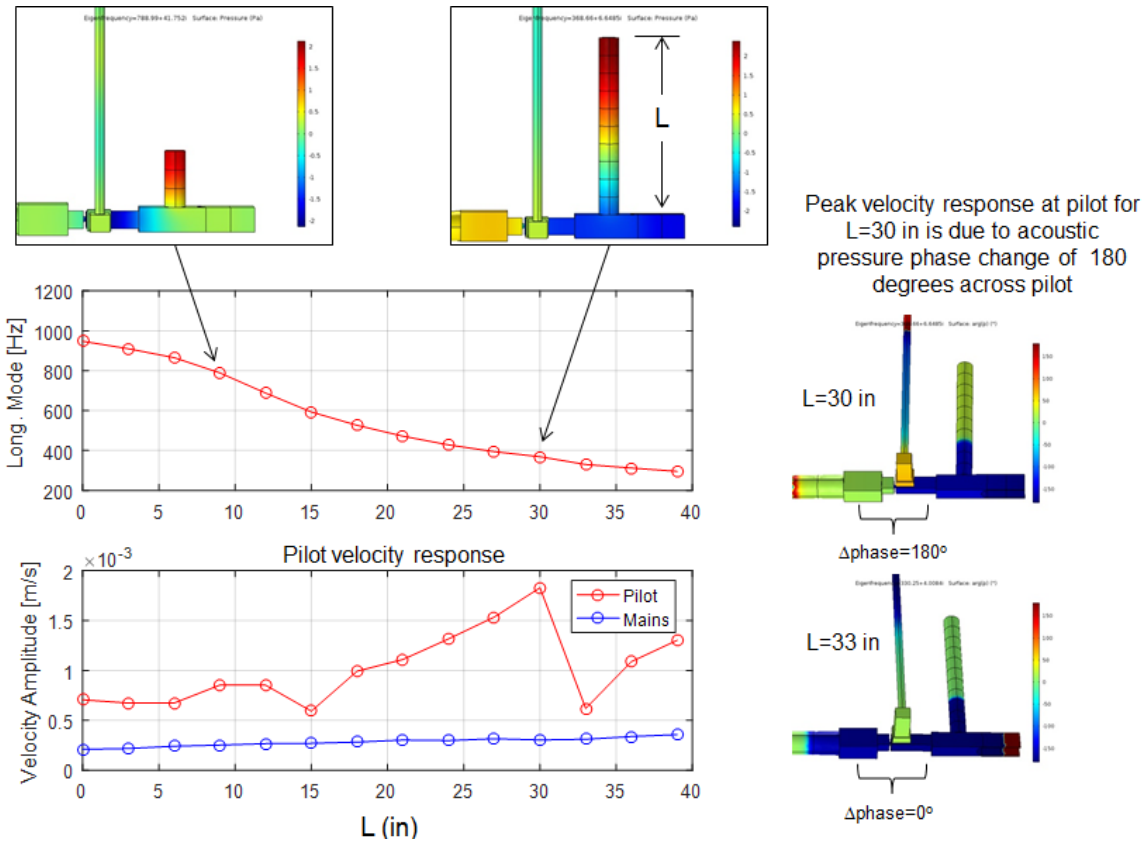

Figure I.14.6. *COMSOL acoustic model results for N+3 baseline combustor with choked exit.*

For the N+3 baseline combustor, using the measured impedance values of the pilot and main swirlers, the COMSOL FEA model was used to calculate acoustic modes and frequencies as a function of the tunable side-branch length. These results are shown in Figure I.14.6. The results show that for a sidebranch length of about 30 inches the expected frequency is about 400 Hz, and the acoustic velocity amplitude at the pilot swirler will be a maximum. Therefore modeling and testing initially focused on this 400 Hz frequency, since it is in the rough frequency range at which engine acoustic modes are sometimes observed, and since it is expected that the large acoustic velocity at the pilot swirler may excite combustion dynamics and enable learning from the models and experiments.

Design and Fabrication of Alternative Pilot Hardware

In preparation for testing multiple styles of fuel injection and mixing devices for the N+3 pilot, to determine which is most prone to combustion dynamics in the ACS combustor, candidate pilots were sought which would be appropriate for the small-core N+3 combustor. It was specifically desired to identify designs which used airblast type fuel atomization, as well as hybrid airblast and pressure atomization. Ideally, the pilot injector for the ACS combustor should be simple, stable and mature. It should be able to be scaled as small as possible yet still perform well, especially in terms of PM emissions. It should also be able to handle challenging relight conditions for advanced high-bypass N+3 engines. Two existing designs were identified, with hardware available for modification and testing: a production P&W airblast fuel injector, and a production P&W Canada fuel injector, with both having potential to be an alternative pilot for the N+3 ACS combustor. These injectors were acquired and modified for installation and testing in the N+3 combustor rig at UTRC.

Acoustically-forced Spray Testing

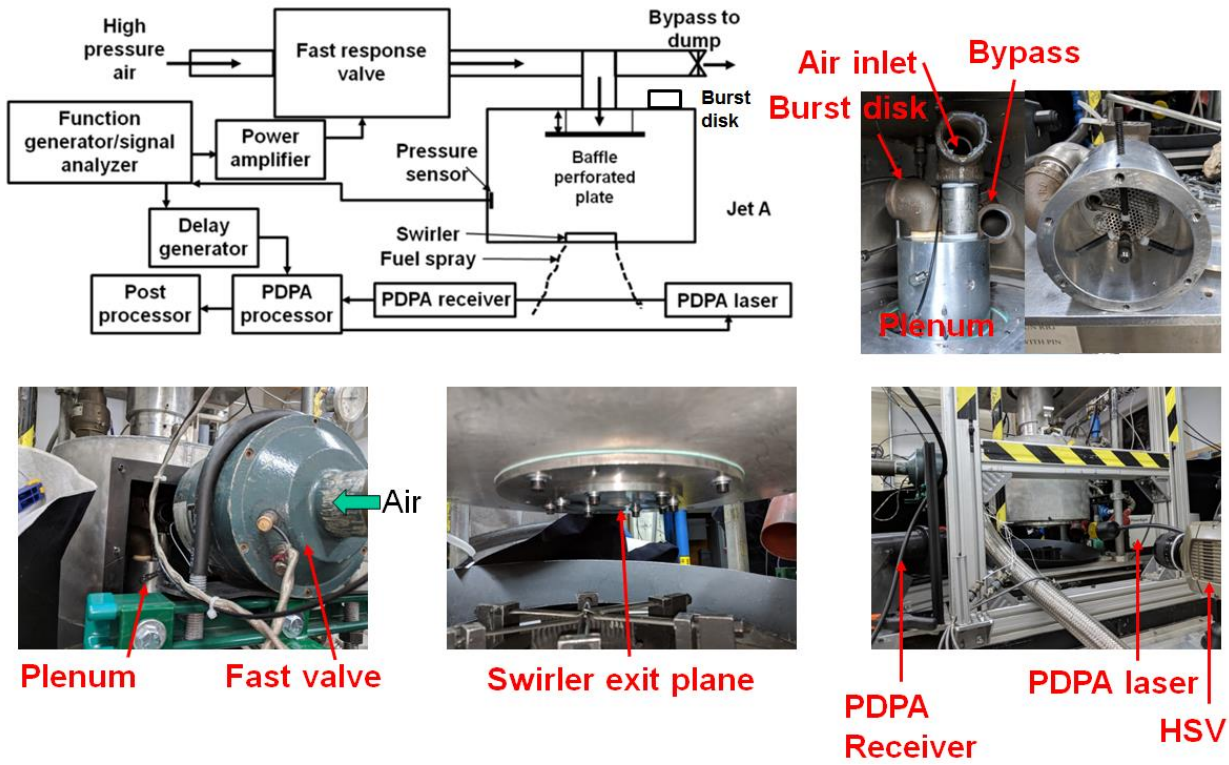

Figure I.14.1. *A schematic and photographs of forced PDPA setup*

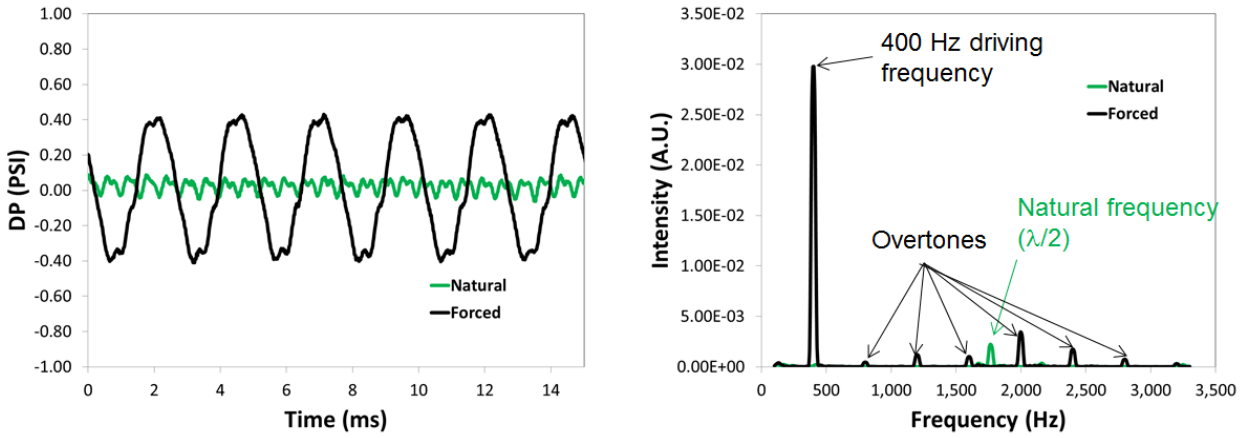

Figure I.14.2. *Natural (green) and forced (black) acoustic characteristics of plenum in time (left) and frequency (right) domains*

During the 4th Quarter of 2017, acoustically-forced PDPA spray tests on the N+3 baseline pilot were carried out to characterize velocity and droplet size dependences on upstream air pressure fluctuation. As shown in the schematic of Fig 1.14.1, the fluctuation of air was produced by a fast response solenoid valve driven by pneumatic (high pressure air) and electrical (stereo amplifier) energy sources. The air provided dynamics in a 3.5" internal height, 4" ID cylindrical shape plenum where swirler was

implemented on its bottom. Phase locked PDPA measurements were performed at 0.75" and 1.1" downstream planes from the swirler exit. A trigger signal for the phase lock was produced by a function generator which also fed the power amplifier for the valve control, so that the actuation of air could be synced with PDPA measurements.

The flow condition of this ambient test was scaled from actual N+3 operating conditions. The forced fluctuation frequency (~ 400 Hz) was from the corresponding CFD simulation condition (see forced spray modeling discussion below). Fluctuation amplitude (0.9 psid p-p target, 0.82 psid p-p actual) was obtained by matching air velocity between the combustion and ambient conditions under quasi-steady state assumption.

Figure 1.14.2 shows the acoustic characteristics of plenum measured by a high frequency pressure transducer located at approximately 0.5" above the bottom of plenum and flush with the side wall. The measured natural frequency of the plenum (green data in the figure) was around 1700 Hz in the absence of forced air, but during forced-acoustic testing it was to be dominated by the forced frequency once air was driven by the valve (black data in the figure).

CFD analysis of acoustically-forced spray for the N+3 baseline pilot using UTRC's HiMIST CFD tool. UTRC's first-principle-based High-fidelity Multiphase Injection Simulation Tool (HiMIST) was applied to simulate the acoustically-forced spray for the N+3 baseline pilot swirling flow injector. Forced spray simulations were performed for a 400 Hz forcing frequency, and compared to the results of the experimental acoustically-forced spray tests, showing good qualitative agreement.

UTRC Dynamics Testing with Rig Optical Access (Window) and High-Speed Imaging

During the current reporting period (FY2018), dynamics tests were performed in UTRC's N+3 combustor rig for multiple pilot configurations. This included high-speed videos of combustion during both stable and unstable conditions. For this purpose, the N+3 combustor rig was setup with a variable-area choked exit and the tunable acoustic side branch, as used during previous dynamics studies, was installed along with a quartz window in the sidewall to provide optical access to the flame regions (Figures I.14.3 and I.14.4). The window design features a thick outer quartz window to take the pressure load of the combustor, and a thin inner window to take the thermal load. Purge air is passed between the two quartz windows and then injected as a film along the inside of the window in the same direction as the bulk combustor flow.

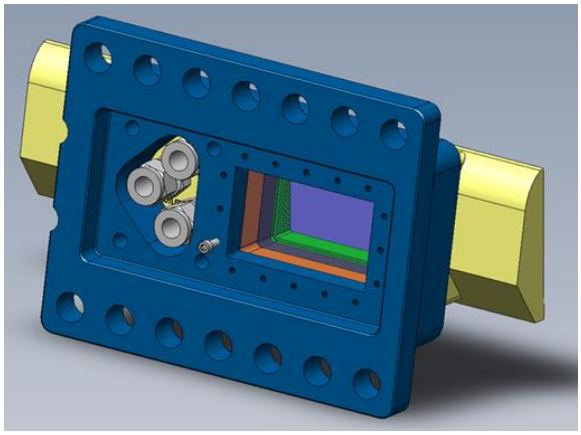

Figure I.14.3. *Illustration of window frame and sidewall insert to provide view into combustor cross-section. The tube connections (fittings) are for frame cooling water (closed circuit) and window purge air (open circuit). The window purge air forms a film along the combustion-side of the inner window.*

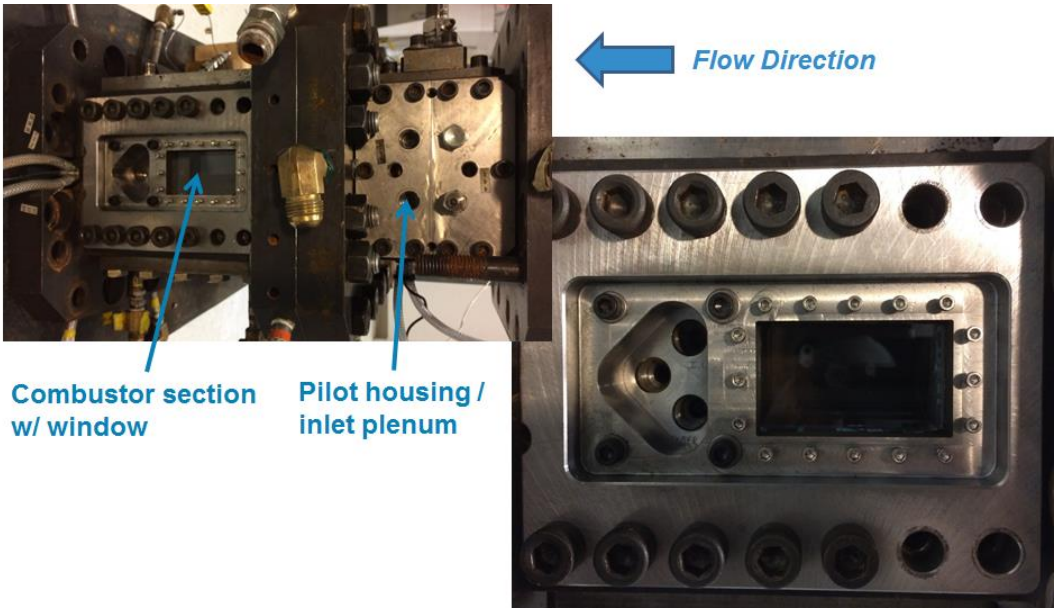

Figure I.14.21. *Photographs of window installed in N+3 combustor rig, showing orientation and flow direction. The high-speed video images have the same orientation and flow direction (i.e. right-to-left).*

Data Acquired and To-Be-Acquired With Window

High speed video has been captured for the baseline N+3 pilot swirler configuration and alternative pilot configurations. Data were acquired using Jet-A fuel in the combustor.

Dynamic Pressure Measurements

Dynamic pressure measurements were captured using Infinite Tube Probes (ITPs). ITPs were located in the feed plenums, combustor (bulkhead, mid and aft), and side-branch cylinder. Voltage signals from the ITPs were passed through a Vishay signal conditioner with a built-in 10 kHz low-pass filter for anti-aliasing. The signal was then read by a high-speed National Instruments data acquisition system. Corrections were applied to the measured ITP amplitudes to account for signal attenuation in the ITP sense-line, as calculated using UTC Standard Work to account for temperature and pressure variations along the sense-line length.

High Speed Camera Setup

High speed video of flame emissions was recorded with a Vision Research Phantom v12 CMOS-based high speed camera. Unfiltered and filtered (CH*, 430 nm narrow bandpass filter) movies were recorded with a 512x256 pixel setting. Unfiltered movies were recorded at 10,000 frames-per-second (fps), with the exposure time adjusted from 100 µs down to 1 µs to prevent saturation of the movies as the equivalence ratio of the mains was increased (resulting in increased flame luminosity at higher equivalence ratios). The CH*-filtered movies were recorded at 10,000 fps with a constant exposure time of 100 µs. The camera was fitted with a 50 mm lens and the f/stop was set to 1.4 (fully open).

Camera Triggering

The high speed DAQ and high speed camera were triggered simultaneously with a source signal from an HP Spectrum Analyzer. High speed data (e.g. from the pressure transducers) was recorded for 30-seconds. High speed video was recorded for a total of 5000 frames, or 0.5-seconds total time record.

The low-speed data for rig operating conditions was triggered manually and recorded for 30-seconds. Reported rig operating conditions were averaged over this 30-second window. Real-time monitoring of the pressure oscillations was performed with an HP Spectrum Analyzer which computed a running FFT of the signals for four rig ITP's.

Results from Baseline and Airblast Pilots

A total of 140 high speed videos were captured for the N+3 baseline and first alternative pilot configurations, both for unfiltered visible emission and filtered (430-nm narrowpass, CH*-filter) light emission. These videos cover a range of acoustic oscillation amplitudes from quiet to loud, and provide a good initial dataset with which to compare configurations.

Section II – Current Problem(s)

At this time there are no problems to report.

Section III – Risk Management

There are no Open Risks remaining. Figure III.1 lists the principal risks that were identified for this N+3 combustor effort, along with their potential mitigation plans if needed. The right-hand column includes notes and a color code to identify significance of the risk: green for not currently significant, yellow for potentially significant, and red for risks that have become significant concerns to the project. All identified potential risks were successfully addressed, as indicated by the green status in all cases.

Technical Risk (TRL-3)	Cost Risk	Schedule Risk	Mitigation Plan	Barriers/Issues & Status ● ● ●
Combustion dynamics in lean-burn system	N/A	Complex prediction required ASAP	Address early & use ERA Ph-2 learning	Working altern. pilot designs for mitigation
Autoignition vs. premixing in low-emissions system (at high OPR)	Hardware damage	Failure to obtain adequate mixing for low emissions	Early sub-component testing at full pressure & temperature	Autoignition testing complete, for Jet-A & alternative fuels
Thermal management of fuel-system & combustor (at high OPR)	N/A	Coking requires cleaning / replacing, or redesign of injectors	Detailed thermal design & anti-coke test procedures	Hardware designed with double-walled tubing & manifolds
Manufacturability at small-scale	Fabrication costs	Fabrication failures & time required to learn workable fab process	Address fab. issues early (sub-component test activity) & apply ERA Ph-2 learning	Fabrication quality achieved for small-core N+3 hardware / combustor
Analysis tools insufficiently mature (dynamics, comb. models, alternative fuels)	N/A	Desired solutions not available in time for design input	Revert to lower-order or lower-resolution models	Learning & decisions based on both modeling and experimentation
Availability of key personnel	N/A	Delays in starting or completing tasks	Early planning & assignment of staff	Design & testing activities on-track
Accurate prediction of N+3 combustor conditions	Re-work to updated conditions	Delays in selecting conditions, or re-work for updated conditions	Design to worst-case conditions; Develop best estimates w/ PW	UTRC coordinating w/ N+3 compressor effort and PW AEP

Figure III.1. *Risk Mitigation Plan, showing principal risks, status, and potential mitigation plan if needed.*

Section IV – Work Planned.

The N+3 small-core combustor effort has been successfully completed, and has accomplished all its milestones and met all its delivery requirements, with no additional work now planned under this effort. Recommendations for related further work under future efforts include the following:

- Application of axially-controlled stoichiometry (ACS) lean-burn combustion to engines for supersonic transport aircraft, as an enabler for low cruise-NOx emissions at supersonic speeds in the stratosphere. Specific attributes of the N+3 combustor technology developed here that make it attractive for supersonic propulsion are its capability for operating over a wide range of fuel-air ratio, its low NOx performance even at the high temperatures and fuel-air ratios expected at supersonic cruise, and the robustness of its fuel-injection and mixing technology even at these conditions.
- Exploration of transient combustor operation, especially with regard to fuel staging, and development of staging methods (sequencing) and technologies that both meet emissions requirements and meet engine operability requirements during aircraft mission segments such as approach and landing with its attendant thrust variation (and potential need for rapid staging).
- Engine integration of axially-controlled stoichiometry (ACS) combustor architectures, including exploration of interfaces to the compressor and turbine such as prediffuser design and tailoring of pattern factor (exit temperature profile to turbine).
- Investigation of main-zone contribution to combustion dynamics, and approaches to mitigating combustion dynamics in potential engine applications.

Section V – New Technology

New technology developed under this N+3 combustor development effort was in the area of fuel injection and mixing for both the pilot and mains. Specifically, an alternative high-shear pilot design was developed with shape changes to the airflow path in the region of fuel-injection, to better mix fuel and air and to prevent fuel-rich zones which lead to Particulate Matter (PM) formation. The alternative injector was developed using CFD tools to evaluate fuel and air mixing, and resulted in a modified filmer shape as well as a modified fuel-nozzle tip, both of which were manufactured and tested at UTRC. In addition to this pilot development, improved main-mixers were developed and demonstrated which provided improved low-NOx emissions performance as a result of their high-degree of mixing, and which were demonstrated to be robust to flashback and autoignition while operating on multiple alternative fuel types. An annular main-mixer was also developed, but not tested, for potential use at larger scale either for larger engines or for reduced injector part count in a small-core engine as described above.

Learning from this N+3 combustor development effort included the following:

- The small-core N+3 combustor developed here, using an axially-controlled stoichiometry (ACS) architecture and optimized main-mixer technology, was demonstrated to meet the NASA N+3 emissions targets on both Jet-A and alternative fuel (a 50/50 blend of Jet-A and Rentech fuel).
- The axial-controlled stoichiometry (ACS) architecture used for the N+3 combustor is viable using multiple alternative pilots. This learning resulted from tests that compared data (as discussed above in this report) acquired using the baseline-type high-shear pilot versus alternative airblast- and hybrid-type pilots. All methods of piloting resulted in emissions performance that can meet the NASA N+3 targets when applied to the ACS combustor architecture developed here. This learning was not anticipated (or considered) during initial planning of the project, but was valuable additional information acquired during the execution of the project.

- The pilot injector is critical to both Particulate Matter (PM) emissions and to combustion dynamics (acoustic tones), and the pilot design can strongly influence performance in both of these areas.
- Based on engine cycles anticipated for future engines, such as the N+3 engine for subsonic commercial transport as well as potential supersonic commercial aircraft engines, achieving low cruise NOx engines will be especially challenging because these engines will cruise at higher fuel-air-ratios and higher overall-pressure-ratios than legacy engines. The axially-controlled stoichiometry (ACS) combustor technology developed here provides a path to mitigating these potential future NOx emissions.

References

Dai, Z., Smith, L.L., & McCormick, D.C., "Evaluation of a CFD Design Tool for Gas Turbine Diffusers," AIAA Paper No. AIAA-2019-1186, AIAA Science & Technology Forum (SciTech), January 7-11, 2019, San Diego, California.

Colket, M.B., Hall, R.J., & Stouffer, S.D., "Modeling Soot Formation in a Stirred Reactor" ASME Paper No. GT2004-54001, Proceedings of ASME Turbo Expo 2004, Vienna, Austria, June 14-17, 2004..

Cumpsty, N.A., "Preparing for the Future: Reducing Gas Turbine Environmental Impact – IGTI Scholar Lecture," Journal of Turbomachinery, Vol. 132 (October 2010).

Epstein, A.H., "Aeropropulsion for Commercial Aviation in the Twenty-First Century and Research Directions Needed," *AIAA Journal*, Vol. 52, No. 5 (May 2014).

Greitzer, E.M., Bonnefoy, P.A., De la Rosa Blanco, E., Dorbian, C.S., Drela, M., Hall, D.K.; Hansman, R.J., Hileman, J.I., Liebeck, R.H., Lovegren, J., Mody, P., Pertuze, J.A., Sato, S., Spakovszky, Z.S.. Tan, C.S., Hollman, J.S., Duda, J.E., Fitzgerald, N., Houghton, J., Kerrebrock, J.L., Kiwada, G.F., Kordonowy, D., Parrish, J.C., Tylko, J., Wen, E.A., & Lord, W.K., "N+3 Aircraft Concept Design and Trade Studies Final Report," NASA Contract NNX08AW63A, Final Report (March 2010).

Lefebvre, A.H., "Gas Turbine Combustion," Taylor & Francis, Bristol, PA (1983).

Lord, W.K., Suciu, G.L., DiOrio, A.G., Greitzer, E.M., & Tan, C.S., "Aircraft and Technology Concepts for an N+3 Subsonic Transport Phase II: Final Report on High-Efficiency, High-Pressure Ratio Small Core Engines," NASA Contract NNX11AB35A, Final Report (October 2014).

Lord, W.K., Suciu, G.L., Hasel, K.L., & Chandler, J.M., "Engine Architecture for High Efficiency at Small Core Size," Paper No. AIAA-2015-0071, 53rd AIAA Aerospace Sciences Meeting, Kissimmee FL (Jan 2015).

Zeppieri, S., Smith, L.L., & Colket, M., "Autoignition Characteristics of Selected Alternative Fuels at High OPR Conditions," AIAA Paper No. AIAA-2017-4985, AIAA Propulsion & Energy Forum (P&E), July 10-12, 2017, Atlanta, Georgia.